

**An Experimental Investigation of the Oxidation Characteristics
of Diesel Particulate Matter**

BY

HWANSOO CHONG
B.E., Dong A University, South Korea, 1996
M.S., Pusan National University, South Korea, 2000

THESIS

Submitted as partial fulfillment of the requirements
for the degree of Doctor of Philosophy in Mechanical Engineering
in the Graduate College of the
University of Illinois at Chicago, 2012

Chicago, Illinois

Defense Committee:

Suresh K. Aggarwal, Chair and Advisor
Kenneth Brezinsky
Rodica Baranescu
Micheal Mcnallan, Civil and Materials Engineering
Kyeong O. Lee, Argonne National Laboratory

ACKNOWLEDGMENTS

The completion of this thesis would not have been possible without the help of many people. The most influential is Prof. Suresh K. Aggarwal, who has always been a great mentor and instructor over the many years that I have known him. To practically approach and solve engineering problems with confidence, you have provided me with the knowledge and resources. To Dr. Kyeong O. Lee, I truly appreciate the patience, guidance, and time that you both afforded me during my journey to complete this thesis. This journey would not have begun without your encouragement and support. Thank you, Dr. Lee, again. Moreover, the education that I received at Argonne National Laboratory goes far beyond any classroom lecture. It is true that a good thesis is not possible without an outstanding committee. My sincere thanks to my committee members – Prof. Kenneth Brezinsky, Prof. Rodica Baranescu, and Prof. Michael McNallan – for their excellent feedbacks, comments on the thesis and their valuable time.

This project is supported by the combustion and emissions program of the U.S. Department of Energy, Office of Vehicle Technologies.

Finally, the completion of this thesis is dedicated to my family, mother and father.

Chong, Hwansoo

TABLE OF CONTENTS

<u>CHAPTER</u>		<u>PAGE</u>
1	INTRODUCTION.....	1
1.1	General.....	1
1.2	Diesel Particulate Matter.....	2
1.3	Environmental Regulations.....	5
	1.3.1 U.S.A. Emission Standards.....	6
	1.3.1.1 On-highway Diesel Truck and Bus Engines.....	6
	1.3.1.2 Off-highway Diesel Engines.....	9
	1.3.1.3 Stationary Engines.....	12
	1.3.1.4 Marine Diesel Engines.....	12
	1.3.1.5 Locomotives.....	16
	1.3.2 European Emission Standards.....	17
	1.3.2.1 Heavy Duty Diesel Truck and Bus Engines.....	17
	1.3.2.2 Off-highway Diesel Engines.....	18
1.4	Diesel PM After-treatment Systems.....	21
	1.4.1 Diesel Particulate Filters.....	23
	1.4.2 DPF Regeneration Systems.....	24
1.5	Soot Oxidation Kinetics and Modeling.....	27
	1.5.1 Global n-th Order Rate Equation.....	27
	1.5.2 Heterogeneous Solid-Gas Thermo-Oxidation Kinetics.....	29
	1.5.3 Langmuir-Hinshelwood Kinetics.....	31
	1.5.4 Reaction-Diffusion Model.....	32
	1.5.5 Thesis Objectives and Outline.....	33
2	EXPERIMENTAL METHODOLOGY.....	38
2.1	Diesel PM Sampling.....	38
2.2	Instrumentation and Calibration.....	40
3	MEASUREMENT OF THE HEAT RELEASE RATE.....	43
3.1	Introduction.....	43
3.2	Oxidation Experimental Scheme.....	44
3.3	Result and Discussion.....	45
3.4	Conclusion.....	57

TABLE OF CONTENTS (Continued)

<u>CHAPTER</u>		<u>PAGE</u>
4	OXIDATION CHARACTERISTICS OF DIESEL PARTICULATES	59
4.1	Introduction.....	59
4.2	General Concept of Kinetics.....	63
4.3	Theory of Reaction Rates.....	65
4.3.1	The Arrhenius Law.....	65
4.3.2	Hard Sphere Collision Theory.....	66
4.3.3	Activated Complex Theory.....	71
4.4	Oxidation Experimental Scheme.....	74
4.5	Result and Discussion.....	75
4.5.1	Oxidation Experiments with Surrogate Soot....	75
4.5.2	Oxidation Experiments with Diesel PM.....	84
4.5.3	Effect of SOF on Diesel PM Oxidation.....	93
4.5.4	Effect of Thermal Aging on Diesel PM Oxidation.....	95
4.6	Conclusion.....	102
5	MODELING OF HEAT RELEASE RATE	106
5.1	Introduction.....	106
5.2	Modeling of the Heat Release Rate.....	107
5.3	Result and Discussion.....	111
5.4	Conclusion.....	121
6	CONCLUSIONS	124
6.1	Summary	124
6.2	Future Work.....	127
	REFERENCES	129
	VITA	138

LIST OF TABLES

<u>TABLE</u>		<u>PAGE</u>
I	13-MODE SUPPLEMENTAL EMISSION TESTING (SET) CYCLE.....	8
II	EPA TIER 2 AND 4 NON-ROAD DIESEL ENGINE EMISSION STANDARDS.....	10
III	ISO 8178 C1, 8-MODE STEADY-STATE TEST CYCLE AND WEIGHTING FACTORS.....	11
IV	EPA TIER2 MARINE DIESEL ENGINE EMISSION STANDARDS AND BLUE SKY PROGRAM.....	14
V	ISO 8178 E1-5 TEST CYCLES AND WEIGHTING FACTORS.....	15
VI	EPA LOCOMOTIVE DIESEL PM EMISSION STANDARDS.....	16
VII	EUROPEAN DIESEL PM EMISSION STANDARDS FOR HEAVY-DUTY DIESEL ENGINES	17
VIII	EUROPEAN STATIONARY CYCLE (ESC) TEST MODE.....	19
IX	STAGE I-IV PM EMISSION STANDARDS FOR NON-ROAD DIESEL ENGINES IN EUROPE.....	20
X	EUROPEAN PM EMISSION STANDARDS FOR DIESEL ENGINES USED IN INLAND WATERWAY VESSELS (STAGE III-A).....	22
XI	EUROPEAN PM EMISSION STANDARDS FOR RAILROAD LOCOMOTIVE DIESEL ENGINES.....	22
XII	REACTION MODELS FOR SOLID-STATE REACTION KINETICS.....	30

LIST OF TABLES (Continued)

<u>TABLE</u>		<u>PAGE</u>
XIII	TOTAL HEAT EVOLVED AND HEAT EVOLVED PER UNIT SAMPLE MASS DURING THE OXIDATION OF SURROGATE SOOT SUBJECTED TO DIFFERENT TEMPERATURE HEATING RATES IN DSC EXPERIMENTS.....	47
XIV	PEAK HEAT RELEASE RATE, TOTAL HEAT RELEASE AND HEAT RELEASE PER UNIT MASS IN THE OXIDATION OF SURROGATE SOOT SAMPLE SUBJECTED TO DIFFERENT ISOTHERMAL CONDITIONS IN DSC EXPERIMENTS.....	50
XV	SAMPLE MASS (M_o), RESIDUE MASS (M_r), NET MASS OXIDIZED (M_o-M_r), MASS OF VOLATILE COMPONENT OF SOF (M_v), TOTAL AMOUNT OF HEAT RELEASE, AND SPECIFIC HEAT RELEASE IN THE OXIDATION OF DIESEL PM, DRY DIESEL PM AND SURROGATE SOOT WITH RESPECT TO DIFFERENT TEMPERATURE PROFILES IN DSC EXPERIMENTS.....	56
XVI	PREVIOUS RESEARCH ON THE OXIDATION OF DIESEL PM.....	61
XVII	MEASURED REACTION ORDERS WITH RESPECT TO CARBON FOR THE SURROGATE SOOT SAMPLES SUBJECTED TO DIFFERENT HEAT TREATMENTS IN INERT AND OXIDIZING ENVIRONMENTS.....	82
XVIII	MEASURED ACTIVATION ENERGY, REACTION ORDER WITH RESPECT TO OXYGEN, AND PRE-EXPONENTIAL FACTOR FOR SURROGATE SOOT SAMPLES SUBJECTED TO DIFFERENT HEAT TREATMENTS.....	83
XIX	MEASURED AMOUNT OF EVAPORATED VOLATILE COMPONENTS OF SOF, REACTION ORDER WITH RESPECT TO SOOT AND OXYGEN, ACTIVATION ENERGY AND PRE-EXPONENTIAL FACTOR FOR DIESEL PM SAMPLES SUBJECTED TO DIFFERENT HEAT TREATMENTS.....	94

LIST OF TABLES (Continued)

<u>TABLE</u>		<u>PAGE</u>
XX	MEASURED AMOUNT OF EVAPORATED VOLATILE COMPONENTS OF SOF, REACTION ORDER WITH RESPECT TO SOOT AND OXYGEN, ACTIVATION ENERGY AND PRE-EXPONENTIAL FACTOR FOR DIESEL PM SAMPLES EXPOSED TO HELIUM ENVIRONMENT FOR 1 HOUR AND 5 HOURS AT 550 °C, PRIOR TO OXIDATION.....	98
XXI	MEASURED KINETIC PARAMETERS (REACTION ORDERS WITH RESPECT TO SOOT AND OXYGEN, ACTIVATION ENERGY, AND PRE-EXPONENTIAL FACTOR) FOR DIESEL PM SAMPLES EXPOSED TO HELIUM AND AIR ENVIRONMENT DURING HEAT TREATMENT WITH A HEATING RATE OF 10 °C/MIN.....	100
XXII	COMPARISON OF THE KINETIC PARAMETERS FOR THE OXIDATION OF SURROGATE SOOT AND DIESEL PM SAMPLES AT 550 °C WITH DIFFERENT HEAT TREATMENTS.....	103
XXIII	DSC SPECIFICATION AND OXIDATION EXPERIMENT CONDITION.....	109
XXIV	THERMOPHYSICAL PROPERTIES OF AIR AT 550°C AND ATMOSPHERIC PRESSURE.....	110

LIST OF FIGURES

<u>FIGURE</u>		<u>PAGE</u>
1	Illustration of diesel particulate matter (PM) emission (Maricq, 2007).....	3
2	GC profiles for the SOF from the diesel PM emissions, diesel fuel, and lube oil (Farrauto and Voss, 1996).....	4
3	Transient federal test standard (FTP) testing cycle (www.dieseln.net.com).....	7
4	Normalized speed and torque over non-road transient cycle (NRTC)...	11
5	Example of exhaust gas flow through wall flow filter.....	23
6	Example of exhaust gas flow through non-blocking filter (Farafontov et al., 2007).....	24
7	Example of continuously regenerating particulate filter systems.....	26
8	Example of a DPF melted during DPF regeneration.....	34
9	DPF test system connected to the exhaust pipe of a 1.9L 4-cylinder light-duty diesel engine.....	39
10	Diesel PM in the cordierite DPF membrane taken out from the thermal reactor in the DPF test system.....	41
11	DSC, TGA, and data acquisition system for oxidation experiment	42
12	Temporal variation of heat release rate during the oxidation of surrogate soot sample in air under a specified temperature profile for the baseline case.....	46
13	Temporal variation of the net heat flow rate associated with the oxidation of model soot samples in air subjected to two different temperature profiles with ramp rate of 10°C/min. The peak temperatures at isothermal conditions are 535 °C and 525 °C in Figs. 13a and b, respectively.....	49

LIST OF TABLES (Continued)

<u>FIGURE</u>		<u>PAGE</u>
14	Instantaneous mass of diesel PM exposed to a nitrogen environment in a heating mode of temperature gradients of 10°C/min and isothermal condition for 1hr at 550°C.....	51
15	Instantaneous mass of diesel PM exposed to a nitrogen environment in a heating mode of heating rate of 10°C/min with three isothermal temperatures of 300°C, 550°C, and 700°C.....	52
16	Temporal variation of the net heat flow rate measured during the oxidation of SOF-containing diesel PM sample and dry diesel soot sample in DSC experiments.....	53
17	Temporal variation of the heat release rate during the oxidation of dry diesel soot, diesel PM, and surrogate soot samples in air subjected to three different temperature profiles with ramp rate of 10°C/min. The peak temperatures at isothermal conditions are 550 °C, 535 °C and 525 °C in Figs. 17a, b, and c respectively.....	54
18	Temporal variation of the instantaneous mass for the surrogate soot sample exposed to helium environment in heating mode with temperature gradient of 10°C/min, then maintained at an isothermal temperature of 550°C for 1 h, and then to oxidizing (air) environment at temperatures 500°C, 550°C, and 600°C in Figs. 18a, b, and c, respectively. Initial sample mass: 5.865mg (a), 5.241mg (b), and 6.267mg (c).....	76
19	Logarithmic plot for the rate of mass loss as a function of $\ln[m_c]$ for the three isothermal temperatures of 500°C, 550°C, and 600°C. The slope yields the reaction order with respect to carbon for the surrogate soot sample.....	77
20	Evaluation of activation energy for the surrogate soot sample using Eq, (4-37).....	78
21	Variation of the measured activation energy plotted versus the initial mass of the surrogate soot sample, covering a mass range of 1-4.5 mg.....	79
22	Evaluation of reaction order of oxygen using Eq. (4-37) for surrogate soot samples subjected to different oxygen partial pressures.....	81

LIST OF TABLES (Continued)

<u>FIGURE</u>		<u>PAGE</u>
23	Instantaneous mass of diesel PM exposed to a helium environment in heating mode with temperature gradients of 10°C/min, isothermal condition for 1h at 550°C, temperature control mode to arrive at the specific isothermal temperature, and then exposed to air environment under isothermal temperatures of 500°C, 550°C, and 600°C, in Figs. 23a, b, and c, respectively. Initial sample mass and residue mass: 4.653mg and 0.266mg in (a), 4.992mg and 0.612mg in (b), and 4.592mg and 0.583mg in (c).....	87
24	Temporal variation of the rate of mass loss during the oxidation of dry diesel soot and surrogate soot samples under isothermal temperatures of 500°C, 550°C, and 600°C, in Figs. 24a, b, and c, respectively.....	88
25	The rate of mass loss plotted as a function of sample mass, normalized by the initial mass of sample measured at the start of oxidation, during the oxidation of dry diesel soot and surrogate soot under isothermal temperatures of 500°C, 550°C, and 600°C, in Figs. 25a, b, and c, respectively.....	89
26	Logarithmic plot for the rate of mass loss of diesel PM samples as a function of $\ln[m]$ for the three isothermal temperatures of 500°C, 550°C, and 600°C. The slope yields the reaction order of soot for the diesel soot sample.....	90
27	Evaluation of activation energy for the diesel soot sample in zones 1 and 2 using Eq. (4-37).....	91
28	Evaluation of reaction order of oxygen in zones 1 and 2 for diesel soot samples subjected to different oxygen partial pressures.....	92
29	Temporal variation of the rate of mass loss during the oxidation of diesel PM samples subjected to three different heat treatments with heating rates of 100°C/min, 10°C/min, and 1 h isothermal period at 550°C in helium, followed by oxidation at isothermal temperature of 600°C. Initial sample mass and residue mass: 4.317mg and 0.155mg for experiment with the heating rate of 100°C/min; and 4.086mg and 0.312mg for 10°C/min, and 4.592mg and 0.583mg for 1h isothermal.....	96

LIST OF TABLES (Continued)

<u>FIGURE</u>		<u>PAGE</u>
30	Temporal variation of the rate of mass loss during the oxidation of two diesel PM samples subjected to heat treatments of 1 h and 5 h isothermal period in helium environment, respectively, prior to oxidation at temperatures of 550°C and 600°C in Figs. 30a and b. Initial sample mass and residue mass: For 1 h isothermal, 4.992mg and 0.612mg in (a), and 4.592mg and 0.583mg in (b). For 5 h isothermal, 3.848mg and 0.415 mg in (a), and 4.286mg and 0.412 mg for 5h in (b).....	97
31	Instantaneous mass and rate of mass loss (oxidation rate) of diesel PM samples exposed to air environment in heating mode with ramp rate of 10°C/min, followed by isothermal condition at temperatures 500°C, 550°C, and 600°C in Figs. 31a, b, and c, respectively. Initial sample mass and residue mass: 5.41mg and 0.593mg in (a), 5.26mg and 0.372mg in (b), and 6.861mg and 0.367mg in (c).....	101
32	A schematic of differential scanning calorimeter (DSC) and heat dissipation from the soot to the platform and the air.....	108
33	Instantaneous heat flow rate of dry surrogate soot samples subjected to a specific temperature profile in helium, and the baseline determined for the data. Initial sample mass: 6.831mg in sample#1, 6.685mg in sample#2, and 6.525mg in sample#3.....	112
34	Evaluated heat capacity in the temperature range of 318K(45°C) and 823K(550°C) for all surrogate soot samples using Eq. (5.11), average values at each temperature, the specific heat function obtained by linear regression analysis for the average data, and a standard NBS graphite reference data. Initial sample mass: 6.831mg in sample#1, 6.685mg in sample#2, and 6.525mg in sample#3.....	112
35	Temporal variation of the instantaneous mass for the surrogate soot sample exposed to helium environment in heating mode with temperature gradient of 10°C/min, then maintained at an isothermal temperature of 550°C for 10 min., and then to oxidizing (air) environment at temperatures 550°C. Initial sample mass: 5.786 mg.....	113

LIST OF TABLES (Continued)

<u>FIGURE</u>		<u>PAGE</u>
36	Temporal distribution of heat flux transferred to the temperature sensor (q_1'') and the air (q_2'') and the total heat flux (q_t'') to both the air and temperature sensor during the oxidation of surrogate soot in the isothermal temperature at 550°C in the DSC.....	115
37	Comparison of data between computation and experiment in terms of heat flow rate (surrogate soot).....	116
38	Evaluated heat capacity in the temperature range of 318K(45°C) and 823K(550°C) for four different dry diesel PM samples using Eq. (5.11). Initial sample mass: 4.81mg in sample#1, 4.852mg in sample#2, 4.845mg in sample#3, and 4.91mg in sample#4.....	117
39	Temporal variation of the instantaneous mass for the dry diesel PM sample exposed to helium environment in heating mode with temperature gradient of 10°C/min, then maintained at an isothermal temperature of 550°C for 10 min., and then to oxidizing (air) environment at temperatures 550°C. Initial sample mass and ash: 5.982mg and 0.285 mg, respectively.....	118
40	Temporal distribution of heat flux transferred to the temperature sensor (q_1'') and the air (q_2'') and the total heat flux (q_t'') to both the air and temperature sensor during the oxidation of dry diesel PM in the isothermal temperature at 550°C in the DSC.....	119
41	Comparison of data between computation and experiment in terms of heat flow rate (dry diesel soot). The zone 1 and the zone including transition and zone 2 are from the start to 80% of the total heat release and the last 20%, respectively.....	120

LIST OF ABBREVIATIONS

DPF	Diesel Particulate Filter
DSC	Differential Scanning Calorimeter
EGR	Exhaust Gas Recirculation
EPA	Environmental Protection Agency
ESC	European Stationary Cycle
ETC	European Transient Cycle
FTP	Federal Test Standard
GVWR	Gross Vehicle Weight Rating
HHD	Heavy Heavy Duty
LAFY	Los Angeles Freeway
LANF	Los Angeles Non Freeway
LHD	Light Heavy Duty
MHD	Medium Heavy Duty
NYNF	New York Non Freeway
NRSC	Non-Road Steady Cycle
NRTC	Non-Road Transient Cycle
NSPS	New Source Performance Standards
NTE	Not-To-Exceed standards
PAH	Polycyclic Aromatic Hydrocarbon
PM	Particulate Matter
SET	Steady-state supplemental Emission Testing
SOF	Soluble Organic Fraction
TGA	Thermogravimetric Analyzer
VGT	Variable Geometry Turbocharger

SUMMARY

Most diesel engines require diesel particulate filter (DPF) systems to meet increasingly stringent emissions regulations, which are equipped with a passive or active regeneration system. Although extensive research has been reported focusing on the development of efficient DPF systems, significant improvements are still needed in their performance. This includes reducing back pressure due to soot and ash build-up, improving material durability and filtration efficiency, and developing smart DPF control management systems for optimum regeneration strategies. In particular, an effective thermal management system is necessary to prevent the failure of a DPF system caused by the thermal runaway. To this end, there has been significant research on the oxidation behavior of diesel PM. However, most of studies have analyzed PM samples taken from the engine exhaust pipe. It is important to investigate the heat release characteristics and the oxidation behavior of PM for designing optimum DPF regeneration algorithms. Such information is important not only for devising efficient thermal management systems for DPF regeneration, but also for developing accurate predictive models. Furthermore, PM contain various chemical components, such as elemental carbon, soluble organic fractions (SOFs), sulfur oxides, and metal oxides. Moreover, the particulates display significant differences in morphology, depending upon speed and load. Researchers have often used surrogate soot such as commercially available graphite or soot samples collected from lab-scale burners. However, oxidation experiments with surrogate soot often provide inaccurate data due to the differences in composition and morphology of diesel PM and surrogate soot.

The present study aims to characterize the oxidation and heat release behaviors of diesel PM collected directly from the filter membrane of a DPF system connected to a diesel engine

SUMMARY (Continued)

exhaust pipe of 1.9L four cylinder light duty diesel engine, and examine the effects of volatile component of SOF and thermal aging on the oxidation of diesel PM. In addition, differences in the oxidation behavior of diesel PM and surrogate soot are characterized by performing experiments under the identical conditions. For oxidation experiments, a differential scanning calorimeter (DSC) and a thermogravimetric analyzer (TGA) were used to measure temporal rate of heat release and mass or mass loss rate in the oxidation of soot samples, respectively.

The results of DSC experiments revealed that the amounts of heat released from the oxidation of SOF-containing diesel PM sample, dry diesel soot, and surrogate soot were approximately 14.67 kJ/g, 17.3 kJ/g, and 14.02 kJ/g, respectively, indicating that the largest heat release was obtained from the dry diesel soot sample. Results also indicated significant differences in the temporal rates of heat release in the oxidation of SOF-containing diesel PM, dry diesel soot and surrogate soot. In the TGA experiments, the oxidation rate of surrogate soot decreased continuously as the soot was oxidized, while that of diesel soot was nearly constant until about 80% of the sample mass was oxidized, and then decreased as the sample was completely oxidized. In addition, the oxidation behavior of surrogate soot was found to be essentially independent of the heat treatment schemes used, while that of diesel soot was strongly influenced by them. The effects of SOF and thermal aging on diesel PM oxidation were characterized. Results indicated that the PM oxidation was only weakly influenced by the presence of volatile components of SOF, whereas it was noticeably affected by thermal aging. The global kinetic parameters were determined for the diesel PM and surrogate soot samples. Finally, a model for predicting heat release rate was developed with the experimental data.

CHAPTER 1

INTRODUCTION

1.1 General

The diesel engine is one of the most widely-used power sources available for industrial, commercial, and personal transportation, owing to its high efficiency, reliability and durability. These advantages of diesel engine are leading to its continued increase in the global use, yet exhaust emissions from diesel engines have caused air pollution problems. The complete combustion of hydrocarbon fuels would only generate CO₂ and H₂O. In the practical engine operations, however, the combustion process is often incomplete, due to the heterogeneity of the air-fuel mixture in cylinder.

It has been reported in literature (Jelles, 1999; Johnson et al., 1994) that typical diesel exhaust emissions are composed of a wide range of organic and inorganic compounds distributed in gaseous and particulate emissions. These emissions include CO, CO₂, NO, NO₂, N₂O, NH₃, volatile organic compounds, water vapor, hydrocarbon (HC), poly-cyclic aromatic hydrocarbons, carboxyl compounds, organic acid, halogenated organic compounds, sulfur dioxides, and dioxins. Particulate matter (PM), organic compounds, carbon monoxide, carbon dioxide, HCs, and NO_x are major products in engine combustion. In addition, diesel exhaust emissions contain inorganic constituents such as metal oxides and sulfur oxides.

Reduction of diesel PM from combustion in diesel engines is of prime important in terms of environmental pollution (Chameides and Bergin, 2002) and potential human health impacts (Seaton et al., 1995; Bünger et al., 2000). In particular, it has been significantly investigated that diesel PM is hazardous to human health due to its potential mutagenic (Berisario et al., 1984;

Ohe, 1984) and carcinogenic activity (Bhatia et al., 1998; IARC, 1989; Kreyling et al., 2007). In addition, diesel particulate emissions are reported to cause respiratory inflammations (Riedl et al., 2005; Schwarze et al., 2006).

These negative effects of diesel exhaust emissions on human health have led to many governmental agencies legislating stricter emissions standards. In order to meet these regulations and reduce diesel particulates emitted to the atmosphere, diesel engines typically require after-treatment in the exhaust system, such as particulate filter system. As the filter accumulates diesel particulate emissions, it builds up backpressure causes many negative effects, such as decreased combustion efficiency or possible filter failure. Therefore, diesel particulate filters (DPFs) have been developed to efficiently remove the accumulated PM emissions in the regeneration process, although they still require significant improvement in performance, such as reducing the back pressure caused by soot/ash build-up, improving high filtration efficiency, material durability, and optimum regeneration strategies.

1.2 Diesel Particulate Matter

In general, the particulate matter is formed by incomplete combustion of gaseous fuels. These particulates start to grow from small carbon particles to large porous agglomerates through several processes, such as pyrolysis, nucleation, surface growth, coalescence, aggregate, and oxidation. The compositions of diesel PM depend on where and how they are collected. The US Environmental Protection Agency (EPA) defined PM emissions as all compounds collected on a preconditioned filter in dilute diesel exhaust gases at a maximum temperature of 52 °C. Typically, diesel particulates contain various chemical components, such as elemental carbon, soluble organic fractions (SOFs), sulfuric acids, and metal oxides. Figure 1 illustrates the

structure of soot particle and other compounds. (Maricq, 2007). In the exhaust tailpipe, most of volatile components are of gaseous phase because of high exhaust temperatures. In emissions measurements, consequently, the dilution and cooling processes affect not only the amount of volatile components condensed in elemental carbons but formation of particulates (Kasper et al., 2000).

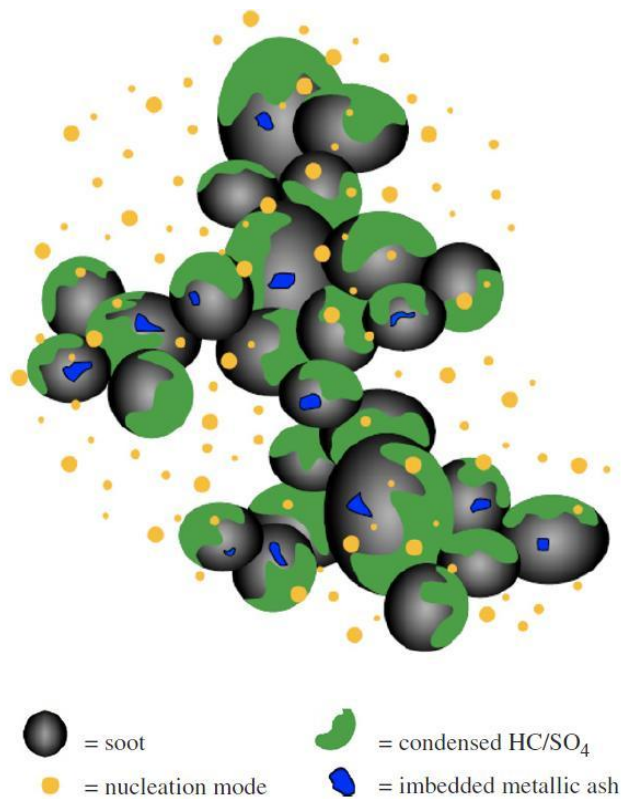


Figure 1. Illustration of diesel particulate matter (PM) emission (Maricq, 2007).

The SOF is a major component often contained in diesel PM emissions. It mainly consists of heavy hydrocarbons (Levsen, 1988), such as aliphatic hydrocarbons, polycyclic aromatic

hydrocarbons (PAHs), nitric PAHs, and oxygenated PAHs, and aldehydes, which are produced due to incomplete combustion of diesel fuels (Durán et al., 2002) or lubricating oils (Farrauto and Voss, 1996; Froelund and Schramm, 1997). Figure 2 shows the chromatograms of SOFs contained in diesel PM, diesel fuel, and lube oil. As shown in the figure, the SOF portion of particulates was comprised primarily of lube oil with a small amount of unburned fuel.

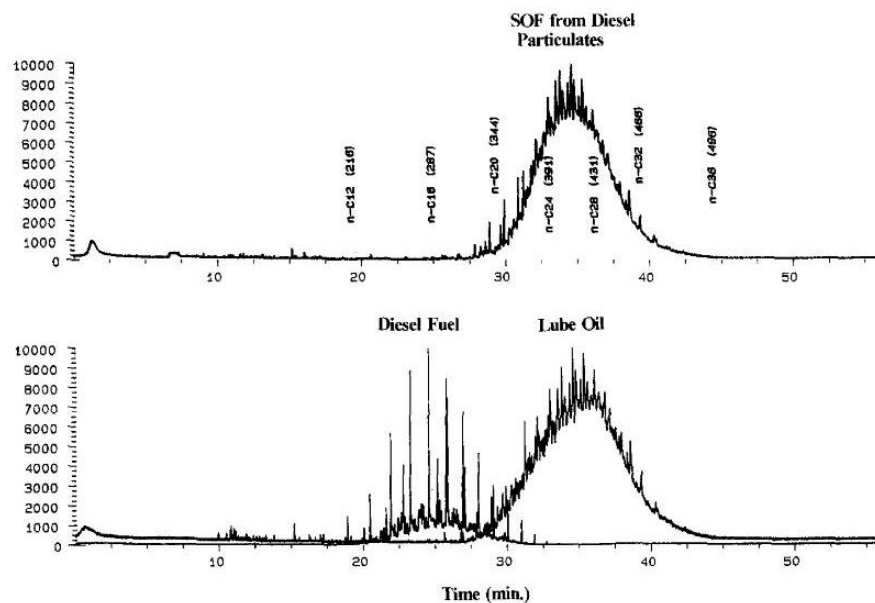


Figure 2. GC profiles for the SOF from the diesel PM emissions, diesel fuel, and lube oil (Farrauto and Voss, 1996).

An important observation reported in previous studies (Lee et al., 2002a; Lee et al., 2003b) was that the amount of SOF in diesel PM strongly depends on engine speed and load conditions, and, consequently, particulates sampled at different engine operating conditions displayed significant differences in morphology. Particles sampled at low engine speed and loads appeared to be amorphous and nebulous, while those sampled at high engine speed/load conditions

exhibited graphitic structures. The authors attributed the amorphous structures to a saturation of SOFs initially residing in exhaust gas emissions, where combustion temperatures were relatively low. In contrast, graphitic structures are formed under high temperature and pressure conditions. Although any direct linear relation has not shown in the literature, the Raman spectroscopic analyses indicated that the degree of graphitic structures increased linearly with engine speed. In addition, metal compounds in lubrication oils lead to a small amount of inorganic ash (Kittelson, 1998).

1.3 Environmental Regulations

Diesel PM emissions have been well known to be responsible for air pollution and human health hazards. In particular, the heavy hydrocarbons (HCs) condensed in particulates are of particular concern, because several of them have shown carcinogenicity and mutagenicity, as reported in various investigations. Once diesel PM emissions including HCs are in the lungs, they can be trapped and deposited in the bronchial passage and alveoli of the lungs, and then result in inflammatory reaction (Schwarze et al., 2006). If the particles are small enough, they can penetrate the blood stream, and then deposit in living organs, such as liver, spleen, kidneys, heart, immune system, and central nerve system. The inflammation can be caused where the particles are accumulated, and can act as carcinogens (Kreyling et al., 2007).

To resolve these problems of diesel particulates, diesel engines typically require after-treatment devices. Furthermore, upcoming strict emissions regulations in U.S. and Europe are providing a motivation to engine manufactures for developing advanced after-treatment systems that can significantly reduce tail-pipe diesel particulate emissions.

1.3.1 U.S.A. Emission Standards

1.3.1.1 On-highway Diesel Truck and Bus Engines

The Following emission standards apply to diesel engines used in heavy-duty highway vehicles. Heavy-duty vehicles are defined as vehicles of gross vehicle weight rating (GVWR) of above 8,500 lbs in the federal jurisdiction. Diesel engines used in heavy-duty vehicles are further divided into three different classes by GVWR. The diesel engine models used for the 8,500 – 19,500 lbs, 19,500 – 33,000 lbs, and over 33,000 lbs vehicle category are classified into light heavy-duty (LHD), medium heavy-duty (MHD), and heavy heavy-duty (HHD), respectively. Current federal emissions standards are expressed in g/bhp·hr and require emission testing over the transient federal test standard (FTP) engine dynamometer cycle and steady-state supplemental emission testing (SET).

The transient FTP testing cycle consists of four phases: 1) NYNF (New York Non Freeway) phase typical of light urban traffic with frequent stops and starts, 2) LANF (Los Angeles Non Freeway) phase typical of crowded urban traffic with few stops, 3) LAFY (Los Angeles Freeway) phase simulating crowded expressway traffic in Los Angeles, and 4) repetition of the first NYNF phase. To simulate the operation of the vehicle that corresponds to the engine being tested, it includes a cold start after a parking overnight, idling, acceleration and deceleration phases, and a wide variety of different speeds and loads sequences, as seen in Figure 3. There are few stabilized running conditions, and the average load factor is about 20 to 25% of the maximum horsepower available at a given speed.

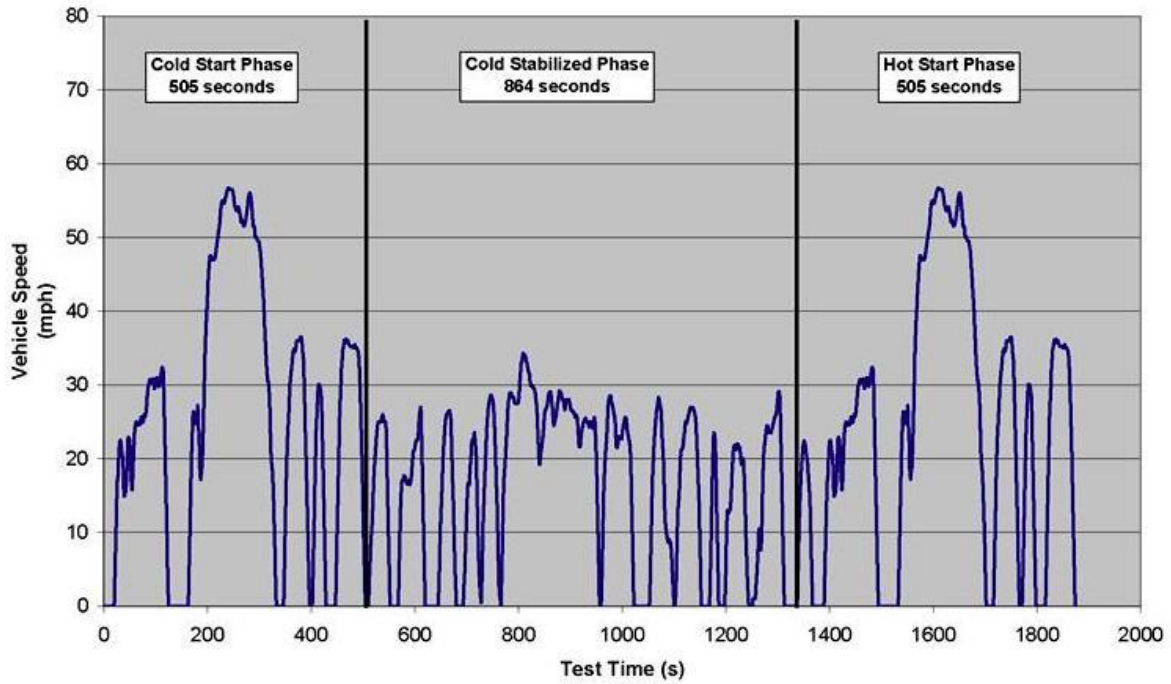


Figure 3. Transient federal test standard (FTP) testing cycle (www.dieselnet.com).

In addition to the transient FTP testing, the steady-state testing, SET, consisting of 13 modes is required for heavy-duty diesel engines. Table I summarizes 13-mode SET cycles. In the table, the engine speeds, A, B, and C, are defined as $A = n_h + 0.25 (n_l - n_h)$, $B = n_h + 0.5 (n_l - n_h)$, and $C = n_h + 0.75 (n_l - n_h)$, respectively. n_h and n_l are the high and low speed determined by calculating 50% and 70% of the declared maximum net power.

TABLE I

13-MODE SUPPLEMENTAL EMISSION TESTING (SET) CYCLE.

Mode		Time, s	Speed, rpm	Torque, %	Mode		Time, s	Speed, rpm	Torque, %
1a	steady-state	170	IDLE	0	8a	steady-state	194	B	100
1b	Transient	20	Linear transition	Linear transition	8b	Transient	20	B	Linear transition
2a	steady-state	173	A	100	9a	steady-state	218	B	25
2b	Transient	20	Linear transition	Linear transition	9b	Transient	20	Linear transition	Linear transition
3a	steady-state	219	B	50	10a	steady-state	171	C	100
3b	Transient	20	B	linear	10b	Transient	20	C	Linear transition
4a	steady-state	217	B	75	11a	steady-state	102	C	25
4b	Transient	20	Linear transition	Linear transition	11b	Transient	20	C	Linear transition
5a	steady-state	103	A	50	12a	steady-state	100	C	75
5b	Transient	20	A	Linear transition	12b	Transient	20	C	Linear transition
6a	steady-state	100	A	75	13a	steady-state	102	C	50
6b	Transient	20	A	Linear transition	13b	Transient	20	Linear transition	Linear transition
7a	steady-state	103	A	25	14	steady-state	168	IDLE	0
7b	Transient	20	Linear transition	Linear transition	-	-	-	-	-

On December 21, 2000 the EPA signed emission standards for model year 2007 and later heavy-duty highway engines. On comparison of the PM emission standards applied to 1998-2006 model year engines and model year 2007 and later, the PM emission standard was stringent from 0.05 to 0.01 g/bhp·hr, and this took full effect in the 2007 heavy-duty engine model year.

1.3.1.2 Off-highway Diesel Engines

The non-road diesel emission regulation, Tier 1-4, covers mobile non-road diesel engines of all sizes used in a wide range of construction, agricultural and industrial equipment. Based on the mobility and portability of diesel engines, the non-road diesel engine includes engines installed on self-propelled equipment, on equipment that is propelled while performing its function, or on equipment that is portable or transportable. The non-road diesel emission regulations are not applicable to all non-road diesel engines. Engines used in railway locomotives, marine vessels, and underground mining equipment are exempted in the non-road engine categories.

Since the first federal standards, Tier 1, for non-road diesel engines were adopted in 1994 for engines over 37 kW, the regulation introduced more stringent Tier 2 standards for all equipment with phase-in schedules from 2000 to 2008. Tier 3 standard for PM was not adopted. On May 11, 2004, the EPA signed the final rule introducing Tier 4 emission standards, which are to be phased-in over the period of 2008-2015. On comparison of Tier 2 and 4, the PM emission standard was much stricter in the Tier 4. The Tier 2 and 4 diesel PM emission standards are listed in Table II. The non-road regulations are in the metric system of units, with all standards expressed in g/kWh. In the Tier 4 phased-in from 2008-2015, PM emission standard of 19-560 kW rated power were phased-in over a few year period, as indicated in this table.

Non-road engine emissions are measured on a steady-state test cycle that is nominally the same as the ISO 8178 C1, 8-mode steady-state test cycle. The ISO 8178 is an international standard designed for non-road engine applications. The ISO 8178 test cycle or its 8-mode schedule C1 in particular can be also referred to as the non-road steady cycle (NRSC). Table III presents 8-mode steady-state test cycle. Tier 4 standards have to be met over both the steady-state test and the

non-road transient cycle (NRTC). The NRTC test is a transient driving cycle for mobile non-road diesel engines. The cycle is an engine dynamometer transient driving schedule of total duration of about 1200 seconds. The speed and torque during the NRTC test are shown Figure 4. The transient testing requirements begin with model year 2013 for engines below 56 kW, in 2012 for 56-130 kW, and in 2011 for 130-560 kW engines. Engines above 560 kW are not tested on the transient test.

TABLE II

EPA TIER 2 AND 4 NON-ROAD DIESEL ENGINE EMISSION STANDARDS.

Tier	Engine power	Year	PM emission, g/kWh
2	kW < 8	2005	0.8
	8 ≤ kW < 19	2005	0.8
	19 ≤ kW < 37	2004	0.6
	37 ≤ kW < 75	2004	0.4
	75 ≤ kW < 130	2003	0.3
	130 ≤ kW < 225	2003	0.2
	225 ≤ kW < 450	2001	0.2
	450 ≤ kW < 560	2002	0.2
	kW ≥ 560	2006	0.2
4	kW < 8	2008	0.4
	8 ≤ kW < 19	2008	0.4
	19 ≤ kW < 37	2008	0.3
		2013	0.03
	37 ≤ kW < 56	2008	0.3
		2013	0.03
	56 ≤ kW < 130	2012-2014	0.02
	130 ≤ kW < 560	2011-2014	0.02
	kW ≥ 560	2011-2014	0.1
2015		0.04	

TABLE III

ISO 8178 C1, 8-MODE STEADY-STATE TEST CYCLE AND WEIGHTING FACTORS.

Mode	Weighting factors	Speed, rpm	Torque, %
1	0.15	Rated speed	100
2	0.15		75
3	0.15		50
4	0.1		10
5	0.1		100
6	0.1	Intermediated speed	75
7	0.1		50
8	0.15	Idle	0

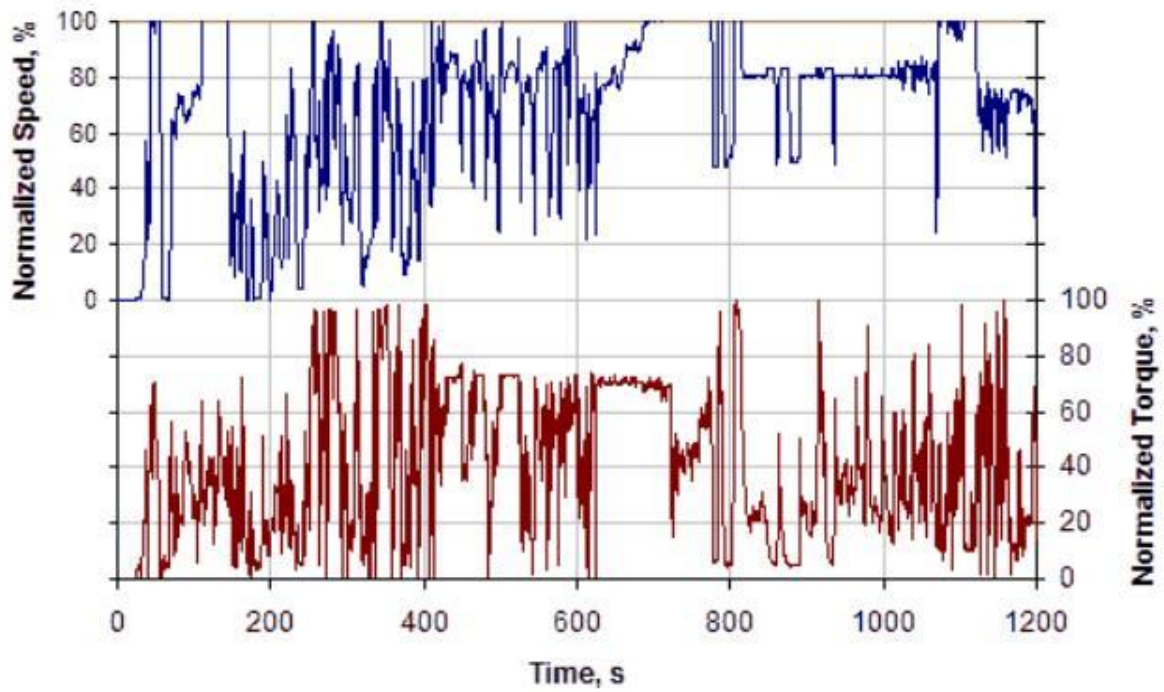


Figure 4. Normalized speed and torque over non-road transient cycle (NRTC).

In Tier 4, non-road engines also have to meet not-to-exceed standards (NTE), which are measured without reference to any specific test schedule. The NTE standards become effective in 2011 for engines above 130 kW; in 2012 for 56-130 kW; and in 2013 for engines below 56 kW. Instead of the specific driving cycle, it involves driving of any type that could occur within the bounds of the NTE control area, including operation under steady-state or transient conditions and under varying ambient conditions. Emissions are averaged over a minimum time of thirty seconds and then compared to the applicable NTE emission limits.

1.3.1.3 Stationary Engines

In 1979, the EPA proposed new source performance standards (NSPS) to control emissions for stationary diesel engines, but they were never finalized. In the absence of federal regulations, emissions from stationary engines gradually became subject to a complex system of state and local regulations. On June 28, 2006, the EPA adopted emission regulations for stationary engines, which require that most new stationary diesel engines meet the Tier 1-4 emission standards for mobile non-road engines. Engines of displacement below 10 liters per cylinder must meet Tier 1 through Tier 4 emission standards for mobile non-road diesel engines, while engines of displacement above 10 liters per cylinder must meet emission standards for marine engines.

1.3.1.4 Marine Diesel Engines

Marine diesel engines are divided into three categories based on displacement per cylinder. Category 3 marine diesel engines typically are over 30 m³ in displacement per cylinder and range in power from 2,500 to 70,000 kW. These are very large diesel engines used for

propulsion power on ocean-going vessels such as container ships, oil tankers, and bulk carriers. Category 1 and Category 2 marine diesel engines are below 5 m³ and from 5 m³ to 30 m³ in displacement, respectively, and range in power from about 500 to 8,000 kW. These engines are used to provide propulsion power on many kinds of vessels including tugboats, supply vessels, and other commercial vessels in and around ports. Emissions from marine diesel engines have been regulated, since emission regulation was issued in 1999.

Emission standards for engines Category 1 and 2 are based on the land-based standard for non-road and locomotive engines. The regulation introduced Tier 2 standards for marine diesel engines in these two categories. The 1999 regulation also set a voluntary “Blue Sky Series” program which permits manufacturers to certify their engines to more stringent emission standards. The qualifying PM emission limits in Tier 2 and blue sky program are listed in Table IV. The Blue Sky program begins upon the publication of the rule and extends through the year 2010.

Table V shows ISO 8178 E1-5 cycles for engines tested in Category 1, depending on types of propulsion engines. Engines belonging to Category 2 are tested on locomotive test cycles. In addition to the test cycle measurement, which is an average from several test modes, the regulations set NTE emission limits.

TABLE IV

EPA TIER2 MARINE DIESEL ENGINE EMISSION STANDARDS AND BLUE SKY PROGRAM.

Category	Displacement per cylinder, m ³	PM emission, g/kWh	
		Tier 2	Blue sky program
1	$D < 0.9$	0.4	0.24
	$0.9 \leq D < 1.2$	0.3	0.18
	$1.2 \leq D < 2.5$	0.2	0.12
	$2.5 \leq D < 5.0$	0.2	0.12
2	$5.0 \leq D < 15$	0.27	0.16
	$15 \leq D < 20$ power < 3300 kW	0.5	0.3
	$15 \leq D < 20$ power \geq 3300 kW	0.5	0.3
	$20 \leq D < 25$	0.5	0.3
	$25 \leq D < 30$	0.5	0.3

TABLE V

ISO 8178 E1-5 TEST CYCLES AND WEIGHTING FACTORS.

Type	E1					E2			
Mode	1	2	3	4	5	1	2	3	4
Torque, %	100	75	75	50	0	100	75	50	25
Speed, rpm	Rated speed		Intermediate speed		Idle	Rated speed			
Weighting factors	0.08	0.11	0.19	0.32	0.3	0.2	0.5	0.15	0.15
Type	E3				E4				
Mode	1	2	3	4	1	2	3	4	5
Power, %	100	75	50	25	100	80	60	40	0
Speed, rpm	100	91	80	63	100	71.6	46.5	25.3	Idle
Weighting factors	0.2	0.5	0.15	0.15	0.06	0.14	0.15	0.25	0.4
Type	E5								
Mode	1	2	3	4	5				
Torque, %	100	75	50	25	0				
Speed, rpm	100	91	80	63	Idle				
Weighting factors	0.08	0.13	0.17	0.32	0.3				

1.3.1.5 Locomotives

For railroad locomotives, the first emission regulation was adopted on 17 December 1997. Tier 0-2 standards are met through engine design methods, without the use of exhaust gas after-treatment. A regulation introduced more stringent emission requirements on 14 March 2008. Tier 3 standards become effective from 2011/12, and Tier 4 standards become effective from 2015. The emission standards are summarized in Table VI.

TABLE VI

EPA LOCOMOTIVE DIESEL PM EMISSION STANDARDS.

Operation type	Tier	Manufacture year	PM emissions, g/bhp·h
Line haul	0	1973 - 1992	0.22
	1	1993 - 2004	0.22
	2	2005 - 2010	0.1
	3	2012 - 2014	0.1
	4	2015 and later	0.03
Switch	0	1973 - 2001	0.26
	1	2002 - 2004	0.26
	2	2005 - 2010	0.13
	3	2012 - 2014	0.1
	4	2015 and later	0.03

Locomotive diesel emissions are measured over two steady-state test cycles which represent two different types of service, line-haul and switch locomotives. The duty cycles are used to idle, dynamic brake modes, and different power levels, and they include different weighting factors for each of the 8 throttle notch modes. The line-haul operation is characterized by a much higher percentage of time in the high power notches, whereas the switch operation involves much time in idle and low power notches.

1.3.2 European Emission Standards

1.3.2.1 Heavy Duty Diesel Truck and Bus Engines

Table VII summarizes the PM emission standards (Euro I-VI) for heavy-duty diesel engines and their implementation dates. Dates in the table refer to new type approvals. Since the

TABLE VII
EUROPEAN DIESEL PM EMISSION STANDARDS FOR HEAVY-DUTY DIESEL ENGINES.

Type	Date	Test	PM emissions, g/kWh
Euro I	kW < 85, 1992	ECE-R49	0.612
	kW ≥ 85, 1992		0.36
Euro II	1996.10		0.25
	1998.10		0.15
Euro III	1999.10 EEV only	ESC & ELR	0.02
	2000.10		0.1
Euro IV	2005.10		0.02
Euro V	2008.10		0.02
Euro VI	2013.01		0.01

Euro III standard, diesel engines have been tested in two testing cycles, European Stationary Cycle (ESC) and the European Transient Cycle (ETC). As indicated in this table, heavy-duty diesel engines with PM emissions under 0.01 g/kW·h will be certified for heavy-duty trucks driving in Europe. This value in Euro VI shows a lowering to PM emissions standard of the order of 50% than that of Euro V.

The ESC test is performing for emission certification of heavy-duty diesel engines in Europe. The engine is tested on an engine dynamometer over a sequence of steady-state modes, as seen in Table VIII. The engine must be operated for the prescribed time in each mode, completing engine speed and load changes in the first 20 seconds. The specified speed shall be held to within ± 50 rpm and the specified torque shall be held to within $\pm 2\%$ of the maximum torque at the test speed. Emissions are measured during each mode and averaged over the cycle using a set of weighting factors. Particulate matter emissions are sampled on one filter over the 13 modes.

1.3.2.2 Off-highway Diesel Engines

To regulate emissions from non-road mobile equipment in European countries, the regulations for non-road diesels were introduced in two stages. Stage I and Stage II were implemented in 1999 and from 2001 to 2004, respectively, depending on the engine power output. On 21 April 2004 Stage III and IV emission standards for non-road engines were adopted by the European Parliament. Stage III standards are phased-in from 2006 to 2013, Stage IV standards enter into force in 2014. The Stage III and IV standards added railroad locomotive engines and marine engines used for inland waterway vessels to the engine categories regulated.

Stage I-IV PM emission standards for non-road diesel engines are shown in Table IX., where the limit values for the Stage III and IV apply to all non-road diesel engines of indicated power range for use in applications other than propulsion of locomotives, railcars and inland waterway vessels. The implementation dates in the table refer to the first registration dates, after which all new engines placed on the market must meet the standard. As indicated well in Table IX, Stage III B and IV standards introduce PM limit of 0.025 g/kWh, representing about 90% emission reduction relative to the previous stage.

TABLE VIII
EUROPEAN STATIONARY CYCLE (ESC) TEST MODE.

Mode	Engine speed, rpm	Load, %	Weighting factor, %	Duration, min.
1	Idle	0	15	4
2	A	100	8	2
3	B	50	10	2
4	B	75	10	2
5	A	50	5	2
6	A	75	5	2
7	A	25	5	2
8	B	100	9	2
9	B	25	10	2
10	C	100	8	2
11	C	25	5	2
12	C	75	5	2
13	C	50	5	2

TABLE IX

STAGE I-IV PM EMISSION STANDARDS FOR NON-ROAD DIESEL ENGINES IN EUROPE.

Category	Power	Date	PM emissions
Stage I			
A	$130 \leq \text{kW} \leq 560$	1999. 01	0.54
B	$75 \leq \text{kW} < 130$	1999. 01	0.7
C	$37 \leq \text{kW} < 75$	1999. 04	0.85
Stage II			
D	$130 \leq \text{kW} \leq 560$	2002.01	0.2
E	$75 \leq \text{kW} < 130$	2003.01	0.3
F	$37 \leq \text{kW} < 75$	2004.01	0.4
G	$18 \leq \text{kW} < 37$	2001.01	0.8
Stage III-A			
H	$130 \leq \text{kW} \leq 560$	2006.01	0.2
I	$75 \leq \text{kW} < 130$	2007.01	0.3
J	$37 \leq \text{kW} < 75$	2008.01	0.4
K	$18 \leq \text{kW} < 37$	2007.01	0.6
Stage III-B			
L	$130 \leq \text{kW} \leq 560$	2011.01	0.025
M	$75 \leq \text{kW} < 130$	2012.01	0.025
N	$56 \leq \text{kW} < 75$	2012.01	0.025
P	$37 \leq \text{kW} < 56$	2013.01	0.025
Stage IV			
Q	$130 \leq \text{kW} \leq 560$	2014.01	0.025
R	$56 \leq \text{kW} < 130$	2014.10	0.025

To meet this limit value, engines have to be typically equipped with particulate filters. Emissions are measured on the ISO 8178 C1 8-mode cycle and the non-road transient cycle (NRTC). In particular, the NRTC is run twice with a cold and a hot start. The final emission results are weighted averages of 10% for the cold start and 90% for the hot start run.

The Stage III-A standards also cover engines used in inland waterway vessels. Engines are divided into categories based on the displacement per cylinder and net power output. There are no Stage III-B or Stage IV standards for waterway vessels. Stage III-A and III-B standards

have been adopted for engines above 130 kW used for the propulsion of railroad locomotives. The PM emission standards for diesel engines used in inland waterway vessels and railroad locomotives are summarized in Table X and XI.

1.4 Diesel PM Aftertreatment Systems

Diesel engines typically require after-treatment devices to control exhaust emissions. Increasingly strict emissions standards in U.S. and Europe are motivated to engine manufactures to develop advanced after-treatment systems that can significantly reduce tail-pipe exhaust emissions. As emission standards become more stringent, advanced diesel engine technologies and diesel particulate filters (DPFs) systems are required to be implemented in diesel vehicles. In particular, DPF systems have been developed to remove PM emissions. To oxidize the trapped diesel particulates, primarily carbon into gaseous emissions such as CO₂, the DPF regeneration systems include the use of catalysts (Chatterjee et al., 2001; Pfeifer et al., 2005; Soeger et al., 2005; Vincent et al., 2001), creating oxidant (Cooper and Thoss, 1989; Hoard, 2001; Levendis and Larsen, 1999; Yamamoto et al., 2003) and the addition of energy such as post fuel injection and combustion (Fayard, 2006; Joshi, 2006; Michelin, 2000), electric heating (Kobashi, 1993; Shirk, 1995), and microwave heating (Zhi, 1995). All of these systems have limitations and strongly depend on the duty cycle of the engine or vehicle. Typically, engines operating at low speeds and loads have difficulty oxidizing the diesel PM emissions trapped on the filter. Furthermore, significant improvements are needed in their performance, which include reducing back pressure due to soot and ash build-up, improving material durability and filtration efficiency, and developing smart DPF control management systems with optimum regeneration strategies.

TABLE X

EUROPEAN PM EMISSION STANDARDS FOR DIESEL ENGINES USED IN INLAND WATERWAY VESSELS (STAGE III-A).

Categories	Displacement per cylinder, m ³	Date	PM emission, g/kWh
V1:1	$D \leq 0.9, P > 37 \text{ kW}$	2007.01	0.4
V1:2	$0.9 \leq D < 1.2$		0.3
V1:3	$1.2 \leq D < 2.5$		0.2
V1:4	$2.5 \leq D < 5$	2009.01	0.2
V2:1	$5 \leq D < 15,$ $P \leq 3300 \text{ kW}$		0.27
V2:2	$15 \leq D < 20$ $P > 3300 \text{ kW}$		0.5
V2:3	$15 \leq D < 20$		0.5
V2:4	$20 \leq D < 25$		0.5
V2:5	$25 \leq D < 30$	0.5	

TABLE XI

EUROPEAN PM EMISSION STANDARDS FOR RAILROAD LOCOMOTIVE DIESEL ENGINES.

Category	Power	Date	PM emissions
Stage III-A (Railroad locomotives)			
RC A	$130 > P$	2006.01	0.54
RL A	$130 \leq P < 560$	2007.01	0.7
RH A	$3P > 560$	2009.01	0.85
Stage III-B (Railcars)			
RC B	$130 > P$	2012.01	0.025
R B	$130 \leq P$	2012.01	0.025

1.4.1 Diesel Particulate Filters

There are two main types of DPFs available commercially, blocking and non-blocking filters. Most commonly used are blocking filters such as wall flow filters, as seen in Figure 5. The wall flow filters are highly effective and can achieve 99% filtration of diesel PM emissions (Locker et al., 2004). They are made of various materials such as cordierite, silicon carbide, and metal fleece. The blocking filters have parallel channels with alternating ends plugged, allowing the exhaust emissions to flow through the porous wall, while the diesel particulates are trapped. If diesel PM emissions are continuously trapped on the filter without oxidation, backpressure will be built up in the exhaust pipe, which can cause power loss or failure of the DPF system. To maintain the engine operation and the DPF system, it is necessary to regenerate the filter by oxidizing the diesel particulates. Non-blocking filters consisted of open channels, in general, use conversion flow channels and hydrodynamic pressure differentials across the filter media.

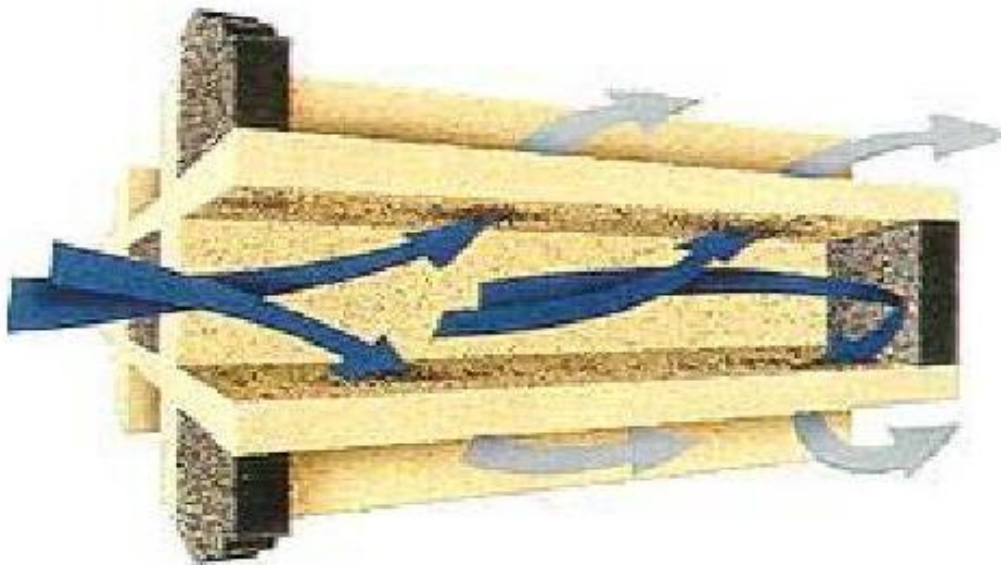


Figure 5. Example of exhaust gas flow through wall flow filter.

The open structure protects the engine by preventing backpressure increases by bypassing the exhaust flow around the filter media if it becomes full, as represented in Figure 6. The filtration efficiency is, however, lower and can be in the range of 0 and 60%.

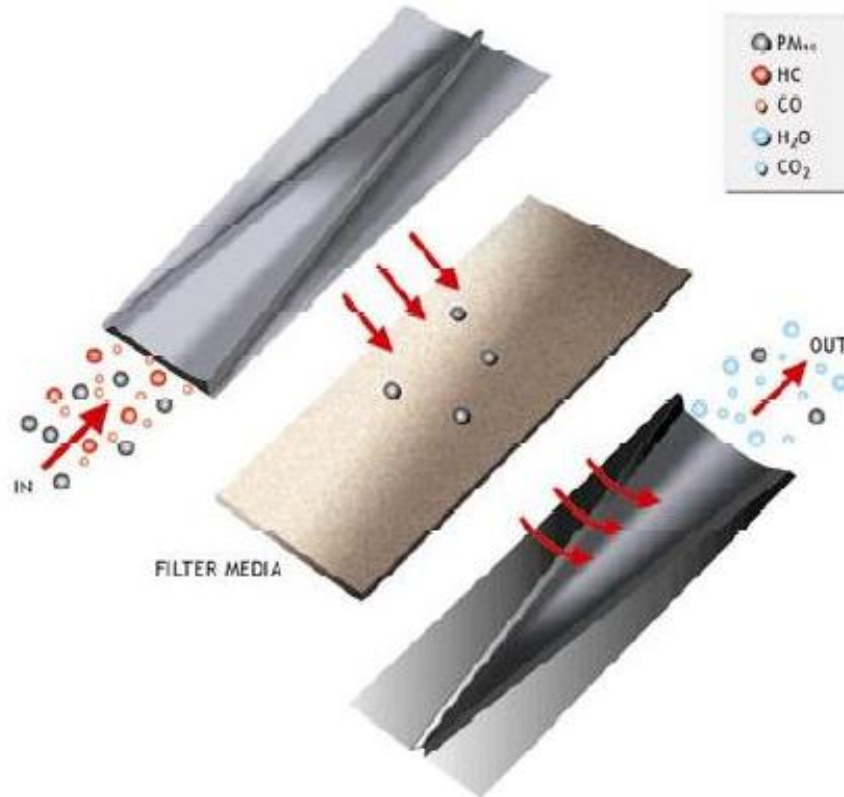


Figure 6. Example of exhaust gas flow through non-blocking filter (Farafontov et al., 2007).

1.4.2 DPF Regeneration Systems

Most of diesel PM on the filter can react with oxygen to form carbon dioxide. However, the reaction of PM with exhaust gas in the filter take place over 550°C, which is usually higher than the temperature of exhaust gas during normal operation of diesel engines. There are two practical strategies for regenerating DPFs, depending on the application; passive and active regeneration.

The passive DPF regeneration uses a combination of exhaust gas temperature and a catalyst to initiate the regeneration process. Active regeneration uses an outside source to supply the heat for regeneration. The former is to lower the temperature at which the PM starts to oxidize. This can be achieved either by the use of a catalyst or by letting diesel particulates react with NO_2 . Active regeneration is usually attained either by post fuel injection, fuel-rich operation, electric heating, or microwave heating.

Diesel particulate emissions can be collected using either by a catalyzed or non-catalyzed coating DPF. In general, PM begins to burn in diesel exhaust around 550°C without a catalyst. To lower the temperature at which the PM reacts, DPF membrane (i.e. washcoated filter) are coated with catalyst materials. The substrate of DPFs is coated with highly porous inorganic oxides such as $\gamma\text{-Al}_2\text{O}_3$, SiO_2 or ZrO_2 , that can retain the noble metal such Pt, Pd, Rh. These DPFs give balance point temperatures of $380\text{-}420^\circ\text{C}$. For instance, Pt based DPFs are in the 350 to 400°C . Balance point temperature is a critical temperature, at which the production rate of particulate emissions is equal to the removal or oxidation rate. However, the contact between catalyst and soot particles is too poor to enforce catalytic reaction. To improve the catalyst-soot contact, catalytic additives, such as cerium and iron, have been used in fuels. The organic part of the fuel is oxidized in the engine combustion chamber and the metallic part of fuel additives is incorporated with soot particles. However, the additives cause extra ash build up in the DPF, thereby increase back pressure. Therefore, it is necessary to remove ash periodically or replace it.

The NO_x -aided continuously regenerating trap (CRT) was commercialized by Johnson Matthey for trucks and buses (Cooper et al., 1989; Allanson et al., 2002), as illustrated in Figure 7. It uses Pt/ Al_2O_3 as an oxidation catalyst placed in the first chamber, upstream of the DPF converts the CO and hydrocarbons to CO_2 and H_2O . This has been reported to remove diesel

particulates at a balance point temperature of 320°C, but is strongly dependent on the NO content in the exhaust stream, the NO and NO₂ thermal equilibrium, exhaust temperature and sulfur content in the fuel. By adding catalysts to the filter, it is possible to convert the NO to NO₂, thereby improve the overall efficiency of soot removal. This, so-called, catalyzed continuously regenerating trap (CCRT) is being used on selected heavy-duty diesel applications where the duty cycle does not always provide sufficient by high temperature for proper functioning of the CRT (Allansson et al., 2004). While this system functions well in Europe where ultra low sulfur diesel fuel is widespread, the system may fail in countries with high sulfur fuels.

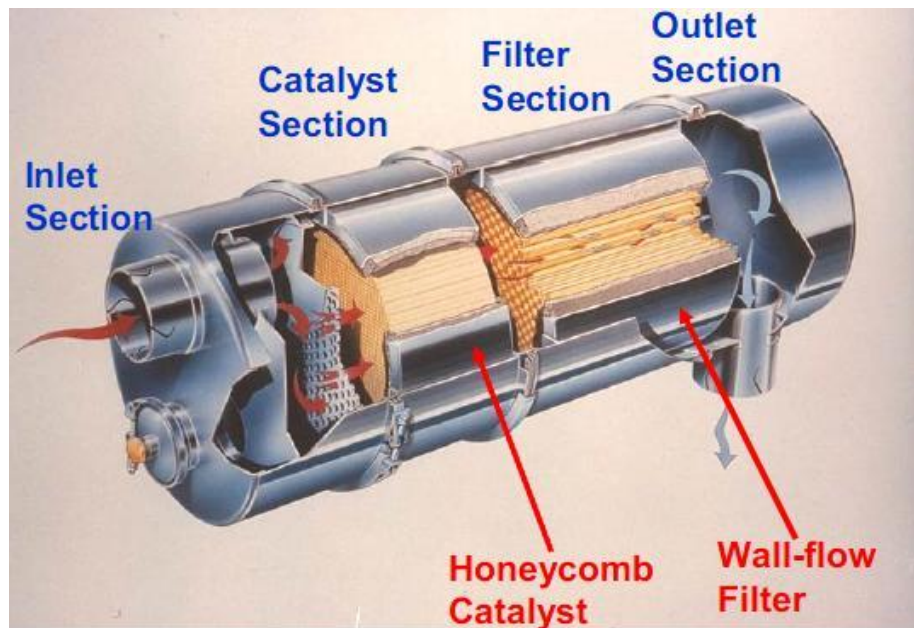


Figure 7. Example of continuously regenerating particulate filter systems.

The PM removal can be effectively accomplished in DPFs by the use of various catalysts and NO₂. However, additional heating of the exhaust gas is also necessary to reach appropriate gas temperature ranges. The preferred methods are post fuel injection, electric heating, and

microwave heating. Ultimately, a DPF system needs minimal maintenance, requires no additional power input, uses molecular oxygen, or NO₂ gases, and so on. Although extensive research has been performed with various strategies, significant efforts are still needed to develop optimum DPF regeneration strategies and achieve the efficient removal of diesel PM.

1.5 Soot Oxidation Kinetics and Modeling

In general, oxidation models for the quantitative prediction of carbon particles can be classified into two main categories, global and intrinsic models. Global models consider impermeable carbon particles to pore diffusion effects into the oxidation rate constants. These oxidation models are often in the form of semi-empirical correlations, based on the kinetic rate expression of the external surface area and of the oxidizer concentration at the external surface. In contrast, intrinsic models consider the active surface area involved in the oxidation, and the concentration profile of oxygen within the particle is assumed to be non-uniform. Therefore, pore structure models have been developed to describe gaseous diffusion through complex pore structures and to model the local oxygen concentration at the active surface area in the particle.

1.5.1 Global n-th Order Rate Equation

An empirical n-th order rate equation is often used to describe kinetics of various solid carbons such as flame soot (Fábio et al., 2008; Higgins et al., 2006; Nejar et al., 2007), char (Hurt and Mitchell, 1992; Monson et al., 1995), and diesel soot (Gilot et al., 1993; Marcucilli et al., 1994; Messerer et al., 2006; Otto et al., 1980; Setiabudi et al., 2004). The most common form of the n-th order rate equation is

$$r = k_s [P_{O_2}]^{n_{O_2}} = A \cdot \exp\left(-\frac{E_a}{R_u \cdot T}\right) \cdot [P_{O_2}]^{n_{O_2}} \quad (1.1)$$

where r is the global oxidation rate, A the pre-exponential factor, E_a the activation energy, R_u the universal gas constant (8.31447 kJ/mol·K), T the temperature (K), P_{O_2} the partial pressure of oxygen, and n_{O_2} the reaction orders with respect to oxygen.

Due to the simple equation form, this equation is often used in comprehensive computer models for diesel soot oxidation. However, the global n -th order rate equation does not explicitly account for pore diffusion effects on the oxidation of solid carbon. In addition, the various values for reaction order with respect to oxygen have been reported to be 0.5 (Petersen, 1987), 0.76-0.94 (Neeft et al., 1997), 0.8 (Du et al., 1991; Ciambelli et al., 1994), and unity (Gilot et al., 1993; Marcucilli et al., 1994; Messerer et al., 2006; Otto et al., 1980; Setiabudi et al., 2004), depending on experimental conditions. Presently no theory can satisfactorily explain or predict how the reaction order would change with experimental conditions. In addition, variations of activation energies indicate the inadequacy of the n -th order rate equation in correlating these data. The observed activation energy were 85 (Bradley et al., 2000), 111 (Pauli et al., 1983), 126-146 (Yezerets et al., 2003), 142 (Otto et al., 1980), and 150 kJ/gmol (Koltakis et al., 1997).

Darcy et al. (2007) reported kinetics of soot oxidation in a diesel engine by following equation:

$$r = -\frac{dm}{dt} = k_s [x_{O_2}]^\alpha \cdot m_o \cdot \left[\frac{m}{m_o}\right]^\beta = A \cdot \exp\left(-\frac{E_a}{R_u \cdot T}\right) \cdot [x_{O_2}]^\alpha \cdot m_o \cdot \left[\frac{m}{m_o}\right]^\beta \quad (1.2)$$

where x_{O_2} is the partial pressure of oxygen in the gas phase; m_o and m are respectively the initial and instantaneous soot mass in the reactor. The kinetics parameters such as A , E_a , α , and β were 8.5×10^7 1/s, 164 kJ/mol, 0.9, and 0.5, respectively, which were determined from isothermal

oxidation experiment. In addition, the oxidation of diesel PM was characterized by two distinct zones, fast and slow oxidation zone.

1.5.2 Heterogeneous Solid–Gas Thermo-Oxidation Kinetics

Kinetic analysis of solid state reactions is normally performed to obtain a mathematical representation of reaction data. The search for a mathematical description of experimental data is mainly sought in terms of kinetic parameters such as pre-exponential factor, activation energy, and the reaction model. A number of investigation on heterogeneous solid and gas thermo-oxidation have been carried out to evaluate these kinetic triplets by means of thermoanalytical methods such as thermogravimetry, differential thermal analysis, and differential scanning calorimetry (Gamlin et al., 2003; Lee et al., 2003; Sorai, 2004).

In an effort of linking heterogeneous solid-gas thermo-oxidation kinetics and soot oxidation, solid state reaction kinetic has been investigated for determining the kinetic parameters from the experimental data of soot oxidation (Jiang et al., 2000; Dernaika et al., 2003).

Kinetic studies are frequently performed under isothermal or non-isothermal conditions. Equation (1.3) is used to describe the kinetics of these reactions under linear heating, where $f(\alpha)$ is the reaction model. The reaction models commonly used to represent solid-state reaction kinetics are listed in Table XII.

$$\frac{d\alpha}{dT} = \frac{k_s}{\beta} f(\alpha) = \frac{A}{\beta} \cdot \exp\left(-\frac{E_a}{R_u \cdot T}\right) \cdot f(\alpha) \quad (1.3)$$

where α the extent of conversion, k_s the Arrhenius rate constant, T the absolute temperature, β the constant heating rate, A the pre-exponential factor, and E_a is the activation energy.

Table XII

REACTION MODELS FOR SOLID-STATE REACTION KINETICS.

Reaction model	f(a)
Avrami–Erofeev equation (1D)	$2(1-\alpha)(-\ln(1-\alpha))^{1/2}$
Avrami–Erofeev equation (2D)	$3(1-\alpha)(-\ln(1-\alpha))^{1/3}$
Avrami–Erofeev equation (3D)	$4(1-\alpha)(-\ln(1-\alpha))^{1/4}$
Phase boundary controlled reaction (contracting linear)	1
contracting area	$3(1-\alpha)^{2/3}$
contracting volume	$2(1-\alpha)^{1/3}$
1-D diffusion	$(1/2)\alpha^{-1}$
2-D diffusion	$[-\ln(1-\alpha)]^{-1}$
3-D diffusion	$2(1-\alpha)^{2/3}(1-(1-\alpha)^{1/3})^{-1}$
Ginstling–Brounshtein equation	$(2/3)(1-\alpha)^{1/3}[1-(1-\alpha)^{1/3}]^{-1}$
First order chemical reaction Random nucleation	$1-\alpha$
Generalized n-th order	$(1-\alpha)^n$
Power law I	$4\alpha^{3/4}$
Power law II	$3\alpha^{2/3}$
Power law III	$2\alpha^{1/2}$
Power law IV	$2/3\alpha^{-1/2}$
Zhuravlev equation	$(2/3)(1-\alpha)^{5/3}[1-(1-\alpha)^{1/3}]^{-1}$

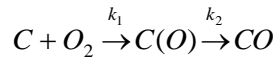
1.5.3 Langmuir-Hinshelwood Kinetics

The global n-th order rate equation and heterogeneous solid-gas thermo-oxidation kinetics has been criticized for lack of theoretical basis and inadequacy for predicting rates over wide ranges of experimental conditions. To account for carbon-oxygen reaction in detail, several reaction processes have been mainly considered, such as chemisorption, oxygen surface diffusion, and desorption of surface oxygen complexes (Essenhigh, 1991; Du et al., 1991).

In the studies, they have suggested two main processes in carbon-oxygen reaction; adsorption of oxygen molecules to the outer surface of carbon particles and desorption of carbon-oxygen compound. Based on this idea, a more meaningful equation of carbon-oxygen reaction has been developed, which is called Langmuir-Hinshelwood form (Laurendeau, 1978). The commonly applied form of this is the two-step Langmuir-Hinshelwood equation.

$$r = \frac{k_1 k_2 P_{O_2}}{k_2 + k_1 P_{O_2}} \quad (1.4)$$

where k_1 and k_2 are two rate constants, which is from the reaction as



Eq. (1.4) can be re-written as

$$\frac{1}{r} = \frac{1}{k_1 P_{O_2}} + \frac{1}{k_2} \quad (1.5)$$

This rate equation is the simplest form of Langmuir-Hinshelwood kinetic expressions capable of modeling reaction order shifting between zero and unity.

1.5.4 Reaction-Diffusion Model

A number of comprehensive and detailed investigations on the oxidation characteristics of PM have been carried out, such as oxidation rate and kinetics parameters, as explained above. However, few studies have been reported on the effects of oxygen diffusion on the oxidation behavior of diesel PM, although it has been well known that the oxidation of soot particles is dependent on oxygen mass transfer effects. This study deals with the soot oxidation occurring in presence of external and inter-particle diffusion of oxygen within the soot. In general, the effectiveness factor is used to account for the inter-particle diffusion effects of oxygen molecules on kinetics in solid fuel particles. The effectiveness factor is defined as the ratio of the observed oxidation rate to the oxidation rate evaluated in the case of homogeneous concentration of reactant throughout the interior of the particle.

In Saterfield's work (Saterfield, 1970), a spherical model and an infinite or semi-infinite flat plate model have been developed to describe simultaneous diffusion and reaction in porous materials. In this research, an effectiveness factor was used to represent the influence of mass transfer, and a formula of the Thiele modulus was also given. For a porous flat plate packed with soot particles, Stanmore et al. investigated the effects of oxygen transfer on the oxidation of carbon particles (Stanmore et al., 1994). Gilot et al. carried out the oxidation experiment for carbon black in the temperature range of 600-900 °C to account for oxygen diffusion in the layer and inside the porous sample particles (Gilot et al., 1993).

The oxidation rate of carbon particles is controlled by the single, sequential, or parallel processes of boundary layer diffusion, chemical reaction and pore diffusion. Walker et al. (1959) and Gray et al. (1976) have postulated the existence of the three different temperature zones or regimes in which one or more different processes control the overall oxidation rate of char. In

Zone I, which occurs when chemical reaction is slow compared to diffusion at low temperature or for small particles, chemical reaction is the rate-determining step. In Zone II, reaction rate is controlled by both chemical reaction and diffusion of reactants through pores. In Zone III, which occurs at high temperatures, surface reaction is so fast that the surface oxygen partial pressure approaches zero, and the overall reaction rate approaches the maximum value allowed by boundary layer diffusion. In this case the overall reaction rate is solely controlled by boundary layer diffusion. The effect of external diffusion or internal diffusion of reactants on the oxidation of various carbon particles has been still significantly investigated.

1.6 Thesis Objectives and Outline

As discussed in preceding section, major efforts are needed to achieve high filtration efficiency and develop optimum regeneration strategies for DPF systems. In particular, an effective thermal management system is necessary to prevent the failure of a DPF system caused by the thermal runaway, which can occur during the oxidation of excess soot accumulated in DPF. Figure 8 shows a DPF in which melting occurred during the regeneration (Barry et al., 2001). Therefore, the distribution of thermal energy released in regeneration needs to be monitored with care. To this end, significant research efforts are currently being undertaken to characterize the oxidation behavior of diesel PM relevant DPF regeneration (Collura et al., 2005; Kalogirou et al., 2007; Messerer et al., 2006; Setiabudi et al., 2004; Stratakis and Stamatelos, 2003; Yezerets et al., 2005). Typically these efforts have undoubtedly been invaluable to the significant improvement in DPF system. However, very few studies have focused on heat release and oxidation rates during the oxidation of diesel PM under realistic engine conditions. Such

information is important not only for devising a highly efficient thermal management system for DPF regeneration, but also for developing an accurate predictive tool.

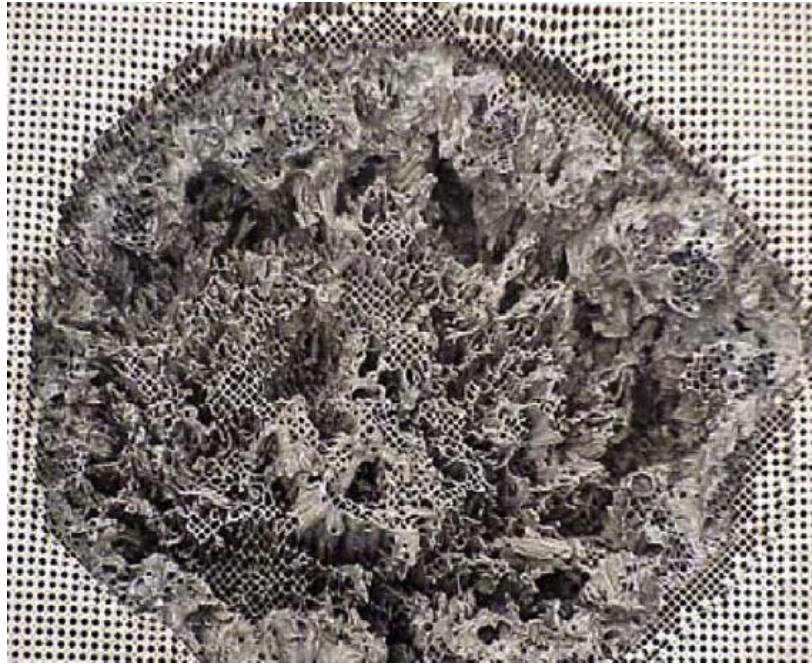


Figure 8. Example of a DPF melted during DPF regeneration.

Since DPF systems offer limited physical access in measuring these rates during regeneration, researchers have used bench-scale experiments to determine the oxidation kinetics parameters, such as reaction order, activation energy, and pre-exponential factor. In addition, researchers have often used surrogate soot, such as commercially available graphite, for oxidation experiments (Jung et al., 2008; Nejar et al., 2007), or soot samples collected from lab-scale burners (Higgins et al., 2006), due to the complexities in the composition and structure of diesel PM. However, the differences in composition and morphology between diesel PM and surrogate soot samples can provide inaccurate results in predicting oxidation rates and thermal

energy distribution during DPF regeneration. Moreover, previous work dealing with diesel PM has generally considered a limited period of oxidation, during which the data exhibited locally linear behavior.

Although SOF-containing PM emissions have been reported to be adverse effect to human health, one possible advantage in utilizing these particulates is the potentially low energy input required for DPF regeneration, because the SOF could enhance the ignition and oxidation of particulates. Practically, the regeneration in DPF systems initially occurs at a localized area where an optimal condition exists for the ignition of soot accumulated. Once ignition occurs, the bed temperature rises rapidly, and the subsequent transfer of thermal energy from the reacting area rapidly evaporates the volatile components of SOF in the unreacted DPF volume. During the evaporation, the diesel PM in the unreacted DPF volume is exposed to exhaust gas emissions containing oxygen, in which the evaporation/oxidation of volatile components of SOF and the oxidation of carbon occur simultaneously over the specific temperature. However, there has been little attention given to the effects of SOF concentration on the thermal energy released during the oxidation of diesel PM, nor has there been any evaluation of the total amount of heat release per unit mass of diesel PM with different SOF concentrations. Furthermore, few studies have characterized the effects of SOF concentration on the oxidation of diesel PM, nor has there been any evaluation of chemical-kinetics parameters of PM subjected to different temperature profiles or thermal treatments.

The objective of this study is to characterize heat release and oxidation behavior during the oxidation of diesel PM collected directly from a DPF under realistic engine conditions. For diesel PM with different levels of SOF concentration and commercially available surrogate soot,

the analysis on the heat release, oxidation rates, and the effects on the oxidation behavior of diesel PM is extensively investigated within the following framework.

Chapter 2 deals with an experimental methodology used in this study, such as the engine specifications, the collection of diesel PM filtered in the DPF membrane, and the operation principle of a thermogravimetric analyzer (TGA) and a differential scanning calorimeter (DSC). In addition, we will describe the calibration procedures for the instrumentations in detail.

Chapter 3 provides the detailed experimental information on the total heat release and the temporal variation of heat release rate from the diesel PM oxidation under realistic conditions. The attention is focused on the elucidation of differences in the heat release characteristics of surrogate soot and diesel soot. Measurements employ the DSC and the TGA. We will mainly report the temporal variation of heat release rate during the oxidation of diesel PM, dry diesel soot, and surrogate soot, using the DSC. For the TGA experiment, the amount of SOF in diesel PM will be also reported.

Chapter 4 deals with the kinetics of diesel PM oxidation, which describes the general dependence of oxidation rates on temperature and reactant concentrations, in understanding the oxidation behavior of diesel particulate emissions. In this chapter, the oxidation kinetics parameters will be determined for diesel PM and surrogate soot, such as reaction order, activation energy, and pre-exponential factor. The differences in the oxidation behavior of diesel PM and surrogate soot will be characterized by performing experiments under the identical conditions. Furthermore, we will investigate the effects of volatile component of SOF and thermal aging in both the inert and oxidizing environments on the oxidation of diesel PM and surrogate soot.

In Chapter 5 the heat release rates during the soot oxidation will be modeled, based on the total specific heat release and the kinetic parameters provided in Chapter 3 and 4. The predictions of heat release rate with the model are compared with experimental data for diesel PM and surrogate soot subjected to the specific heating profile in an air environment.

Since the PM samples analyzed in this work were approximately the same as the soot cake built in commercial DPFs in terms of their properties, our investigation is expected to provide more accurate results in subsequently predicting the thermal energy distributions and the oxidation behaviors of diesel PM during DPF regeneration.

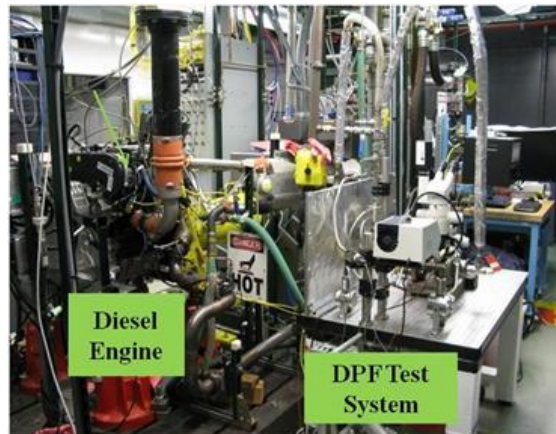
CHAPTER 2

EXPERIMENT METHODOLOGY

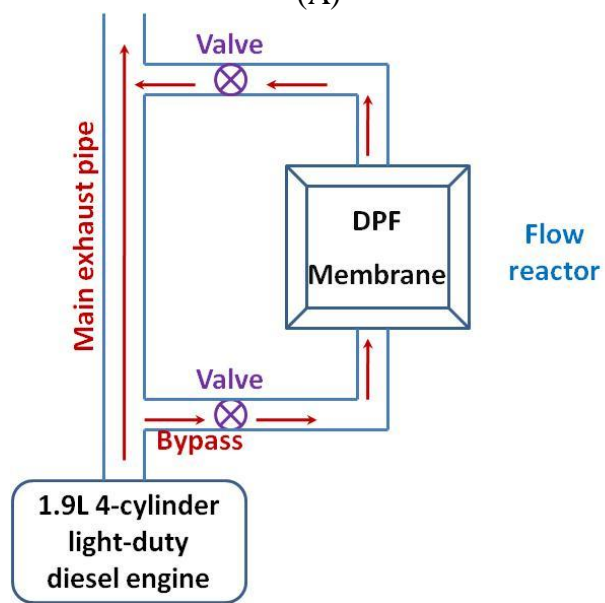
2.1 Diesel PM Sampling

Diesel PM samples used in this study were collected from a non-catalytic cordierite DPF membrane placed in a flow reactor of a laboratory scale DPF test system, where no regeneration was conducted. As illustrated in Figure 9, the DPF system was connected to the exhaust pipe of a 1.9 L four-cylinder light duty diesel engine. This engine is equipped with a variable geometry turbocharger (VGT) to boost the intake air to the desired pressure and has a self-contained exhaust gas recirculation (EGR) system. The engine is capable of producing 150 hp with a maximum speed of 5000 rpm. It has multiple-injection capability, and both the EGR rate and VGT setting are electronically controlled. The common-rail injection system can be operated at a maximum injection pressure of 1600 bar.

The engine was operated at various randomly selected engine speeds and loads in order to simulate conditions that practical DPF systems undergo in vehicle operation. The selected engine speeds were 1000 rpm, 2000 rpm, and 3000 rpm, and at each speed the engine was operated at 25%, 50%, and 75% load for several hours. During the transition period, the diesel PM emissions were continuously filtered in the DPF membrane. At each engine operating condition, the engine was stabilized (by maintaining coolant and lubricating oil temperatures constant) while the target speed/load condition was maintained constant for several minutes. Engine exhaust emissions were bypassed from the main exhaust pipe, of which soot particles were filtered in the DPF filter membrane, while gaseous emissions were ventilated back to the engine exhaust stream. In order to collect enough PM emissions, the engine was operated for several hours, and then soot



(A)



(B)

Figure 9. (A): DPF test system connect to the exhaust pipe of 1.9L four-cylinder light-duty diesel engine, (B): its schematic representation.

were taken from the filter. Figure 10 shows a cordierite DPF membrane loaded with PM emissions in the DPF test bench. The PM samples were carefully collected from the filter membrane and transferred to an environmentally controlled glove box in a clean laboratory. The DPF inlet temperatures were measured in a range of about 80–200°C. Soot oxidation reactions

are not expected to occur at these temperatures, which are fairly low compared to those in the main exhaust pipe, because the exhaust is cooled down through the fairly long sampling line. The uncoated filter membrane was not preconditioned for the soot loading.

An ultra-low sulfur diesel (ULSD) fuel and conventional SAE15 W-40 lubricating oil were used for this work. The diesel fuel had an ash content of about 0.002 wt.%, sulfur content of about 15 ppm, carbon content of about 86.9 wt.%, hydrogen content of about 13.1 wt.%, and a cetane number of 46. The lubricating oil has an ash content of 1.3 wt.%, Zn of 2.5 wt.%, and sulfur content less than 0.005 wt.%.

2.2 Instrumentation and Calibration

As represented in Figure 11, a differential scanning calorimeter (DSC, temperature range between ambient and 550°C; heating rates 0.1-100 °C/min; crucible size 50µL) is used to measure the rate of heat release during the oxidation of diesel PM, dry soot, and surrogate soot under specific temperature profiles. A thermogravimetric analyzer (TGA, temperature range between ambient and 1050°C; heating rates 0.1-100°C/min; crucible size 100µL) measures the temporal variations of sample mass under specific temperature profiles, either by oxidation with air or evaporation in inert gas environment.

In principle, the DSC measures the amount of heat either supplied to a sample or abstracted from it. The generation or consumption of heat in the present case occurs mainly due to chemical reactions, and affects a temperature change in a DSC component that measures the amount of heat exchanged. A control system equipped with the DSC adjusts the temperature difference between these two components, caused by chemical reactions, to zero. Thus, the DSC measures

the total power needed for adjusting the temperature difference to zero, and the data are recorded in terms of heat flow rate (mW).

In DSC calibration, the melting temperature and standard enthalpy of fusion of a reference sample were used as calibration parameters for temperature and heat flow measurements. High purity indium and tin were prepared as the references, and then calibration samples of each substance were weighed and loaded into the aluminum pans. The indium sample was first heated up to 300 °C at a temperature gradient of 10 °C/min in nitrogen to measure the melting temperature and the standard enthalpy of fusion. The values measured for those two parameters were corrected with respect to the melting temperature, 156.6 °C, and enthalpy of fusion, 28.45 J/g of standard indium, respectively. In addition, the same calibration was carried out to assure the accuracy in temperature measurement. The melting temperature measured for tin was corrected with respect to the melting temperature, 231.95 °C, of standard tin and then temperature calibration was completed by two-point temperature calibration.

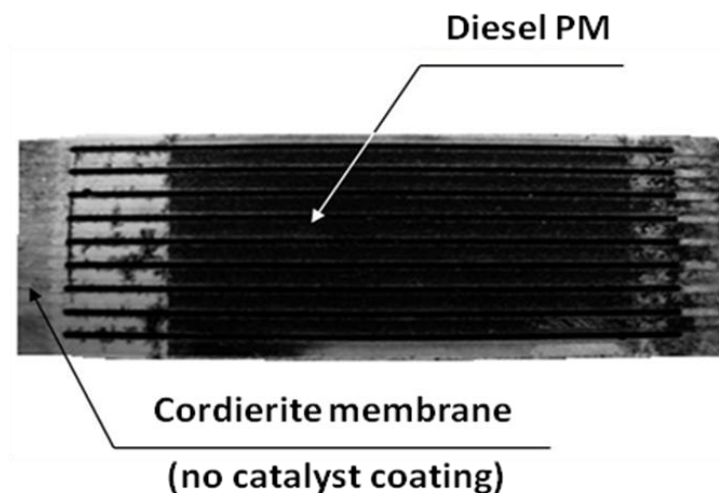


Figure 10. Diesel PM in the cordierite DPF membrane taken out from the thermal reactor in the DPF test system.

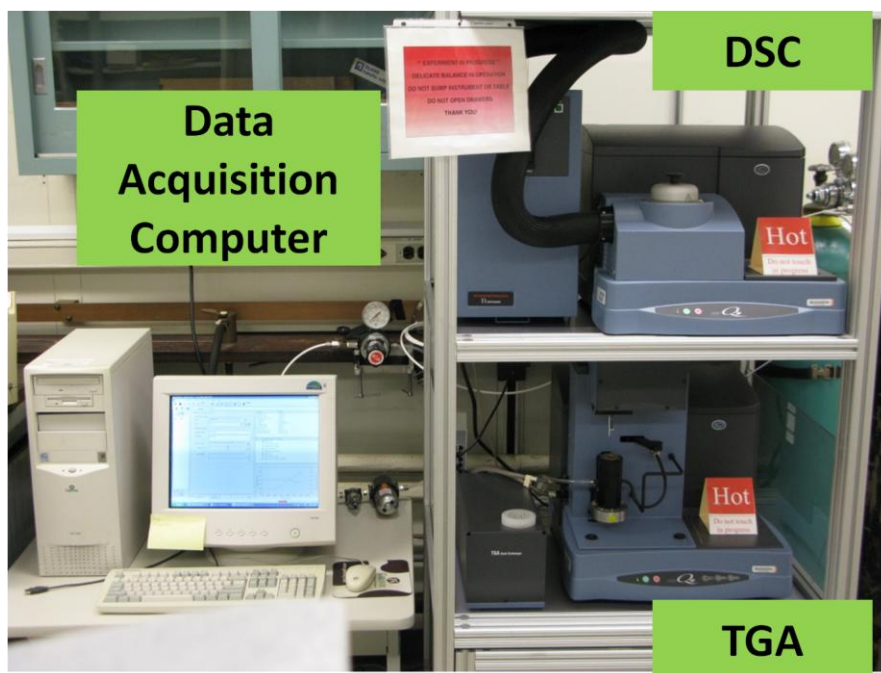


Figure 11. DSC, TGA, and data acquisition system for oxidation experiment.

A TGA measures the temporal variation of a given sample mass under a specified temperature profile. The change in sample mass may occur due to either oxidation with reactants, or evaporation in an inert gas environment. In TGA calibration, two standard weights were used to calibrate the microbalance, while the temperature calibration was performed with alumel and nickel in the heating mode. Calibration samples were accurately weighed and loaded into the TGA pan, and then exposed to an elevated temperature profile of 10 °C/min in a nitrogen atmosphere to measure Curie point temperatures of the calibration samples. The measured temperatures were corrected to 157.0 °C and 368.8 °C, respectively.

CHAPTER 3

MEASUREMENT OF THE HEAT RELEASE RATE

3.1 Introduction

In chapter 3, this investigation is aimed at measuring the instantaneous rate of heat release during the oxidation of diesel PM collected directly from a DPF, as well as the total amount of heat release per unit soot mass. The study is motivated from the consideration of developing optimum thermal management strategies for DPF regeneration. We performed the same analysis by using diesel PM and commercially available synthetic or surrogate soot to examine differences in heat release characteristics. As described earlier, the PM samples used in this work were collected directly from a filter membrane in a DPF system, which was connected to a diesel exhaust pipe. Thus, the PM samples analyzed in this work were approximately the same as the soot cake built in commercial DPFs in terms of their properties, and thereby our experiments are expected to provide more accurate results in subsequently predicting the temporal distributions of thermal energy during DPF regeneration. Experiments using the diesel PM and commercially available synthetic soot were performed using a differential scanning calorimeter (DSC) and a thermogravimetric analyzer (TGA), respectively. First, the heat release data were obtained and analyzed for the oxidation of surrogate soot. The experiments were then performed to evaluate heat release rates during the oxidation of diesel PM with different levels of SOF concentrations. In addition, the heat release rates were measured with SOF-containing diesel PM and dry diesel soot (with no volatile components) under identical conditions. Finally, the experimental results were analyzed to examine differences between the heat release characteristics during the oxidation of diesel PM, dry diesel soot and surrogate soot.

3.2 Oxidation Experimental Scheme

A sample was placed in the reaction chamber of DSC, and subjected to a specific temperature profile in flowing air to measure the total amount of heat and the temporal variation of heat flow rate during the sample oxidation. Because the chemical composition of surrogate soot is less complex than that of diesel PM emission, the analysis for the surrogate soot was carried out in order to optimize the temperature profile used for the sample oxidation and to clarify differences in the temporal variation of heat release rates during the oxidation of real diesel PM and surrogate soot. A DSC was used to measure the instantaneous heat release during soot oxidation under specified temperature profiles in air, while a TGA was used to measure the amount of volatile components of SOF in PM samples and also to provide the dry diesel soot samples.

In DSC experiment, samples were accurately weighed and loaded into the aluminum sample pans. A baseline of experimental data needs to be determined to attain high accuracy in measuring heat release during the sample oxidation. An experiment for determining the baseline was conducted in nitrogen under a specified temperature profile with an empty reference pan and a pan loaded with a sample. For measuring instantaneous heat release rate, the sample was heated to 550 °C and then maintained at this temperature (i.e., isothermal condition) until the oxidation was completed. Prior to the temperature increase, the DSC was stabilized at 45 °C for 10 min to eliminate small data fluctuations detected. For both determination of the baseline and measurement of heat release, the sample and reference pans were open to nitrogen gas, of which the flow rate was set at 60 ml/min.

Dry soot samples were prepared by using a TGA (Chong et al., 2010). The surrogate soot or diesel PM sample taken in a pan of the TGA was heated in a nitrogen atmosphere from 45 °C

up to 550 °C with a temperature gradient 10 °C/min, and then maintained at this temperature for 1 h. During the isothermal condition, the volatile components contained in the soot sample were completely removed in nitrogen. From this thermal treatment by TGA, dry soot samples can be obtained. The mass of sample residues was then accurately measured by a microbalance.

3.3 Result and Discussion

As noted earlier, the DSC experiments were conducted to measure heat release from the commercially available model soot first. Figure 12 presents the temporal variation of heat release rate during the oxidation of a surrogate soot sample in air subjected to a given temperature profile, and the baseline determined for the data. As described earlier, the temperature profile consists of a progressive temperature mode with temperature increasing from 45 °C to 550 °C at a constant rate of 10 °C/min, followed by an isothermal mode. Note that the maximum temperature for the DSC experiments is 550 °C in the isothermal mode. The surrogate soot sample was weighed (3.719 mg) and loaded into an aluminum sample pan of the DSC. For establishing the baseline, a high purity nitrogen gas was used to provide an inert environment to suppress chemical reactions under this temperature profile. The heat flow rate profile for this case clearly indicates the endothermic process associated with the heating of the sample during the temperature heat-up period.

After the baseline was determined, the surrogate soot sample was reacted in an oxidizing environment with an airflow rate of 60 ml/min under the same temperature profile as described above. As shown in the figure, the reaction was stabilized in the initial heating period from 45 °C to about 200 °C for about 20 min, and then increased rapidly with time until the ambient temperature reached the isothermal condition. Subsequently the heat flow rate decreased

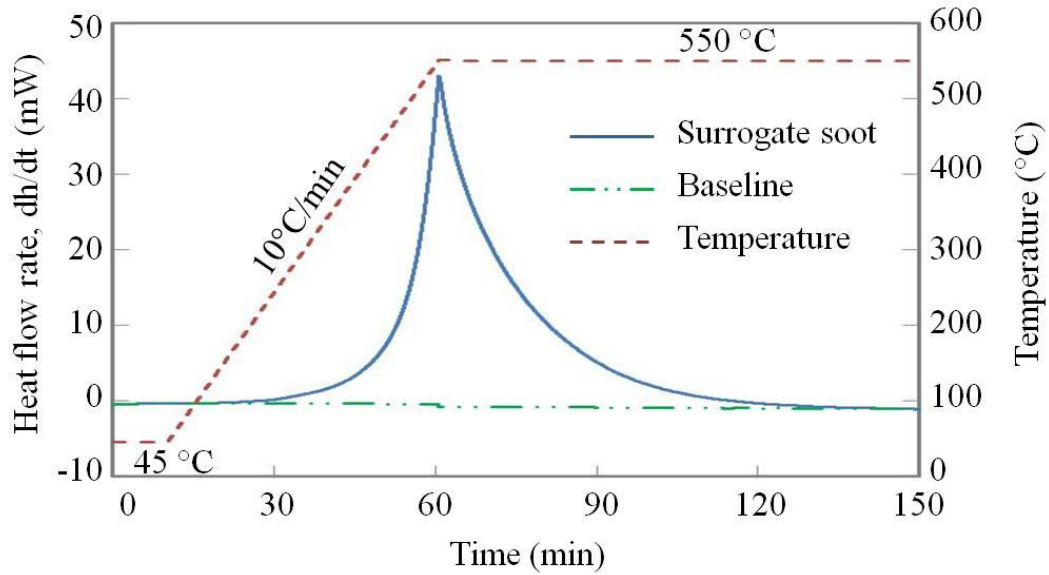


Figure 12. Temporal variation of heat release rate during the oxidation of surrogate soot sample in air under a specified temperature profile for the baseline case.

exponentially with further oxidation of sample soot during the isothermal condition maintained at 550 °C until it eventually became zero, indicating the termination of oxidation reaction.

For a given soot sample, the total amount of heat release per unit sample mass can be evaluated by integrating the heat release rate data with respect to time as:

$$q = \left[\int_{t_1}^{t_2} \frac{dH}{dt} dt \right] \cdot \left(\frac{1}{M_o - M_r} \right) \quad (3.1)$$

where dH/dt denotes the heat flow rate measured by the DSC, t_1 and t_2 correspond to times at the start and termination of oxidation, respectively, and M_o and M_r are initial sample¹ mass, and residue mass, respectively. Note that the integral in Equation (3.1) represents the area under the heat flow rate curve. This net amount of heat release, associated with the soot oxidation, was

¹In experiments with surrogate soot, the residual mass is zero (i.e., $M_r = 0$), since the soot sample undergoes complete oxidation with no ash remaining.

obtained by subtracting the area defined by the baseline from the total heat release computed by Equation (3.1).

Table XIII summarizes results from the DSC experiments using various temperature heating rates (ranging from 3 °C/min to 100 °C/min) for surrogate soot samples. Results are shown in terms of the total heat released and the heat release per unit soot mass. For each heating rate, the temperature profile consisted of increasing the temperature from 45 °C to 550 °C at a given heating rate, and then maintaining an isothermal condition until the sample was completely oxidized. The results indicate that while the total heat release varies with the heating rate, the heat per unit mass is essentially independent of the heating rate, except for the fast heating rates of 80 °C/min and 100 °C/min. For these heating rates, temperature fluctuations were observed during transition from the progressive temperature profile to the isothermal mode. From these experiments, therefore, the amount of heat release per unit mass of surrogate soot was evaluated

TABLE XIII.

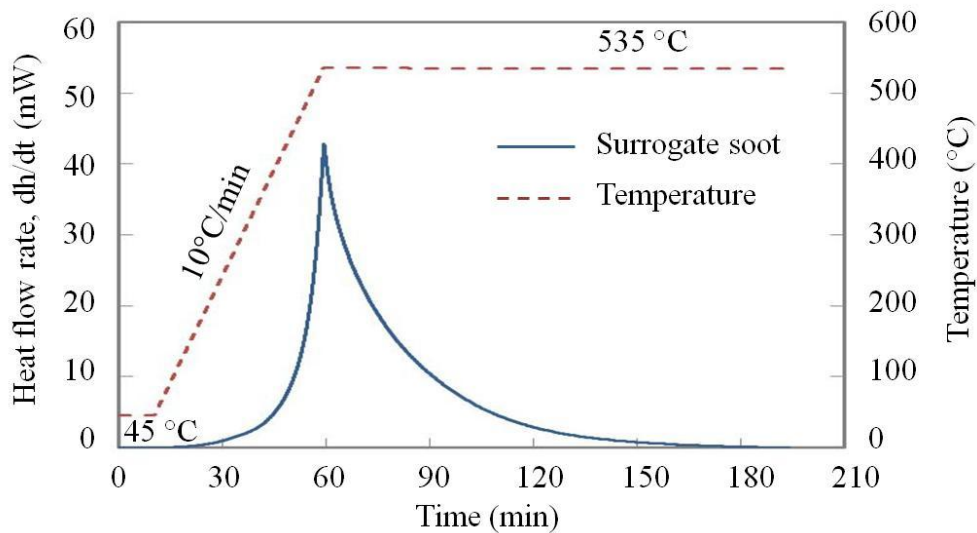
TOTAL HEAT EVOLVED AND HEAT EVOLVED PER UNIT SAMPLE MASS DURING THE OXIDATION OF SURROGATE SOOT SUBJECTED TO DIFFERENT TEMPERATURE HEATING RATES IN DSC EXPERIMENTS.

Heating rate (°C/min)	M _o (mg)	Total Heat Released (J)	Specific Heat Released (kJ/g)
3	5.299	74.35	14.03
5	4.329	60.7	14.02
10	3.719	52.15	14.02
20	4.307	60.4	14.02
40	4.474	62.73	14.02
60	4.741	66.47	14.02
80	4.791	67.93	14.18
100	5.613	81.56	14.53

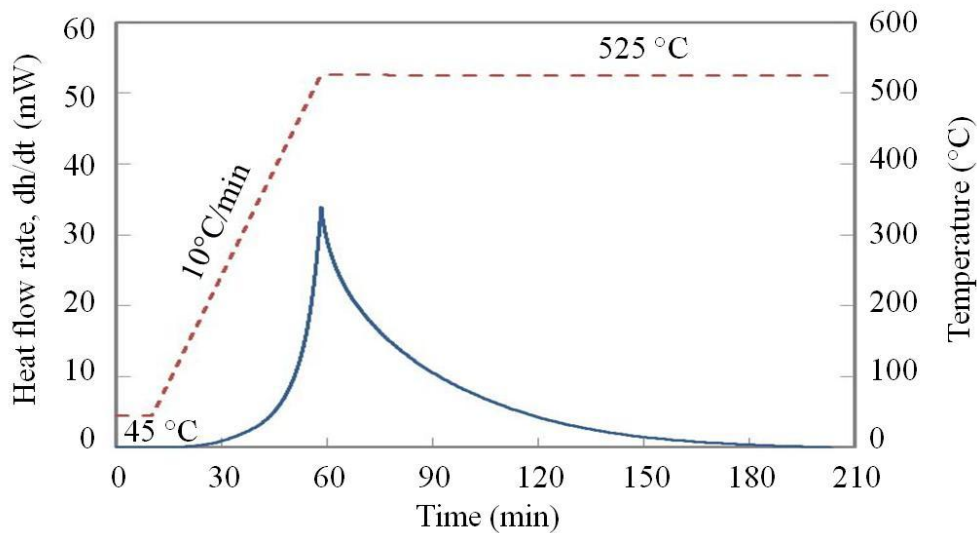
to be 14.02 kJ/g. In addition, an optimum heating rate of 10 °C/min was determined, which offers both high accuracy in data acquisition and time saving in performing the experiments.

The next set of experiments focused on the effects of peak temperatures set for isothermal conditions. Two more surrogate soot samples were individually heated up to 535 °C and 525 °C at a temperature gradient of 10 °C/min in air, respectively, and then maintained at these temperatures until the oxidation was completed, the same as in the previous experiment for 550 °C (cf. Figure 12). The results are shown in Figure 13, which presents the temporal variations of heat release rate for the two soot samples. Note that for each plot, the baseline heat flow rate has already been subtracted so that the data exhibit the heat flow rates generated solely by soot oxidation. The total heat release and heat release per unit soot mass for these three cases are listed in Table XIV. The results indicate that although the peak heat release rate and the total heat release are different for the three different isothermal conditions, the heat release per unit mass remains the same (=14.02 kJ/g) for the three cases.

Further oxidation experiments were performed to illustrate differences in the temporal variation of heat release rate associated with the oxidation of two diesel soot samples with different concentrations of the volatile components of SOF. Oxidation conditions in terms of the temperature profile (10 °C/min) and air flow rate (60 mL/min) were the same as before with an isothermal condition at 550 °C. The dry diesel soot sample was obtained by separating volatile components in SOF from the PM sample using the following procedure. A PM sample was placed in the TGA unit and heated up to 550 °C with a heating rate of 10 °C/min in nitrogen (inert) environment, and then maintained at this temperature for 60 min. During the isothermal condition at 550 °C, volatile components of SOFs contained in the diesel PM sample were completely removed, which was confirmed by no more change in the sample mass.



(A)



(B)

Figure 13. Temporal variation of the net heat flow rate associated with the oxidation of model soot samples in air subjected to two different temperature profiles with ramp rate of $10^{\circ}\text{C}/\text{min}$. The peak temperatures at isothermal conditions are 535°C and 525°C in Figs. 13A and B, respectively.

TABLE XIV

PEAK HEAT RELEASE RATE, TOTAL HEAT RELEASE AND HEAT RELEASE PER UNIT MASS IN THE OXIDATION OF SURROGATE SOOT SAMPLE SUBJECTED TO DIFFERENT ISOTHERMAL CONDITIONS IN DSC EXPERIMENTS.

Isothermal Temperature (°C)	Heating rate (°C/min)	M _o (mg)	Peak heat release rate (mJ/s)	Total Heat Release (J)	Specific Heat Release (kJ/g)
550	10	3.719	43.01	52.15	14.02
535	10	4.893	41.96	68.62	14.02
525	10	4.767	33.10	66.85	14.02

Figure 14 and 15 present results from a representative TGA experiment for the separation of volatile components of SOF in PM samples subjected to two different heat treatments in helium environment. It has been reported that the amount of volatile components of SOF in PM is dependent of heat treatment schemes. Previous studies have used the ramp rates of 0.2°-160°C/min (Fermo et al., 2005; Lapuerta et al., 2007; Setiabudi et al., 2004), maximum temperatures of 380-750°C (Fermo et al., 2005; Lapuerta et al., 2007; Stratakis et al., 2003; Yezerets et al., 2003; Zinbo et al. 1992), and isothermal duration of 2 hours. For the present TGA experiments, the heat treatment parameters include the temperature ramp rate, the maximum temperature, and duration of isothermal condition. For data in Fig. 14, the sample with initial mass of 4.184 mg was heated to 550°C at a ramp rate of 10°C/min, and then maintained at 550°C for an hour. As indicated, the volatile components of SOF adsorbed in the PM sample were completely removed during this time. The reduction of PM mass or the mass of SOF evaporated from the sample was found to be 19.94% of the initial mass. For results in Fig. 15, the PM

sample with initial mass of 4.147 mg was heated at the same ramp rate of 10°C/min, but three different isothermal conditions were applied for an hour each at 300°C, 550°C, and 700 °C, respectively. As expected, the mass profile for this case is significantly different, indicating fraction vaporization of SOF components depending upon volatility, compared to that in Fig. 14. However, the total amount of SOF evaporated for this case was 20.04 % of the initial mass, which is essentially the same as that for the first case.

By the same procedure as described above, the amount of volatile component in SOF evaporated was found to be 0.855 mg or 20% by mass for a PM sample of initial mass of 4.274 mg. This dry diesel soot sample of 3.419 mg then underwent oxidation in air under the same temperature profile as in the DSC experiment. After the complete oxidation of both diesel soot

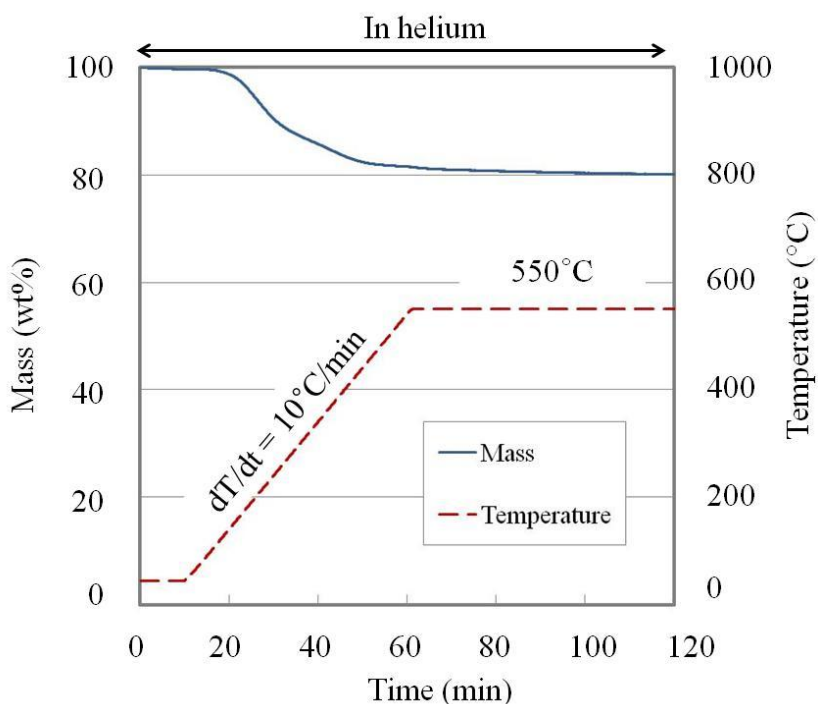


Figure 14. Instantaneous mass of diesel PM exposed to a nitrogen environment in a heating mode of temperature gradients of 10°C/min and isothermal condition for 1hr at 550°C.

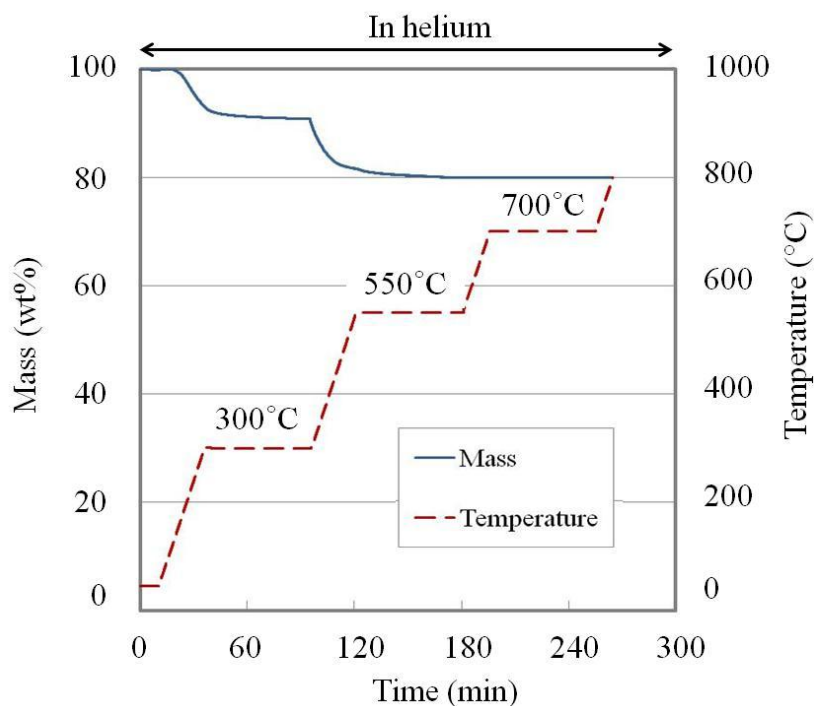


Figure 15. Instantaneous mass of diesel PM exposed to a nitrogen environment in a heating mode of heating rate of $10^{\circ}\text{C}/\text{min}$ with three isothermal temperatures of 300°C , 550°C , and 700°C .

samples, the amount of residue was measured to be 0.266 mg for the PM sample and 0.393 mg for the dry soot sample, respectively.

Results from the DSC experiments for the diesel PM sample and dry soot sample are presented in Figure 16. An important difference in the data is that SOF-containing diesel PM sample shows two peak values of heat flow rate, while the dry diesel soot exhibited one peak. The first peak near $t \approx 40$ min appears due to the exothermic reaction associated with the oxidation of SOFs, while the second peak near $t \approx 60$ min is due to the oxidation of soot. The total amounts of heat release per unit mass calculated by using Equation (1) are 14.67 kJ/g and 17.3 kJ/g for the SOF-containing PM sample and dry diesel soot sample, respectively. These values are in good agreement with those reported previously (Yang et al., 2010). It is also important to

note that the above values are lower than those associated with the pure carbon burning to CO₂, the latter being 32.8 kJ/g. While we did not measure the product species, the lower values of heat release may be attributed to the formation of CO. Evidence of this is provided by Reichert et al. (2008), who observed that the amount of CO formed was higher than that of CO₂, when solid carbon was oxidized at temperatures over 400 °C.

Additional oxidation experiments with diesel PM samples were conducted under two more isothermal conditions, corresponding to maximum (isothermal) temperatures of 535 °C and 525 °C, respectively. Figure 17 presents the temporal variations of heat release rates from the oxidation of diesel PM in air, in comparison with those from dry diesel soot and surrogate soot samples (see Figure 13). Results for the 550 °C case are also included in the figure. The comparison of data for diesel PM and dry diesel soot at three isothermal temperatures of 550 °C/535°C/525°C indicate that the fractions of the energy, representing the integrated heat release rate as percentages of the total heat release of the sample, were 8.18%/7.35%/7.94% in the first

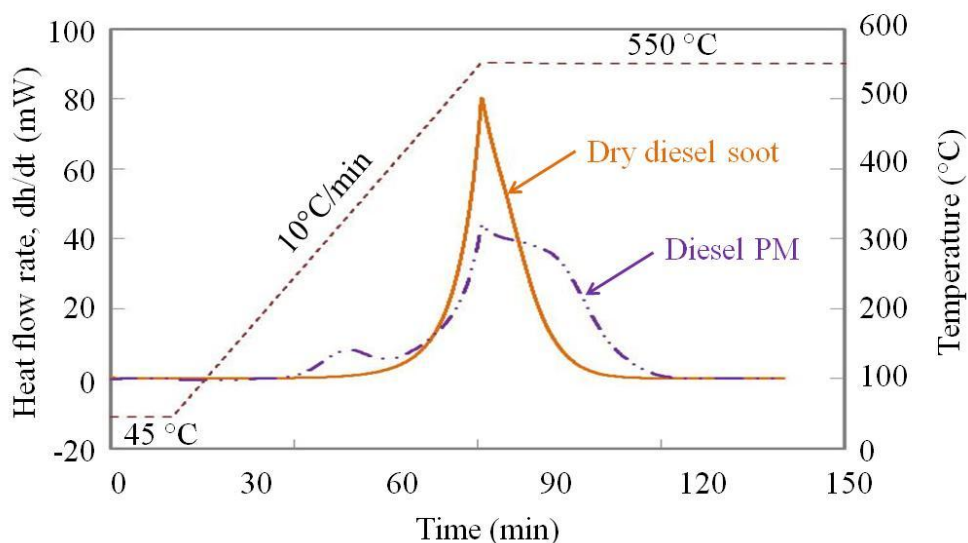


Figure 16. Temporal variation of the net heat flow rate measured during the oxidation of SOF-containing diesel PM sample and dry diesel soot sample in DSC experiments.

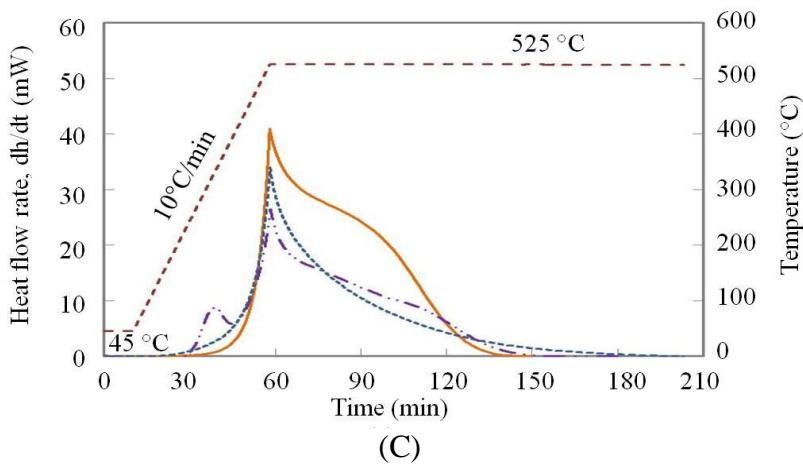
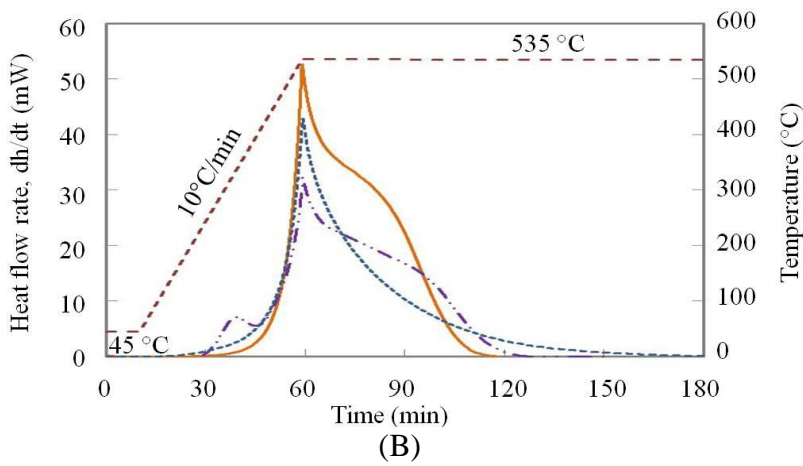
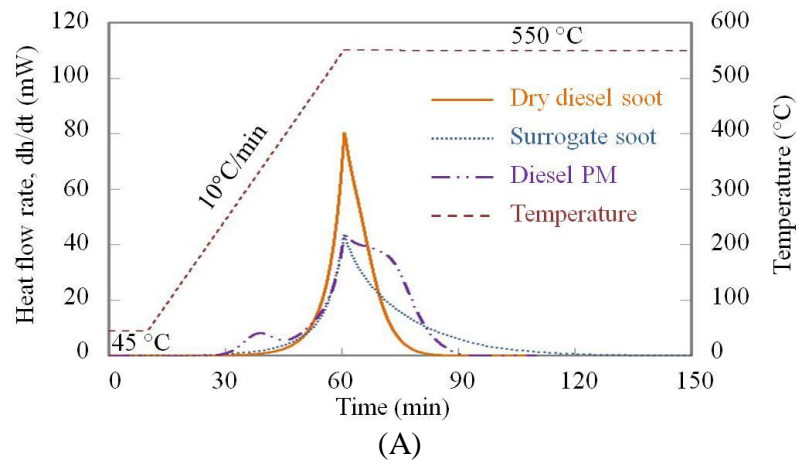


Figure 17. Temporal variation of the heat release rate during the oxidation of dry diesel soot, diesel PM, and surrogate soot samples in air subjected to three different temperature profiles with ramp rate of 10°C/min. The peak temperatures at isothermal conditions are 550 °C, 535 °C and 525 °C in Figs. 17A, B, and C, respectively.

peak and 91.82%/92.65%/92.06% in the second peak. Using the measured amounts of volatile components of SOF as 0.904 mg, 1.004 mg, and 0.982 mg, the amounts of heat released during the oxidation SOFs in diesel PM samples were evaluated to be 5.66 kJ/g, 5.24 kJ/g, and 5.5 kJ/g, respectively. Thus the average specific heat release from the oxidation of SOFs can be approximated as 5.47 kJ/g, which is small compared to that from the oxidation of dry diesel soot.

As indicated in Figure 17, the maximum value of heat release rate decreases for the all the samples, as the isothermal temperature is reduced. However, the total heat release per unit mass of sample is the same for the three temperature cases. Another important observation is that for these cases, there are noticeable differences in the heat release rate curves for the dry diesel soot and surrogate soot samples. These differences can be attributed to the chemical contents in the two soot samples. It is also important to note the difference in the heat release rate profile for the 550 °C case and those for the 535 °C or 525 °C cases for the oxidation of dry diesel soot samples. The profile for the 550 °C case exhibits a continuous sharp decrease after the peak value, while those for the 535 °C and 525 °C cases indicate first a sharp decrease, followed by slow decrease and then sharp decrease again. This indicates sensitivity of the oxidation process to reaction temperature, implying that dry diesel soot contains some chemical species that affect the temporal rate of heat release during oxidation at a given temperature.

The total amounts of heat release during the oxidation of SOF-containing diesel PM, dry diesel soot, and surrogate soot samples were computed using Equation (1), and the results are summarized in Table XV. For these results, the samples were subjected to heating mode at the constant rate of 10 °C/min and three different isothermal temperatures at 550 °C, 535 °C, and 525 °C in an air environment. As shown in the table, the amount of heat release per unit mass of

each sample is the same for the three different temperature profiles, although the instantaneous heat release rates during the oxidation are quite different (cf. Figures 16 and 17).

TABLE XV

SAMPLE MASS (M_o), RESIDUE MASS (M_r), NET MASS OXIDIZED (M_o-M_r), MASS OF VOLATILE COMPONENT OF SOF (M_v), TOTAL AMOUNT OF HEAT RELEASE, AND SPECIFIC HEAT RELEASE IN THE OXIDATION OF DIESEL PM, DRY DIESEL PM AND SURROGATE SOOT WITH RESPECT TO DIFFERENT TEMPERATURE PROFILES IN DSC EXPERIMENTS

Temperature profile		Sample	M_o (mg)	M_r (mg)	$M_o - M_r$ (mg)	M_v (mg)	Total Heat Release (J)	Specific Heat Release (kJ/g)
Isothermal temperature (°C)	Heating rate (°C/min)							
550	10	Diesel PM	4.521	0.266	4.255	0.904	62.5	14.67
		Dry diesel soot	3.419	0.393	3.026	-	52.2	17.3
		Surrogate soot	3.719	0	3.719	-	52.12	14.02
535	10	Diesel PM	5.021	0.158	4.863	1.004	71.32	14.67
		Dry diesel soot	6.233	1.095	5.138	-	88.62	17.3
		Surrogate soot	4.893	0	4.893	-	68.62	14.02
525	10	Diesel PM	4.912	0.274	4.638	0.982	68.02	14.67
		Dry diesel soot	6.119	0.39	5.729	-	98.84	17.3
		Surrogate soot	4.767	0	4.767	-	66.85	14.02

3.4 Conclusion

In order to control the thermal runaway during the oxidation of excess soot deposit in DPF, it is necessary to have detailed experimental information on the total heat release and the temporal variation of heat release rate from the diesel PM oxidation under realistic conditions. Previous studies have often used commercial soot artifacts (surrogate soot) or PM samples collected from lab-scaled burners for oxidation experiments, although there are inherent compositional and structural differences between the diesel PM and surrogate soot. The effect of SOF concentration in the diesel PM on the heat release rate characteristics has also not been considered. Moreover, most previous investigations have focused on the oxidation characteristics of diesel PM. In this study, we report detailed experimental information on the total heat release and the temporal variation of heat release rate during the oxidation of diesel PM, and elucidate differences in the heat release characteristics of surrogate soot and diesel soot. The diesel soot samples were collected from a cordierite particulate filter, where PM emissions bypassing the exhaust pipe of a light-duty diesel engine were deposited. Measurements employed a differential scanning calorimeter (DSC) and a thermogravimetric analyzer (TGA). Important observations are as follows.

Measurements taken at various ramp rates indicated an optimum heating rate of 10 °C/min, which provide high accuracy and efficiency in measuring the temporal variation of heat release rate during soot oxidation. Furthermore, experiments on the heat release during the oxidation of SOF-containing diesel PM and dry diesel soot (with no SOF) revealed two peaks in heat release rate profiles for the diesel PM, and only one peak for the dry diesel soot. For the diesel PM, the first peak corresponds to exothermic reactions associated with the oxidation of SOFs at

temperatures below 400 °C, followed by the second peak corresponding to exothermic reactions for soot oxidation at higher temperatures.

The DSC experiments revealed that the amounts of heat released from the oxidation of SOF-containing diesel PM sample, dry diesel soot, and commercially available surrogate soot were approximately 14.67 kJ/g, 17.3 kJ/g, and 14.02 kJ/g, respectively, indicating that the largest heat release was obtained from the dry diesel soot sample². Furthermore, the specific heat release from the oxidation of SOFs was found to be 5.47 kJ/g. Results also indicated significant differences in the temporal rates of heat release in the oxidation of SOF-containing diesel PM, dry diesel soot, and surrogate soot. In particular, remarkable differences were found on the results for dry diesel soot samples with respect to the oxidation temperatures of 550 °C and below 550 °C in air. The heat release rate of dry diesel soot at the isothermal temperature of 550 °C decreases monotonically as the complete mass is oxidized. In contrast, the rates of heat release at the isothermal temperatures of 535 °C and 525 °C first decrease rapidly, and then slowly. As the complete mass is oxidized, the rapid zone appears again.

²This is consistent with the results of previous studies which indicate that the specific heat release increases if the internal structures of carbon material become more ordered.

CHAPTER 4

OXIDATION CHARACTERISTICS OF DIESEL PARTICULATES

4.1 Introduction

As stated earlier, diesel engines typically require after-treatment devices to control exhaust emissions. Increasingly strict emissions standards in U.S. and Europe are providing a major impetus to engine manufacturers for developing advanced after-treatment systems that can significantly reduce tail-pipe exhaust emissions. In particular, DPF systems have been developed to remove particulate matter emissions in a majority of diesel vehicle classes. However, significant improvements are needed in their performance, which include reducing back pressure due to soot and ash build-up, improving material durability and filtration efficiency, and developing smart DPF control management systems with optimum regeneration strategies. In particular, an effective thermal management system is necessary to prevent the failure of a DPF system by thermal runaway that can occur during the oxidation of excessive soot deposit in DPF regeneration. To this end, while there have been studies dealing with the oxidation characteristics of diesel PM (Awara et al., 1997; Chilumukuru et al., 2009; Darcy et al., 2007; Kalogirou et al., 2007; Messerer et al., 2006; Neeft et al., 1997; Otto et al., 1980; Pauli et al., 1983; Stratakis et al., 2003; Yezerets et al., 2005), detailed experimental data on the heat release and oxidation rates of diesel PM under realistic engine and DPF conditions are still needed. Since DPF systems offer limited physical access in measuring these rates during regeneration, researchers have used bench-scale experiments to determine the oxidation kinetics parameters, such as reaction order, activation energy, and pre-exponential factor.

The kinetics of oxidation, the study of how fast oxidation takes place, is a topic of central importance to develop smart DPF system with optimum regeneration strategies. Knowledge of the phenomenological rates describing the general dependence of oxidation rates on temperature and reactant concentrations is of value for its own sake, in understanding the oxidation behavior of diesel particulate emissions, in improving the efficiency of DPF regeneration, and in preventing the failure of a DPF system by thermal runaway that can occur during the oxidation of excessive soot deposit.

In the previous chapter, it has been described that the oxidation experiments with surrogate soot and commercially available graphite often provide inaccurate data for predicting the oxidation rates and thermal energy distribution during DPF regeneration, and the discrepancies can mainly be attributed to two factors. First, there are significant differences with respect to the composition and morphology of diesel PM and surrogate soot samples. Second, the SOF adsorbed on diesel PM can enhance its ignition and oxidation rate, and, thereby, lower the energy input required for DPF regeneration. However, our literature review indicated only one study (Collura et al., 2005) dealing with the effect of SOF on the oxidation of diesel PM.

Previous research concerning the oxidation of diesel PM is summarized in Table XVI. As indicated, there have been numerous investigations on the oxidation of diesel PM under both catalytic and non-catalytic conditions. However, most of them have analyzed PM samples taken from the engine exhaust. While such studies provide useful fundamental information on the kinetic parameters pertaining to diesel soot oxidation, it is important to characterize the oxidation behavior of PM samples taken directly from a DPF system. The kinetic parameters obtained from such samples provide more relevant information for designing optimum DPF regeneration algorithms.

Table XVI
PREVIOUS RESEARCH ON THE OXIDATION OF DIESEL PM

Reference	Sampling position	Oxidation instrumentation	Rate expression
Awara et al. (1997)	DPF	DPF / diesel engine (bare & catalyzed)	$R = -A \cdot \exp\left(-\frac{E_a}{R_u \cdot T}\right) \cdot [O_2]$
Chilumukuru et al. (2009)	DPF	DPF / diesel engine (catalyzed)	$R = -A \cdot T \cdot \exp\left(-\frac{E_a}{R_u \cdot T}\right)$
Darcy et al. (2007)	DPF	Reactor (non-catalyzed)	$R = -A \cdot \exp\left(-\frac{E_a}{R_u \cdot T}\right) \cdot m_o \left[\frac{m}{m_o}\right]^{n_c} [P_{O_2}]^{n_{O_2}}$
Kalogirou et al. (2007)	Exhaust pipe	Reactor (bare& catalyzed)	$R = -A \cdot \exp\left(-\frac{E_a}{R_u \cdot T}\right) \cdot [P_{O_2}]^{n_{O_2}}$
Messerer et al. (2006)	Exhaust pipe	Reactor (catalyzed)	$R = -A \cdot \exp\left(-\frac{E_a}{R_u \cdot T}\right) \cdot m$
Neeft et al. (1997)	Exhaust pipe	Reactor (non-catalyzed)	$R = -A' \cdot \exp\left(-\frac{E_a}{R_u \cdot T}\right) \cdot [1 - \lambda]^{n_c} [P_{O_2}]^{n_{O_2}} *$
Otto et al. (1980)	Exhaust pipe	Reactor (non-catalyzed)	$R = -A \cdot \exp\left(-\frac{E_a}{R_u \cdot T}\right)$
Pauli et al. (1983)	Exhaust pipe	Reactor (non-catalyzed)	$R = -A \cdot \exp\left(-\frac{E_a}{R_u \cdot T}\right) \cdot [O_2]$
Rodríguez-Fernández et al. (2011)	Between DOC and Teflon filter	TGA (non-catalyzed)	$R = -A \cdot \exp\left(-\frac{E_a}{R_u \cdot T}\right) \cdot [m]^{n_c} [P_{O_2}]^{n_{O_2}}$
Stratakis et al. (2003)	DPF	TGA (bare& catalyzed)	$R = -A \cdot \exp\left(-\frac{E_a}{R_u \cdot T}\right) \cdot [m]^{n_m}$
Yezerets et al.(2005)	DPF	Reactor/ TGA (non-catalyzed)	$R = -A \cdot \exp\left(-\frac{E_a}{R_u \cdot T}\right) \cdot [c]^{n_c} [O_2]^{n_{O_2}} **$

* λ : Ratio of the instantaneous oxidized carbon to total carbon, ** c : Remaining amount of carbon in the reactor

In Chapter 4, we begin with a survey of the specific functional dependence of the reaction rate on temperature, which is referred to as Arrhenius law. We then briefly discuss two theories of reaction rates, the collision theory and the activated complex theory. For a more detailed understanding of any of these aspects and a thorough coverage of the subject, refer to any of the books on chemical kinetics, such as those listed in Reference (Benson, 1960; Laidler, 1969; Levenspiel, 1999). And then the oxidation experiment was performed to examine the oxidation behavior and kinetics parameters of diesel PM collected directly from the filter membrane of a DPF system connected to a diesel engine exhaust pipe. Since the samples were collected from the soot cake built up in commercial DPFs, our experiments are expected to provide more accurate results for predicting the oxidation of diesel PM during DPF regeneration. Another objective is to examine the effects of volatile component of SOF on the oxidation of diesel PM by using samples containing various amounts of SOF. In addition, differences in the oxidation behavior of diesel PM and surrogate soot are characterized by performing experiments under the identical conditions. The temperature-programmable experiments were conducted using a thermogravimetric analyzer (TGA), and the instantaneous mass and the rate of mass loss of a given sample were measured under well characterized conditions. Subsequently, the kinetic parameters such as the activation energy, pre-exponential factor, and reaction orders were determined for both the diesel PM and surrogate soot. The effects of thermal aging in both the inert and oxidizing environments on the oxidation of diesel PM and surrogate soot were characterized by performing experiments for a range of thermal conditions, which include different heating rates, different isothermal periods prior to oxidation, and different isothermal (furnace) temperatures during oxidation.

4.2 General Concept of Kinetics

For a one-step chemical reaction of arbitrary complexity, a stoichiometric relation can be presented by



where ν'_i and ν''_i are the stoichiometric coefficient of reactant and product, respectively, R_i and P_i are the reactant and product, respectively.

The International Union of Pure and Applied Chemist (IUPAC) has recommended that the term “rate of reaction” be restricted to the quantity

$$\dot{\xi} = \frac{1}{\nu_i} \frac{dn_i}{dt} \quad (4.2)$$

where $\dot{\xi}$ is the time derivative of the extent of reaction, and ν_i is the molecularity of the reaction with respect to species i , n_i is the change in number of moles of component i .

For the elementary reaction, the molecularity of a reaction is the number of atoms or molecules that interact with each other, leading to the completion of the reaction. The overall molecularity presents the number of molecules that collide within their molecular range of interaction. Most elementary reactions have overall molecularity of two, representing two-body collisions. For the reactions with overall molecularity of three, it is necessary to recombine two colliding molecules, and a third body is needed to carry away the excess energy. For large, complex molecules the excess energy can be absorbed by the various vibration modes of the combined molecules and a third body may not be needed.

The simplest representation of overall rate of reaction involving the reactants is

$$\omega = k \prod_{i=1}^N c_i^{n_i} \quad (4.3)$$

where k is the rate constant, c_i is the molar concentration (mol/m^3) of species, n_i is the reaction order with respect to the i th species. The reaction rate is usually found experimentally, which is a simple function of these concentrations under the constant of temperature, pressure, and so on. The order of a reaction with respect to a given species is the exponent of that species's concentration in the experimental rate expression. The experimentally determined stoichiometric coefficients based on concentration variations are reaction orders instead of reaction molecularities. When the elementary reaction proceeds, the reaction orders determined are the respective molecularities of the reaction. However, when the species whose concentrations are measured are the starting and final species of a global reaction, the reaction orders represent the net effects of the molecularities of the individual elementary reactions.

The measured reaction order is called pseudo-molecularity of the reaction. By holding all variables constant but one of the reactants in high concentrations, the reaction order of the lean component can be approximately identified as the apparent overall reaction order. Since the reaction order describes both elementary and global reactions, it will be used in specifying all reactions in our reaction study.

A reaction that occurs entirely in a single phase is said to be homogeneous, while one that occurs partly or entirely at an interface between phases is heterogeneous. The significance of the latter is that many reactions have rates strongly influenced by the presence of solid surface. Some crucial step in the reaction can occur on the surface, and the rate may depend on the speed with which reactants can diffuse to the surface. To complicate matters further, some reactions proceed by competing homogeneous and heterogeneous reactions. In one way to distinguish the two, the heterogeneous rate increases with the surface area, while the homogeneous rate remains constant.

Another way is by varying the temperature: The homogeneous rate varies exponentially with temperature, whereas a heterogeneous reaction limited by diffusion should have a rate roughly proportional to $T^{1/2}$.

4.3 Theory of Reaction Rates

4.3.1 The Arrhenius Law

For an elementary reaction the Arrhenius law (Arrhenius, 1889) states that

$$\frac{d \ln k}{dT} = \frac{E_a}{R_u T^2} \quad (4.4)$$

where k is the rate constant, T is the temperature, E_a is the activation energy of the reaction (J/mol), and R_u the universal gas constant. If E_a is a constant with respect to temperature, integrating Eq. (4.4) yields

$$k(T) = A \exp\left(-\frac{E_a}{R_u T}\right) \quad (4.5)$$

where A is the frequency factor or the pre-exponential factor. For constant values of A and E_a , a plot of $\ln k$ versus $1/T$ exhibits a linear relationship, with A and E_a respectively determined from the intercept and slope of such a plot.

A somewhat better fit can often be obtained with an equation of the form, which is called modified Arrhenius equation,

$$k(T) = BT^\alpha \exp\left(-\frac{E_a}{R_u T}\right) \quad (4.6)$$

where B is a constant, and α is temperature exponent. As is usually the case, when $E_a \gg RT$, the exponential factor dominated the temperature dependence. And A has comparatively weak temperature dependence for many elementary reactions.

4.3.2 Hard Sphere Collision Theory

The collision theory is based on the kinetic theory of gases, which examines the interactions between two reactive hard-sphere molecules and the type of collisions they can undergo. The hard sphere collision theory develops the reaction rate with physical transport processes, that is, an expression giving the rate constant in terms of microscopic quantities. It uses kinetic theory to obtain the frequency of collisions between reactive molecules. In the simple hard sphere model, it is assumed that the collision energy is derived from the relative translational energy between the colliding molecules for sufficiently dilute gases. Furthermore, because not all collisions between molecules actually lead to reaction, it is necessary to estimate the fraction of reactive collisions, an expression for the rate at which reactive collisions occur can be derived, which is equivalent to the reaction rate.

Consider two different types of molecule: the one is standing and the other is approaching it. The moving molecule through a gas with a speed is assumed to be equal to the average velocity. The collision rate is proportional to the number of density of two different types of molecule, the reactive speed between these molecules, and their size. To quantify the fraction of reactive collisions, the impact parameter, b , is of importance defined as the distance of a line perpendicular to each of the initial velocities of two colliding molecules. If b is large relative to the range of the force between the molecules, then the molecules hardly interact. Otherwise, the

interaction and deflection may be large. Thus, if a collision occurs, their centers are within the distance

$$b_{\max} = r_1 + r_2 \quad (4.7)$$

where b_{\max} is the maximum value of the impact parameter for which a collision can occur, r_1 and r_2 are the molecular radii of a moving molecule and a stationary molecule, respectively.

In view of one type of molecule striking a molecule of the other type, the colliding area is equal to

$$\pi(r_1 + r_2)^2 = \pi b_{\max}^2 \quad (4.8)$$

The total number of collision of the stationary molecule is

$$Z_2 = \pi b_{\max}^2 v \Delta t n_2 \quad (4.9)$$

where v is the velocity of moving molecule at impact, Δt is the time interval during which a molecule moves, n_2 is the number of stationary molecules per unit volume. The distance that a molecule travels in the time is simply $v\Delta t$, so that all stationary molecules are located in the volume $\pi b_{\max}^2 v \Delta t$.

The number of collisions of the stationary molecule per unit time is

$$Z_2 = \pi b_{\max}^2 v n_2 \quad (4.10)$$

Thus, the total number of collisions of moving molecules with those of stationary molecules per unit time and per unit volume is

$$Z_{12} = \pi b_{\max}^2 v n_1 n_2 \quad (4.11)$$

Since all collisions will not lead to reaction, it is necessary to modify Eq. (4.11). The reactive collision can be affected by the energy at impact. The energy corresponding to the

motion of the center of mass can be conserved, so that the only energy available for overcoming a barrier to reaction can be the relative energy.

The cross section is parameterized in terms of the energy evaluated from the velocity along with the line of centers. The velocity along the line of centers, v_{lc} , is

$$v_{lc} = v \cdot \cos \alpha \quad (4.12)$$

where v is the velocity of moving molecule, α is the angle between the center line at the impact point and the line of moving molecule forward to the stationary molecule. The energy associated with motion along the line of centers is

$$\varepsilon_{lc} = \frac{1}{2} \mu v_k^2 \quad (4.13)$$

where μ is the reduced mass.

Applying Eq. (4.12) to (4.13) with $\varepsilon = \frac{1}{2} \mu v^2$ and $\sin \alpha = \frac{b}{b_{\max}}$, then we obtain

$$\varepsilon_{lc} = \varepsilon \left\{ 1 - \left(\frac{b}{b_{\max}} \right)^2 \right\} \quad (4.14)$$

where b is the impact parameter for which a collision can occur.

Since the reaction occurs when the initial kinetic energy, ε_{lc} , exceeds the threshold energy, ε^* ,

it can be written as

$$\varepsilon_{lc} = \varepsilon \left\{ 1 - \left(\frac{b}{b_{\max}} \right)^2 \right\} > \varepsilon^* \quad (4.15)$$

If we consider that the effective value of the impact parameter and annulus of area of a molecule for reaction are b_{eff} and $2\pi b db$, then the average probability for reaction in this annulus and energy can be expressed as

$$\langle P \rangle = \int_0^{b_{eff}} 2\pi b P db \quad (4.16)$$

For P=1, Eq. (4.15) can be

$$b^2 < b_{max}^2 \left(1 - \frac{\varepsilon^*}{\varepsilon}\right) \quad (4.17)$$

So that the average probability, $\langle P \rangle$, is, where $b_{eff}^2 = b_{max}^2 \left(1 - \frac{\varepsilon^*}{\varepsilon}\right)$

$$\langle P \rangle = 2\pi \int_0^{b_{eff}} b db \quad (4.18)$$

Therefore,

$$\langle P \rangle = \pi b_{max}^2 \left(1 - \frac{\varepsilon^*}{\varepsilon}\right) \quad (4.19)$$

The reaction rate constant at a particular energy at the point of impact can be

$$k(\varepsilon) = \langle P \rangle \cdot v = v b_{max}^2 \left(1 - \frac{\varepsilon^*}{\varepsilon}\right) \quad (4.20)$$

Thus, the average value of reaction rate constant is

$$k(T) = \langle k(\varepsilon) \rangle = \int_{\varepsilon^*}^{\infty} \{k(\varepsilon) \cdot P(\varepsilon)\} d\varepsilon \quad (4.21)$$

The Boltzmann energy distribution is given by

$$P(\varepsilon) d\varepsilon = 2\pi \left(\frac{1}{\pi k_B T}\right)^{3/2} \sqrt{\varepsilon} \exp\left(-\frac{\varepsilon}{k_B T}\right) d\varepsilon \quad (4.22)$$

where k_B is the Boltzmann constant.

Applying Eq. (4.20) and (4.22) to (4.21), then the average value of reaction rate constant can be expressed as

$$k(T) = \int_{\varepsilon^*}^{\infty} \left\{ 2\pi^2 v b_{\max}^2 \left(\frac{1}{\pi k_B T} \right)^{3/2} \left(1 - \frac{\varepsilon^*}{\varepsilon} \right) \sqrt{\varepsilon} \exp\left(-\frac{\varepsilon}{k_B T} \right) \right\} d\varepsilon \quad (4.23)$$

Since the velocity of moving molecule is

$$v = \left(\frac{2\varepsilon}{\mu} \right)^{1/2} \quad (4.24)$$

the reaction rate constant yields

$$k(T) = \pi b_{\max}^2 \left(\frac{8k_B T}{m\pi} \right)^{1/2} \exp\left(-\frac{\varepsilon^*}{k_B T} \right) \int_{\varepsilon^*}^{\infty} \left\{ \left(\frac{\varepsilon - \varepsilon^*}{k_B T} \right) \exp\left(-\frac{\varepsilon - \varepsilon^*}{k_B T} \right) \right\} \frac{d\varepsilon}{k_B T} \quad (4.25)$$

By letting $x = \frac{\varepsilon - \varepsilon^*}{k_B T}$

then

$$k(T) = \pi b_{\max}^2 \left(\frac{8k_B T}{m\pi} \right)^{1/2} \exp\left(-\frac{\varepsilon^*}{k_B T} \right) \int_0^{\infty} \{x \exp(-x)\} dx \quad (4.26)$$

Since $\int_0^{\infty} \{x \exp(-x)\} dx = 1$, the rate constant can be written as

$$k(T) = \pi b_{\max}^2 \langle v \rangle \exp\left(-\frac{\varepsilon^*}{k_B T} \right) \quad (4.27)$$

where

$$\langle v \rangle = \left(\frac{8k_B T}{m\pi} \right)^{1/2}$$

In Eq. (4.27), the factor $\pi b_{\max}^2 \langle v \rangle$ is the number of collisions per unit time per unit volume between two hard sphere molecules. By this simple collision theory, the absolute magnitude of k is usually overestimated, since it can be thought of as the fraction of collisions with sufficient energy that also have the proper orientation for reaction. Accordingly, simple collision theory is modified by including the probability factor, p , which is sometimes called a steric factor. Thus, Eq. (4.27) can be re-written as

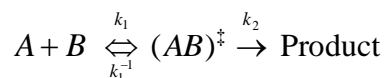
$$k(T) = p \pi b_{\max}^2 \langle v \rangle \exp\left(-\frac{\varepsilon^*}{k_B T}\right) \quad (4.28)$$

Since the temperature is increased, the average relative speed also increases, and hence so does the collision frequency. But if the threshold energy, ε^* , is larger than $k_B T$, then a small increase in temperature increases the fraction of collisions with enough energy for reaction, much more rapidly than the total number of collisions.

4.3.3 Activated Complex Theory

In the activated complex theory, it has been considered that the reaction rates are associated with the transition from the activated state of molecules to reacted state. The reaction rate in this theory describes the dynamics of a reactive collision to equilibrium between the reactants and an intermediate state called the activated complex. On collision between molecules of the reactants with the top of the potential energy barrier, a highly energized and unstable molecule is formed, which is referred to be the activated complex. The activated complex dissociates either into products or back to reactants, depending on the bonding strength.

Consider a bimolecular reaction represented by



where $(AB)^\ddagger$ is the activated complex. The rate constant is given as (Vincenti and Kruger; 1965)

$$k(T) = k_2 \frac{q^\ddagger}{q_A q_B} \exp\left(-\frac{\varepsilon^*}{k_B T}\right) \quad (4.29)$$

where k_2 is the rate constant of activated complex $(AB)^\ddagger$, q^\ddagger is the partition function per unit volume for activated complex, and q_A and q_B are the partition functions per unit volume for the reactants.

The partition function is simply a number which describes how the molecules are distributed over the available energy states at a given temperature in the system. In general, the electronic energy levels are generally very widely separated in energy compared to the thermal energy at room temperature. In each electronic level, there are several vibrational levels and for each vibrational level, there are several rotational states. This is a simplified and useful model to start with. The total energy is a sum of electronic (E_e), vibrational (E_v), rotational (E_r), translation (E_{tr}), and nuclear spin energy (E_n). Assuming the first three to be independent and neglecting the last energy, the molecular partition function is written as the product of electronic, vibrational, rotational and translation partition functions. Therefore,

$$q = q_{\text{electronic}} \cdot q_{\text{vibration}} \cdot q_{\text{rotation}} \cdot q_{\text{translation}} \quad (4.30)$$

Since $E_e > E_v > E_r > E_{tr} > E_n$, there are far too many translational states available compared to the other states such as rotational, vibrational and electronic states.

In the bimolecular reaction, the partition function of molecule i is simply the translational partition function as rotations and vibrations are absent. The translational partition function per unit volume can be expressed as

$$q_i = \frac{(2\pi m_i k_B T)^{3/2}}{h^3} \quad (4.31)$$

where m_i is the mass of molecule i , h is Plank's constant.

The rate constant k_2 is the unimolecular decomposition rate of $(AB)^\ddagger$ going to products. If it is assumed that the rate of $(AB)^\ddagger$ decomposition is equal to the frequency of vibration of the complex, ν^\ddagger . then the complex decomposes to products on every vibration. Thus, the rate constant can simplify to

$$k(T) = \nu^\ddagger \frac{q^\ddagger}{q_A q_B} \exp\left(-\frac{\varepsilon^*}{k_B T}\right) \quad (4.32)$$

Separating the partition function q^\ddagger into two factors, a partition function for the vibration (z^\ddagger) that leads to dissociation of the transition state and a partition function for the remaining degrees of freedom (q'^\ddagger).

z^\ddagger can be calculated as

$$z^\ddagger = \frac{1}{1 - \exp\left(-\frac{h\nu^\ddagger}{k_B T}\right)} \quad (4.33)$$

By Taylor series,

$$z^\ddagger = \frac{k_B T}{h\nu^\ddagger} \quad (4.34)$$

Therefore, the rate constant can be

$$k(T) = \frac{k_B T}{h} \frac{q'^\ddagger}{q_A q_B} \exp\left(-\frac{\varepsilon^*}{k_B T}\right) \quad (4.35)$$

where $\frac{q^\ddagger}{q_A q_B}$ is the ratio of the number of state available to the activated complex to the number of states available to the reactants.

4.4 Oxidation Experimental Scheme

Soot samples were accurately weighed and loaded into the sample pans to measure the instantaneous mass and rate of mass loss during oxidation. As stated earlier, the oxidation behavior was characterized with respect to different heating rates in an inert environment prior to oxidation, as well as by using PM samples containing different levels of volatile components of SOF. Two different heating rates (10°C/min and 100°C/min) and two isothermal durations (1h and 5h) were used to evaporate different amounts of volatile components of SOF in the PM sample, and to characterize the effects of heating mode on the oxidation of dry diesel soot. In addition, the soot samples were directly exposed to oxidizing environment during the heating mode to characterize their oxidation behavior under conditions when carbonaceous matter and volatile components of SOF are being simultaneously oxidized. High purity helium gas was used to provide an inert environment to suppress chemical reactions during evaporation. Following evaporation, helium was replaced with air for the oxidation of PM samples under the specific isothermal conditions with temperature of 500°C, 550°C, and 600°C. The flow rate of helium or air was set at 60ml/min. Subsequently, the data obtained from oxidation experiments were used to determine the reaction orders, activation energy, and pre-exponential factor for each sample. A similar procedure was used for oxidation experiments with surrogate soot samples.

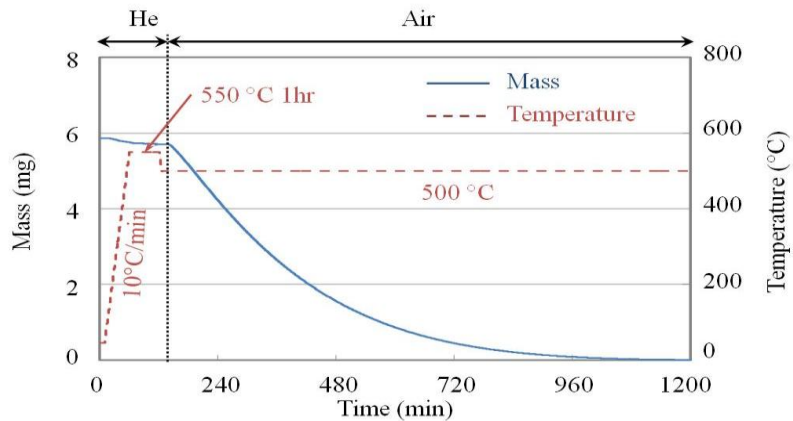
4.5 Result and Discussion

4.5.1 Oxidation Experiments with Surrogate Soot

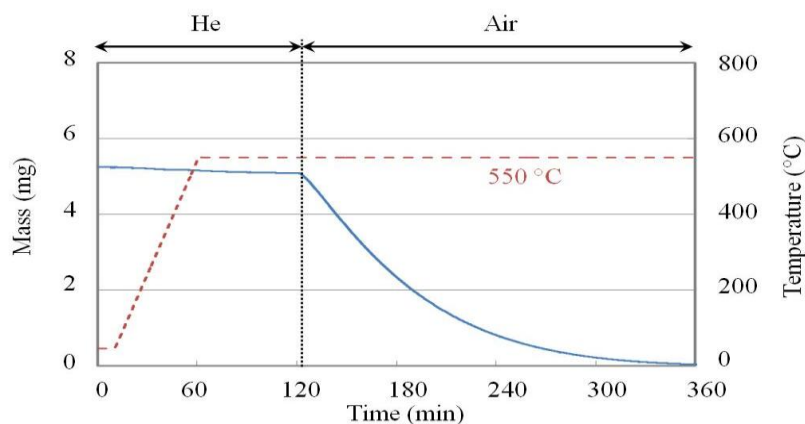
Figure 18 depicts the temporal variation of the instantaneous mass for a surrogate soot sample exposed to helium environment in heating mode with a ramp rate of 10°C/min followed by an isothermal condition at 550°C for 1h, and then exposed to oxidizing (air) environment at a specific temperature. As mentioned earlier, high purity helium gas flow was used to provide an inert environment to suppress chemical reactions during the heat-up mode. The flow rates of both helium and air were set at 60ml/min. The oxidation experiments were performed with surrogate soot samples of 5.865mg, 5.241mg, and 6.267mg. Note that the error in mass measurement in TGA set-up is less than 0.001% for the three furnace temperatures used in this study. As indicated, during the heating period, a relatively small mass ($\approx 2\sim 2.5\%$) is lost due to the evaporation of moisture, organic compounds, etc., contained in the sample. Once the furnace temperature reached the specified isothermal temperature, the helium gas was replaced with air to start oxidation. Consequently, the instantaneous sample mass decreases with time due to oxidation, and the rate of decrease of mass or the oxidation rate can be expressed as (Neeft et al., 1997):

$$r = \frac{dm_c}{dt} = -A \cdot \exp\left(-\frac{E_a}{R_u \cdot T}\right) \cdot [m_c]^{n_c} \cdot [P_{O_2}]^{n_{o_2}} \quad (4.36)$$

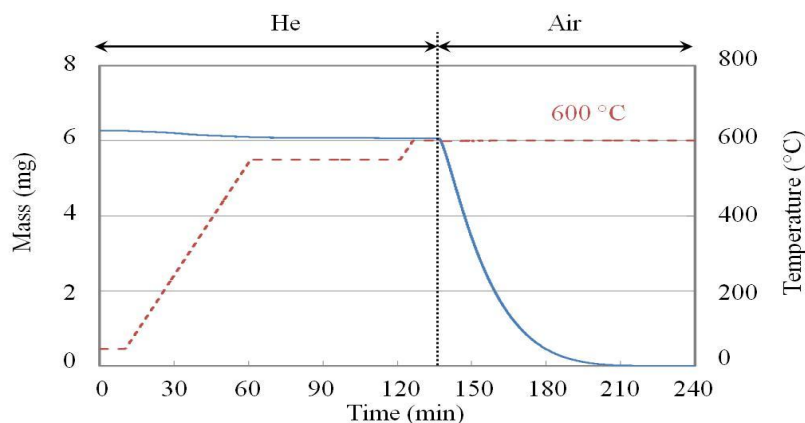
Here m_c is the sample mass, t the time, A the pre-exponential factor, E_a the activation energy, R_u the universal gas constant (8.31447 kJ/mol·K), T the temperature (K), P_{O_2} the partial pressure of oxygen, and n_c and n_{o_2} the reaction orders with respect to carbon and oxygen, respectively.



(A)



(B)



(C)

Figure 18. Temporal variation of the instantaneous mass for the surrogate soot sample exposed to helium environment in heating mode with temperature gradient of 10°C/min, then maintained at an isothermal temperature of 550°C for 1 h, and then to oxidizing (air) environment at temperatures 500°C, 550°C, and 600°C in Figs. 18A, B, and C, respectively. Initial sample mass: 5.865mg (A), 5.241mg (B), and 6.267mg (C).

In order to evaluate n_c , Eq. (4.36) is rearranged by taking the natural logarithm as :

$$\ln\left[-\frac{dm_c}{dt}\right] = n_c \cdot \ln[m_c] - \left(\frac{E_a}{R_u}\right)\frac{1}{T} + n_{O_2} \ln[P_{O_2}] + \ln A \quad (4.37)$$

The logarithmic plot of the rate of mass loss as a function of $\ln[m]$ is shown in Figure 19 for the three isothermal temperatures of 500°C, 550°C, and 600°C. The reaction order n_c was obtained by linear regression and computing the slope of each linear regression plot. Note the fluctuations near the end of oxidation, which may be attributed to measurement errors associated with the oxidation of small sample mass. The effect of these fluctuations on the computed

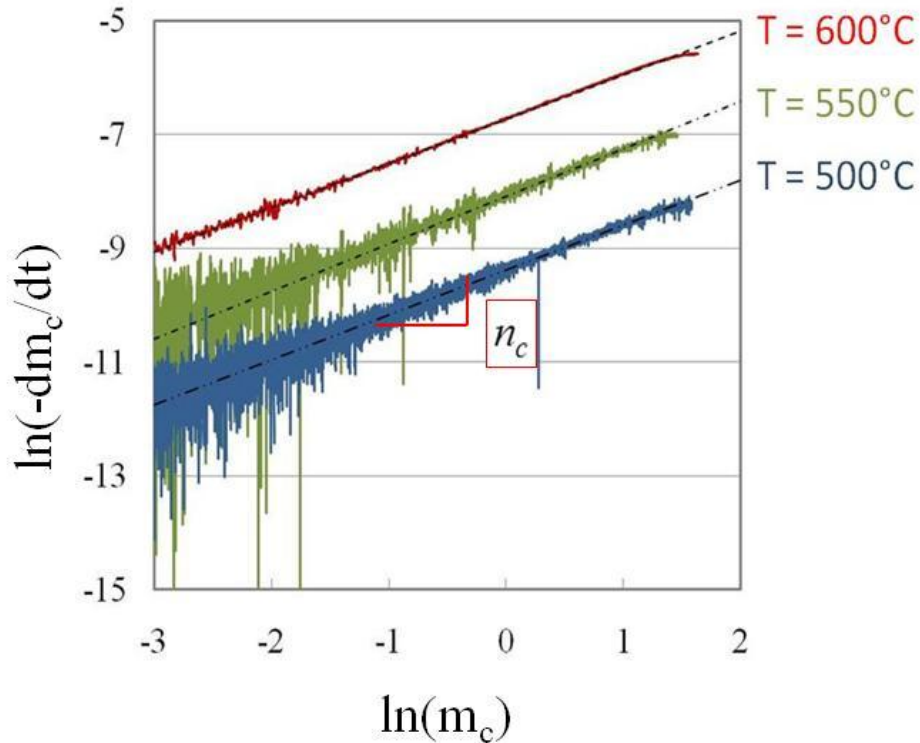


Figure 19. Logarithmic plot for the rate of mass loss as a function of $\ln[m_c]$ for the three isothermal temperatures of 500°C, 550°C, and 600°C. The slope yields the reaction order with respect to carbon for the surrogate soot sample.

reaction order was assessed by determining the reaction order using data from the start of oxidation to (i) 95% mass loss ($\ln m \approx -1.5$), and (ii) 99% mass loss ($\ln m \approx -3$). For the first case, the computed reaction order was $n_c=0.79 \pm 0.02$, while for the second case, the reaction order was $n_c= 0.79 \pm 0.05$. Thus the results indicate that the effect of fluctuations on the measured reaction order is negligible, if the data during the final 5% oxidation period is excluded. In order to determine the activation energy (E_a), Eq. (4.37) is rearranged as:

$$\ln\left[-\frac{dm_c}{dt}\right] - 0.79\ln[m_c] = -\left(\frac{E_a}{R_u}\right)\frac{1}{T} + n_{O_2}\ln[P_{O_2}] + \ln A \quad (4.38)$$

Then the plot of the left-hand term of this equation (with $n_c=0.79$) versus inverse of the temperature yields E_a , as indicated in Fig. 20.

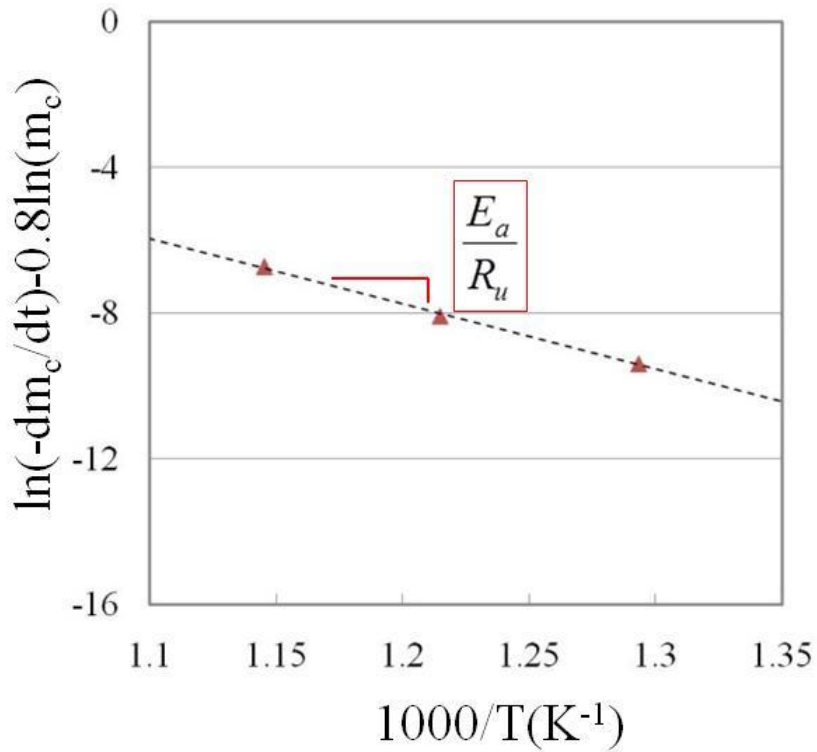


Figure 20. Evaluation of activation energy for the surrogate soot sample using Eq, (4.38).

The three data points in this figure correspond to three isothermal temperatures. Again the gradient of the linear regression line yields $-E_a/R_u$, and the activation energy $E_a = 148.16\text{kJ/mol}$ for the surrogate soot sample.

Experiments were also performed to examine the effect of initial sample mass on the oxidation behavior of surrogate soot. Experiments involved 12 different samples with initial mass ranging from 1mg to 4.5mg. Each sample was heated to an isothermal temperature of 500°C, 550°C, or 600°C with a heating rate of 10°C/min in a helium environment, and then oxidized in air under isothermal conditions. Figure 21 plots the values of activation energy determined from these experiments.

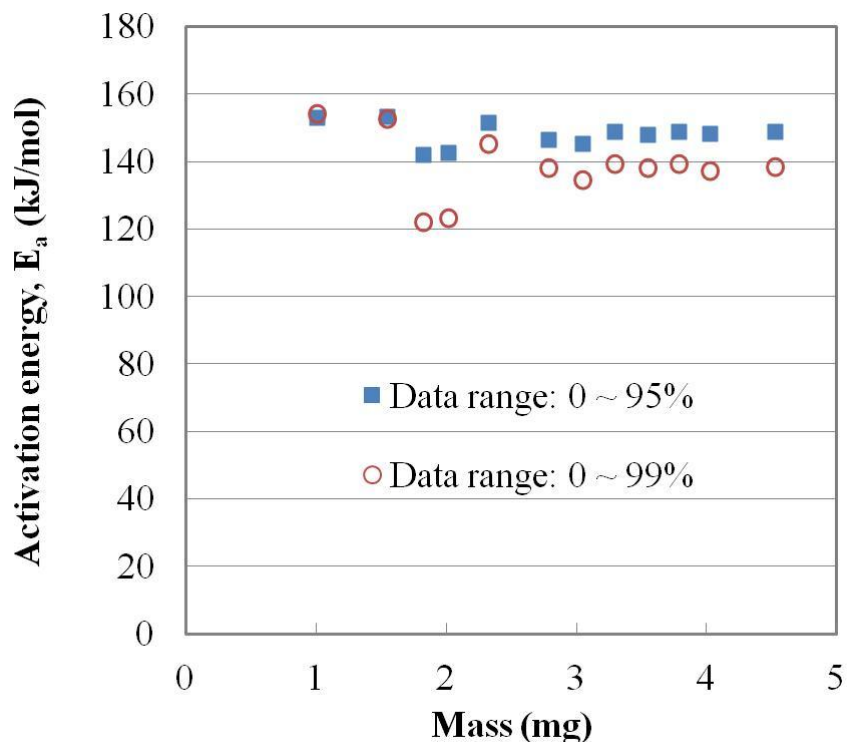


Figure 21. Variation of the measured activation energy plotted versus the initial mass of the surrogate soot sample, covering a mass range of 1-4.5 mg.

While the results exhibit some fluctuations, especially for initial sample mass < 2.5 mg, the activation energies calculated for initial sample mass > 3 mg were nearly identical. For data from the start of oxidation to 99% mass loss and $n_c = 0.74$, the evaluated activation energy was 138 ± 2 kJ/mol corresponding to 6 different samples, whereas for $n_c = 0.79$ and data where the oxidation rate during the final 5% mass loss was excluded, the activation energy was found to be 148 ± 5 kJ/mol. These results suggest that a minimum sample mass of 3 mg is needed to obtain kinetic parameters independent of the initial mass.

Furthermore, it is essential to use data from the start of oxidation to 95% mass loss to assure the accuracy of evaluation in kinetic parameters. It is useful to compare our results for the surrogated soot with those reported in the literature. Yezerets et al. (2005) reported an activation energy of $E_a = 137 \pm 8.7$ kJ/mol for temperatures 400–550°C, oxygen concentrations 3–25%, and total carbon conversion between 15–18%. They assumed the reaction order of soot to be unity. Neft et al. (1997) reported activation energy values of $E_a = 168 \pm 1$ kJ/mol and $E_a = 169 \pm 16$ kJ/mol for soot samples oxidizing in O₂/Ar mixture with 25% O₂ by volume, and in O₂/H₂O/Ar mixture with 10% O₂ and 10% H₂O by volume.

In order to determine the pre-exponential factor (A) and the reaction order of oxygen (n_{O_2}), oxidation experiments were carried out at three different oxygen partial pressures, using (i) 25% air/75% He, (ii) 60% air/40% He, and (iii) 100% air/0% He. Using a similar procedure as described earlier, the soot samples were heated to a temperature of 550°C with a heating rate of 10°C/min followed by isothermal condition at 550 °C for 1h in helium environment, and then exposed to air environment under a specific oxygen partial pressure at temperature of 550°C. The flow rate of air-He mixture was set at 100 ml/min. Figure 22 plots the left-hand term of Eq. (4.38) versus $\ln[P_{O_2}]$. Again using a linear regression analysis, the slope of the linear regression

line yields the reaction order $n_{O_2}=0.93$, while Y-intercept yields the pre-exponential factor $A=4.34 \times 10^6$.

Four additional experiments were performed to investigate the oxidation behavior of surrogate soot subjected to different heating conditions in either helium or air environment. For the first experiment, the soot sample was heated to the oxidation temperature of 500°C, 550°C, and 600°C with a heating rate of 10°C/min in helium environment, and then exposed to oxidizing environment. For the second experiment, the heating rate was changed to 100°C/min (maximum heating rate), while for the third, the sample was exposed to helium environment during the heating rate of 10°C/min, then maintained at an isothermal temperature of 550 °C for

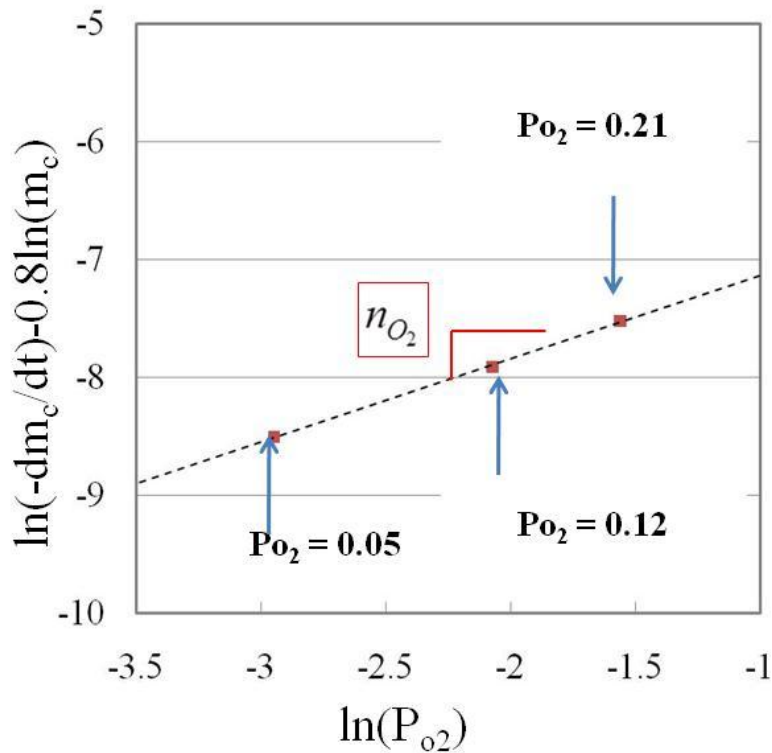


Figure 22. Evaluation of reaction order of oxygen using Eq. (4-37) for surrogate soot samples subjected to different oxygen partial pressures.

5 hours, and then exposed to air environment under isothermal conditions. For the fourth experiment, the sample was directly exposed to oxidizing environment during the heating mode. Table XVII summarizes the reaction orders of surrogate soot obtained from these experiments. As indicated in the table, for heating rates 100°C/min and 10°C/min with no isothermal period, the evaluated reaction orders were 0.79 ± 0.01 and 0.79 ± 0.02 , respectively. The corresponding reaction order for the isothermal periods of 5 hours was 0.78 ± 0.02 . For the sample directly exposed to oxidizing environment during the heating rate of 10°C/min, reaction order was 0.8 ± 0.01 .

Table XVII

MEASURED REACTION ORDERS WITH RESPECT TO CARBON FOR THE SURROGATE SOOT SAMPLES SUBJECTED TO DIFFERENT HEAT TREATMENTS IN INERT AND OXIDIZING ENVIRONMENTS.

Heat treatment scheme		Isothermal oxidation temperature (°C)			Reaction order (n_c)
		500	550	600	
Heating rate	10 °C/min	0.79	0.81	0.77	0.79 ± 0.02
	100 °C/min	0.78	0.8	0.8	0.79 ± 0.01
Isothermal period	1 hr	0.77	0.81	0.79	0.79 ± 0.02
	5 hr	0.8	0.77	0.76	0.78 ± 0.02
Oxidation during heating up (No helium used)		0.79	0.81	0.8	0.8 ± 0.02
Reaction order (n_c)		0.79 ± 0.01	0.8 ± 0.03	0.78 ± 0.02	

Table XVIII summarizes the evaluated activation energy, reaction order with respect to oxygen, and pre-exponential factor for surrogate soot samples subjected to different heat treatments, as discussed above. The E_a values obtained from the other four experiments were 145.22 kJ/mol, 147.79 kJ/mol, 149.07 kJ/mol, 148.02 kJ/mol, respectively. The values of n_{O_2} and A were found to be as $n_{O_2}=0.94 \pm 0.01$ and $A=(3.68 \pm 0.81)\times 10^6$, respectively. An important observation from these results is that the reaction order of surrogate soot is essentially independent of the heating modes in both helium and oxidizing environments.

Table XVIII

MEASURED ACTIVATION ENERGY, REACTION ORDER WITH RESPECT TO OXYGEN, AND PRE-EXPONENTIAL FACTOR FOR SURROGATE SOOT SAMPLES SUBJECTED TO DIFFERENT HEAT TREATMENTS.

Heat treatment scheme		Activation energy (E_a), (kJ/mol)	Reaction order of oxygen (n_{O_2})	Pre-exponential factor, A (1/sec)
Heating rate	10 °C/min	147.8	0.94	3.24×10^6
	100 °C/min	145.2	0.95	2.49×10^6
Isothermal period	1 hr	148.2	0.93	4.34×10^6
	5 hr	149.1	0.95	4.54×10^6
Oxidation during heating up (No helium used)		148.0	0.94	3.78×10^6
Average			0.94	3.68×10^6
Standard deviation			± 0.01	$\pm 0.81 \times 10^6$

4.5.2 Oxidation Experiments with Diesel PM

We now present results of oxidation experiments with diesel PM samples collected directly from a DPF membrane. As described earlier, the amount of SOF in diesel PM strongly depends on engine speed and load conditions, and the particulates sampled at different engine operating conditions display significant differences in morphology, which affects soot reactivity.

The diesel soot reactivity is also influenced by the oxidation temperature and duration due to their influence on the soot structure (Neeft et al., 1996; Ishiguro et al., 1991; Vander Wal et al., 2007). The gas temperature in engine exhaust can vary from 150 °C at idle to 600 °C at full load, depending on the engine and duty cycle, and the amount of SOF in the PM accumulated on the DPF membrane can vary significantly with this temperature, decreasing as the temperature is increased. Therefore, it is important to investigate the oxidation behavior of diesel PM using different heat treatments and PM samples containing different amounts of SOF.

In order to prepare a dry diesel soot sample, the diesel PM sample was first exposed to helium environment to evaporate the volatile components of SOF. As discussed earlier (cf. Fig.14 and 15), the temperature was increased to 550°C at a rate of 10°C/min, and then maintained at 550°C for 1h for the evaporation of additional SOF components from the sample. The dry diesel soot sample was then exposed to the oxidizing (air) environment under the prescribed isothermal condition. Similar to the surrogate soot experiments, the temperatures at isothermal condition were maintained at 500°C, 550°C, or 600°C. Figure 23 presents the temporal variation of instantaneous mass of diesel PM samples subjected to the above heating and oxidizing mode. The flow rates for both helium and air were set at 60ml/min, while the initial sample masses were of 4.653 mg, 4.992mg, and 4.592mg. As indicated in this figure,

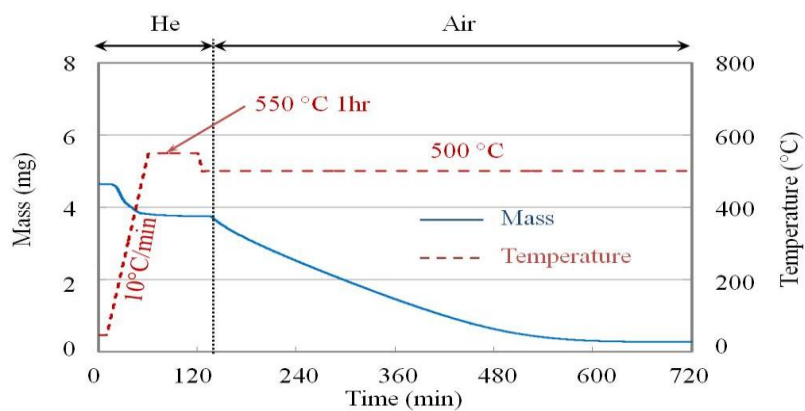
initial reduction in the PM mass is due to the evaporation of SOF components in the helium environment. Approximately 19.4%, 19.6%, and 20.0% of the initial mass was lost during this process for the three PM samples. The subsequent reduction in mass is due to the oxidation of dry diesel soot. After complete oxidation, the amounts of residues were measured to be 0.266mg, 0.612mg and 0.583mg, respectively, for the three samples.

Figure 24 plots the temporal variation of the rate of mass loss or the oxidation rate of dry diesel soot, determined from the measurement of instantaneous mass from the start of oxidation for the three isothermal temperatures. The corresponding plots for the oxidation rate of surrogate soot are also shown in the figure. As expected, there are significant differences in the oxidation behavior of dry diesel soot and surrogate soot. As helium is being replaced by air, the oxidation rate of surrogate soot increases rapidly, and subsequently decreases as the sample is oxidized. The oxidation of diesel soot also exhibits an initial transient period during which the oxidation rate increases rapidly, as helium is being replaced by air. Following this short transient period, as indicated in Fig. 24, the oxidation rate of diesel soot becomes nearly constant for a certain period and then decreases, while that of surrogate soot decreases continuously.

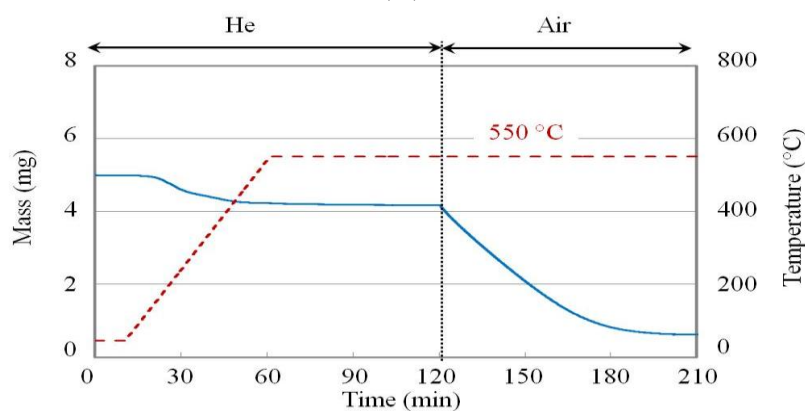
In order to gain further insight into the differences between the oxidation behavior of dry diesel soot and surrogate soot, we plot in Figure 25 their oxidation rates with respect to the instantaneous sample mass normalized by its mass at the start of oxidation. Consistent with the plots in Fig. 24, following a short transient period, the oxidation rate of surrogate soot decreases continuously as the sample mass decreases. In contrast, the oxidation rate of diesel soot is nearly independent of the instantaneous sample mass until about 80% of the mass is oxidized, and then decreases as the sample is completely oxidized. Therefore, the oxidation of diesel soot appears to be characterized by two distinct zones, which are termed here as zones 1 and 2. The transition

between the two zones is more clearly discerned for the 550°C and 600°C cases. Neeft et al. (1997) also observed a similar flat region during the oxidation of diesel soot. Thus an important observation from the present study is the significant difference in the oxidation behavior of diesel soot and surrogate soot.

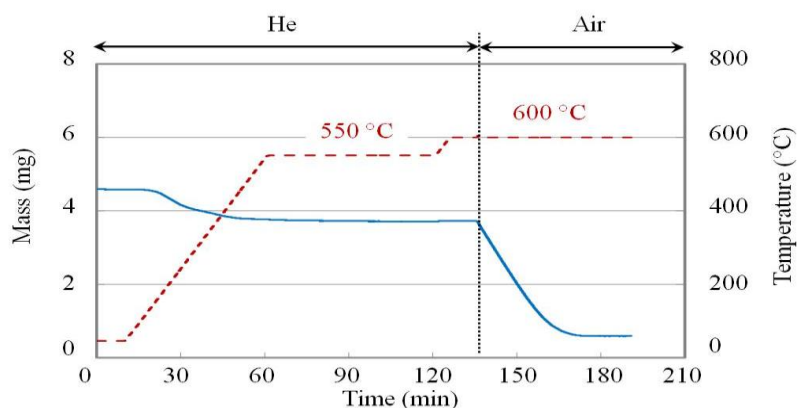
The oxidation rate of diesel soot is nearly independent of the instantaneous sample mass in zone 1 and then decreases as the sample is completely oxidized. In contrast, the surrogate soot oxidation rate decreases continuously during oxidation as the sample mass decreases. While a more in-depth description of these differences will require measurements of soot morphology and speciation, which is beyond the scope of this study, we may ascribe this behavior to several processes. These include (i) formation of surface intermediates or functional groups during heating and oxidation, which are known to enhance the diesel soot reactivity (Müller et al., 2005), (ii) presence of heavier SOF components (Collura et al. 2005), (iii) changes in soot morphology and crystallization (Vander Wal et al., 2007), and (iv) build-up of ash layer which decreases the diesel soot reactivity. Previous studies have observed these processes during diesel soot oxidation. Müller et al. (2005) reported the formation of surface functional groups, such as C=O, C-O-C, and C-OH, based on mass spectrometry measurements. Their investigation revealed the existence of different surface functional groups in diesel soot and surrogate soot, which contributed to differences in the reactivity of two soot samples. Collura et al. (2005) examined the presence of volatile and non-volatile SOF components, as well as surface function groups in the diesel PM, and discussed their effects on reactivity. Vander Wal et al. (2007) noted significant changes in diesel soot morphology during oxidation, while the surrogate soot exhibited a uniform nanostructure. Thus an important inference from these studies and our results is that the oxidation of diesel soot in zone 1 is primarily influenced by the presence of



(A)

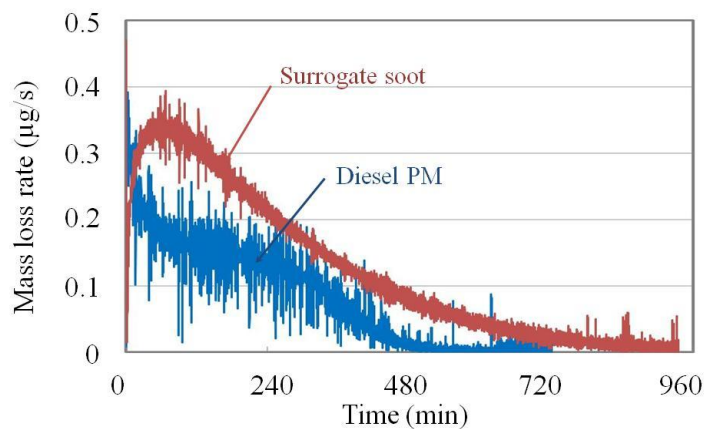


(B)

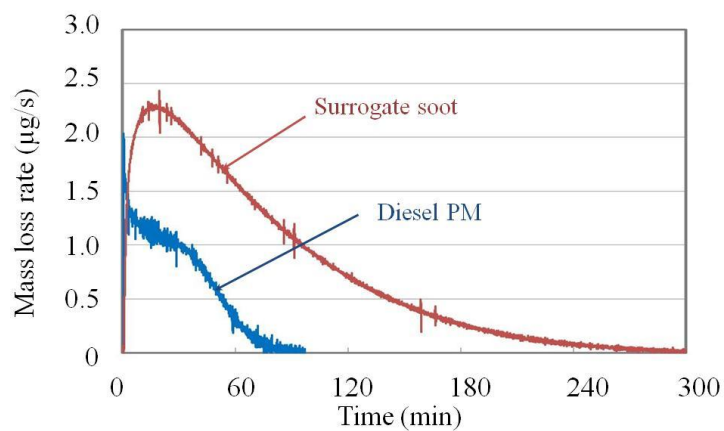


(C)

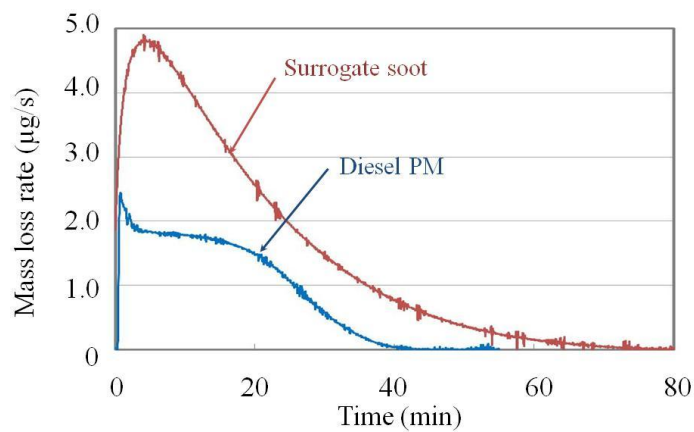
Figure 23. Instantaneous mass of diesel PM exposed to a helium environment in heating mode with temperature gradients of 10°C/min, isothermal condition for 1h at 550°C, temperature control mode to arrive at the specific isothermal temperature, and then exposed to air environment under isothermal temperatures of 500°C, 550°C, and 600°C, in Figs. 23A, B, and C, respectively. Initial sample mass and residue mass: 4.653mg and 0.266mg in (A), 4.992mg and 0.612mg in (B), and 4.592mg and 0.583mg in (C).



(A)



(B)



(C)

Figure 24. Temporal variation of the rate of mass loss during the oxidation of dry diesel soot and surrogate soot samples under isothermal temperatures of 500°C, 550°C, and 600°C, in Figs. 24A, B, and C, respectively.

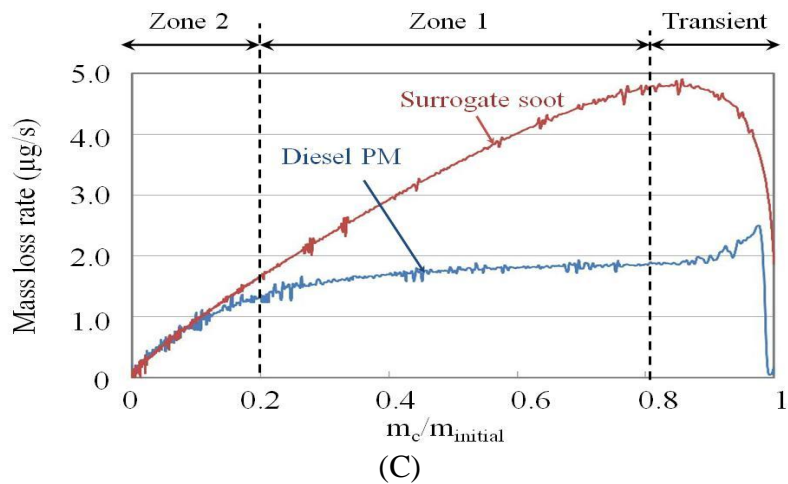
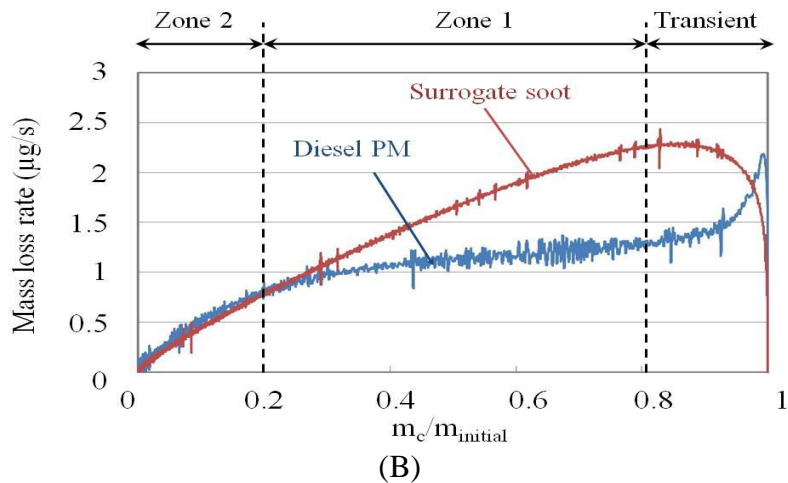
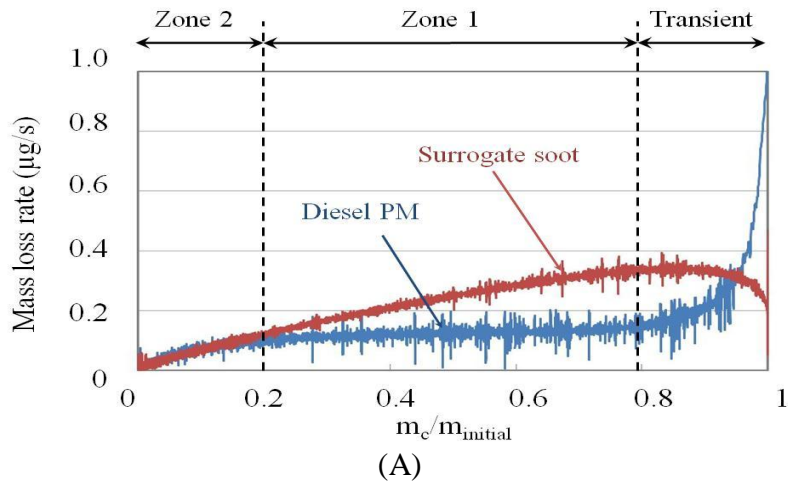


Figure 25. The rate of mass loss plotted as a function of sample mass, normalized by the initial mass of sample measured at the start of oxidation, during the oxidation of dry diesel soot and surrogate soot under isothermal temperatures of 500°C, 550°C, and 600°C, in Figs. 25A, B, and C, respectively.

surface functional groups and heavier SOF components, while that in zone 2 is more strongly affected by the presence of ash layer.

As was the case for the surrogate soot, the data in Fig. 25 were used to determine the reaction order (n_c) and activation energy (E_a) for the dry diesel soot. The logarithmic rate of mass loss, $\ln[-dm/dt]$, is plotted as a function of $\ln[m]$ in Figure 26. The reaction order is then

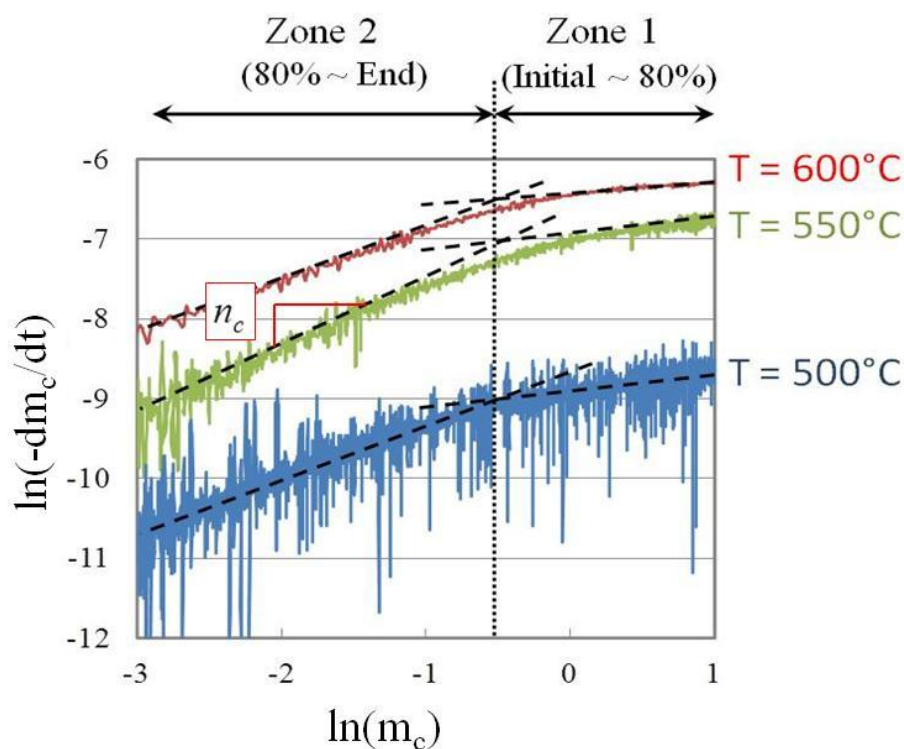


Figure 26. Logarithmic plot for the rate of mass loss of diesel PM samples as a function of $\ln[m]$ for the three isothermal temperatures of 500°C, 550°C, and 600°C. The slope yields the reaction order of soot for the diesel soot sample.

obtained from the slope of the linear regression line. As indicated, two distinct values of reaction order corresponding to zones 1 and 2 were found for each case. The reaction order (n_c) values were 0.25/0.28/0.19 in zone 1, and 0.71/0.83/0.67 in zone 2 for the three temperatures

500°C/550°C/600°C, respectively. The average values of the reaction orders can be written as 0.24 ± 0.05 and 0.74 ± 0.08 in zones 1 and 2, respectively. With these values of reaction orders, activation energy can be determined by plotting the left-hand term of Eq. (4.38) versus the inverse of temperature, as indicated in Figure 27. Again, the slope of the linear regression line yields $-E_a/R_u$, or the activation energies as $E_a=139.55$ kJ/mol and 136.26 kJ/mol in zones 1 and 2, respectively, for the diesel soot sample. The literature review (Marcuccilli et al., 1994; Otto et al., 1980; Stratakis et al., 2003) indicated a wide variation in the reported activation energy values, $E_a = 132$ to 207 kJ/mol, depending on the assumed reaction order and experimental conditions, especially the oxygen partial pressure.

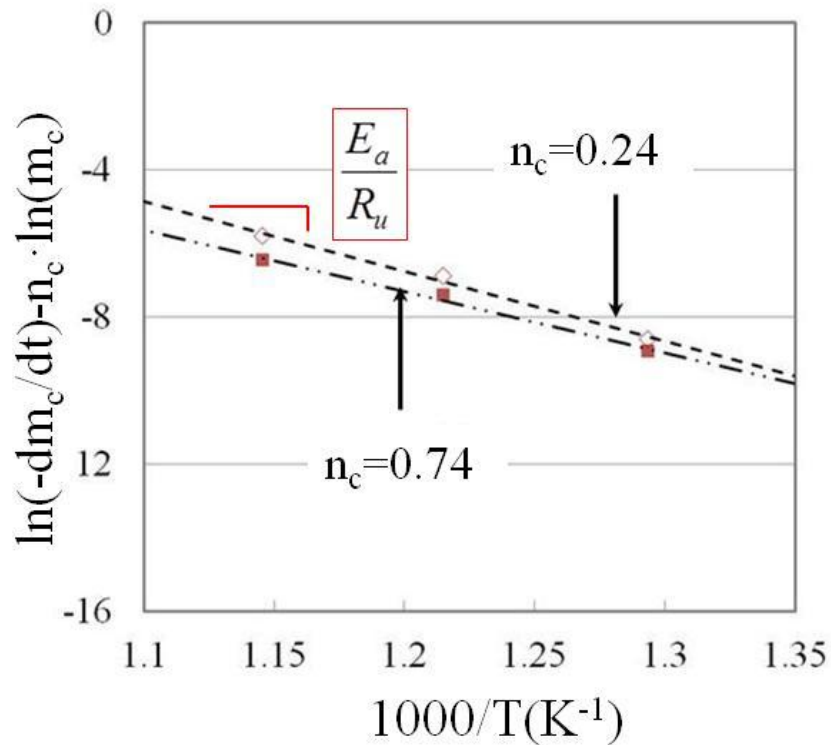


Figure 27. Evaluation of activation energy for the diesel soot sample in zones 1 and 2 using Eq. (4.38).

Similar to the surrogate soot samples, the reaction order of oxygen (n_{O_2}) and pre-exponential factor (A) were determined by conducting oxidation experiments under three different oxygen partial pressures using (i) 25% air/75% He, (ii) 60% air/40% He, and (iii) 100% air/0% He. Again the dry diesel soot samples were first exposed to helium environment in heating mode with temperature gradients of 10°C/min and then to oxidizing environment under a specific oxygen partial pressure and an isothermal temperature at 550°C. The flow rate of air-He mixture was maintained at 100 ml/min. Figure 28 plots the left-hand term of Eq. (4.38) versus $\ln[P_{O_2}]$ for zones 1 and 2.

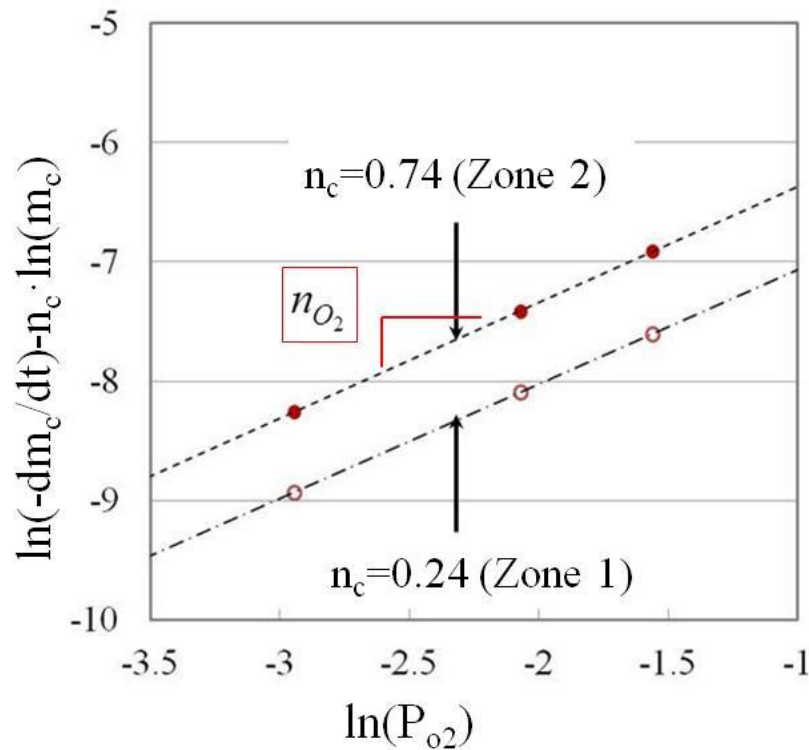


Figure 28. Evaluation of reaction order of oxygen in zones 1 and 2 for diesel soot samples subjected to different oxygen partial pressures.

Again from a linear regression analysis in each zone, the slope of the linear regression line yielded the reaction orders of oxygen as $n_{O_2} = 0.96$ and 0.97 in zones 1 and 2, respectively. Then the pre-exponential factor determined using these values of n_{O_2} and the Y-axis intercept in Fig. 12 were $A = 0.31 \times 10^7$ and 0.05×10^7 in zones 1 and 2, respectively.

4.5.3 Effect of SOF on Diesel PM Oxidation

The effect of SOF on the oxidation behavior of diesel PM was investigated by performing TGA experiments using different heat treatment schemes, as indicated in Table XIX. The first one involved heating the PM sample in helium at a rate of $100^\circ\text{C}/\text{min}$ to a specified temperature (500°C , 550°C , or 600°C), and then subjecting to oxidation at the indicated temperature. For the second scheme, the heating rate was reduced to $10^\circ\text{C}/\text{min}$, while for the third case, the sample was heated in helium at a rate of $10^\circ\text{C}/\text{min}$ to the specified temperature and then maintained at that temperature for 1 hour, prior to oxidation. Using different heat treatment schemes allowed us to vary the amount of volatile components of SOF evaporated from PM samples, and thus perform oxidation experiments with samples containing different amounts of SOF. The amounts of volatile components of SOF evaporated from the sample varied from 4.7% to 21.9% of the initial sample mass, as listed in Table XIX.

For each of the above nine cases, the kinetic parameters were determined from the measurements of the temporal variations of sample mass and rate of mass loss, as described earlier. These parameters, which include the reaction orders with respect to soot (n_c) and oxygen (n_{O_2}), the activation energy, and pre-exponential factor in both zones 1 and 2, are listed in Table XIX. An important observation from these results is that the amount of SOF in diesel PM does not have a significant effect on the oxidation behavior of diesel PM. For instance, for the three cases with

Table XIX

MEASURED AMOUNT OF EVAPORATED VOLATILE COMPONENTS OF SOF, REACTION ORDER WITH RESPECT TO SOOT AND OXYGEN, ACTIVATION ENERGY AND PRE-EXPONENTIAL FACTOR FOR DIESEL PM SAMPLES SUBJECTED TO DIFFERENT HEAT TREATMENTS.

Heating & Flue gas conditions	He	Heating rate (°C/min)	100			10			10		
		Isothermal period at 550 °C (Hr)	-			-			1		
	Air	Oxidation temperature (°C)	500	550	600	500	550	600	500	550	600
Amount of evaporated volatile components of SOF (% of mass)			4.7	7.1	13.1	12.1	16.5	21.9	19.4	19.6	20.0
n_c	Zone1	0.3	0.29	0.18	0.24	0.29	0.19	0.25	0.28	0.19	
	Zone2	0.72	0.87	0.68	0.72	0.87	0.64	0.71	0.83	0.67	
n_{O_2}	Zone1	0.95			0.95			0.96			
	Zone2	0.97			0.96			0.97			
E_a (kJ/mol)	Zone1	139.1			136.8			139.6			
	Zone2	133.1			129.5			136.3			
A (1/sec)	Zone1	0.68×10^7			0.21×10^7			0.31×10^7			
	Zone2	0.18×10^7			0.1×10^7			0.05×10^7			

oxidation at 500°C, the reaction orders of soot (n_c) in zones 1 and 2 are 0.3/0.24/0.25 and 0.72/0.87/0.67, respectively, for diesel PM samples with evaporated volatile components as

4.7%, 12.1%, and 19.4%, respectively. The variation in n_c for oxidation at higher temperatures (550°C and 600°C) is even smaller. The corresponding variation in n_{O_2} with respect to the heat treatment scheme or SOF is also negligibly small. Similarly, the activation energy exhibits a relatively small variation with respect to the amount of SOF in diesel PM; for the three heat treatment schemes, the values of E_a are 139.1 kJ/mol, 136.8kJ/mol, and 139.6kJ/mol in zone 1, and 133.1 kJ/mol, 129.5kJ/mol, and 136.3kJ/mol in zone 2, respectively. The pre-exponential factors, however, exhibit more noticeable variation, with values ranging from 0.21×10^7 to 0.68×10^7 (1/s) in zone 1, and from 0.05×10^7 to 0.18×10^7 (1/s) in zone 2, depending upon the heat treatment scheme.

Thus an important result from the present study is that the kinetic parameters for the oxidation of diesel PM are only weakly influenced by the presence of SOF. This is further illustrated by plotting in Figure 29 the rate of mass loss for the sample subjected three different heat treatments, and then oxidized at the isothermal temperature of 600°C. The oxidation rate profiles for the three heat treatments schemes are essentially the same, although there are some quantitative differences, which are also reflected in the values of the pre-exponential factors.

4.5.4 Effect of Thermal Aging on Diesel PM Oxidation

It has been known that the oxidation behavior of diesel PM is strongly influenced by the soot graphitic structure. Vander Wal et al. (2006) and Su et al. (2004) observed the interior structure of diesel soot to be hollow and disorderly, when exposed to exhaust gas containing oxygen in the temperature range of 150-600°C, and its oxidation rate was higher than that of the ordered diesel soot with no hollow structure. Moreover, thermal aging at 700°C was observed to cause the soot structure to become more graphitic. Müller et al. (2005) also examined the

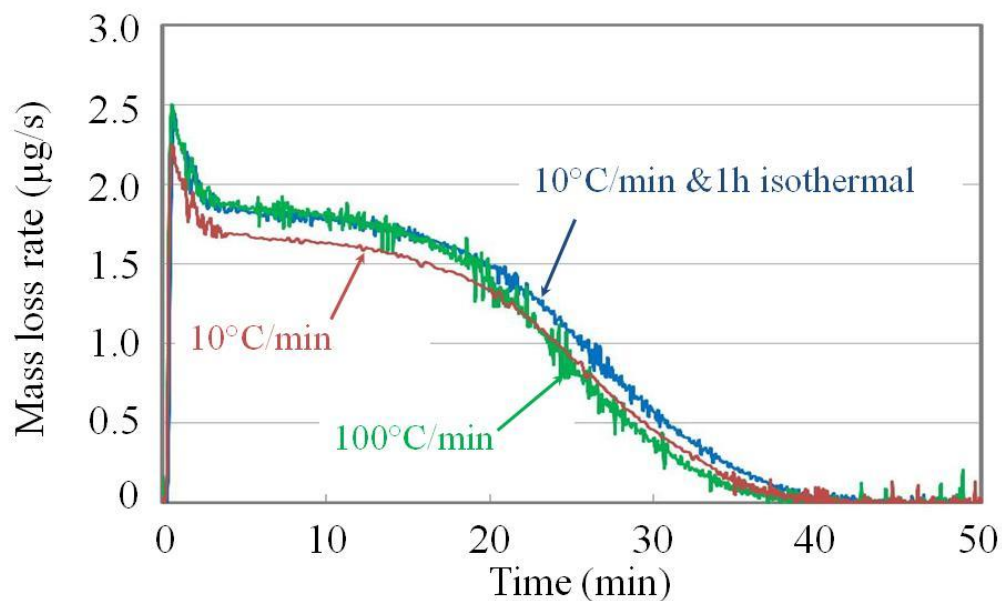
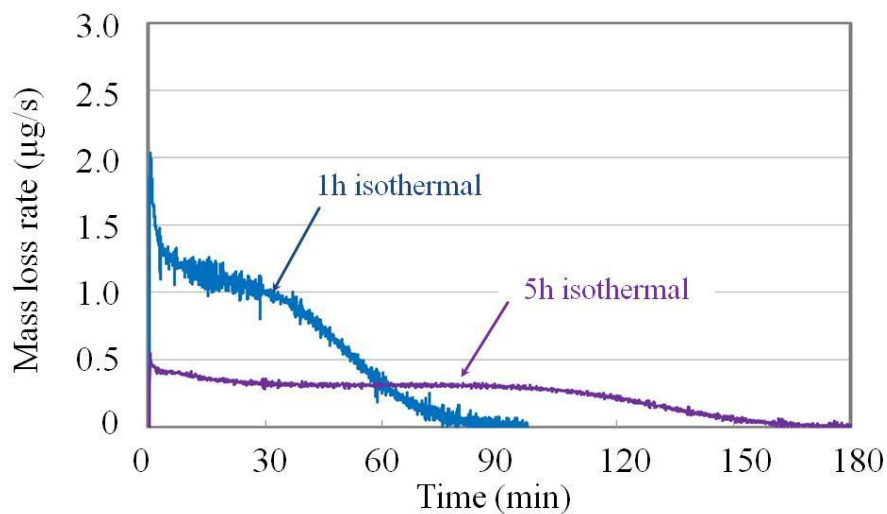


Figure 29. Temporal variation of the rate of mass loss during the oxidation of diesel PM samples subjected to three different heat treatments with heating rates of 100°C/min, 10°C/min, and 1 h isothermal period at 550°C in helium, followed by oxidation at isothermal temperature of 600°C. Initial sample mass and residue mass: 4.317mg and 0.155mg for experiment with the heating rate of 100°C/min; and 4.086mg and 0.312mg for 10°C/min, and 4.592mg and 0.583mg for 1h isothermal.

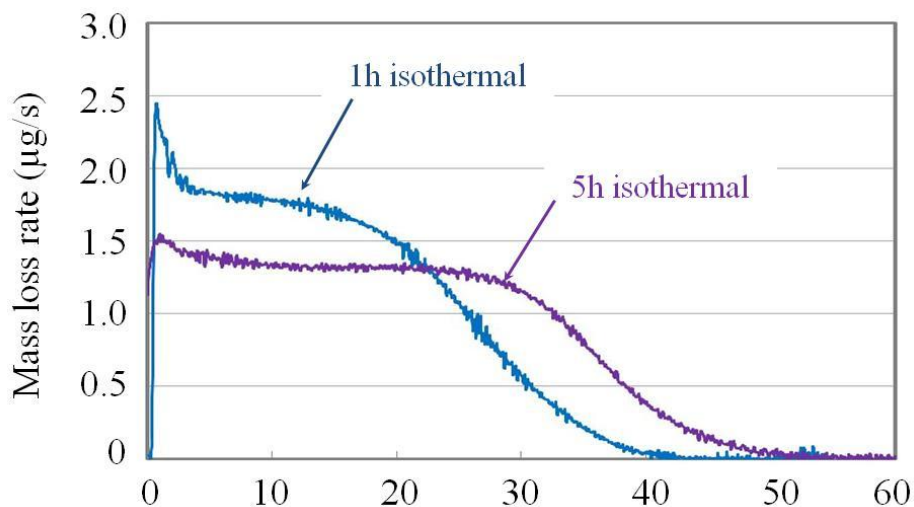
reactivity of soot with respect to the amount of graphitization, and observed reduced reactivity with increased graphitization or more orderly structure.

The effect of thermal aging on the oxidation behavior of diesel PM is depicted in Figure 30, which compares the rate of mass loss for the two samples subjected to different heat treatments, followed by oxidation at temperatures of 550°C and 600°C. As indicated in Table XX, the two heat treatments prior to oxidation consisted of heating the samples to a temperature of 550°C at a rate of 10°C/min and maintaining this temperature in helium for 1 hour and 5 hours. For both cases, the kinetic parameters were determined using the same methodology as described earlier, and the values are also listed in Table XX. As indicated in Fig. 30, the diesel soot reactivity or

the oxidation rate is significantly reduced due to thermal aging, which is expected to make the soot structure more graphitic.



(A)



(B)

Figure 30. Temporal variation of the rate of mass loss during the oxidation of two diesel PM samples subjected to heat treatments of 1 h and 5 h isothermal period in helium environment, respectively, prior to oxidation at temperatures of 550°C and 600°C in Figs. 30A and B. Initial sample mass and residue mass: For 1 h isothermal, 4.992mg and 0.612mg in (A), and 4.592mg and 0.583mg in (B). For 5 h isothermal, 3.848mg and 0.415 mg in (A), and 4.286mg and 0.412 mg for 5h in (B).

Table XX

MEASURED AMOUNT OF EVAPORATED VOLATILE COMPONENTS OF SOF, REACTION ORDER WITH RESPECT TO SOOT AND OXYGEN, ACTIVATION ENERGY AND PRE-EXPONENTIAL FACTOR FOR DIESEL PM SAMPLES EXPOSED TO HELIUM ENVIRONMENT FOR 1 HOUR AND 5 HOURS AT 550 °C, PRIOR TO OXIDATION.

Heating & Flue gas conditions	He	Heating rate (°C/min)	10			10		
		Isothermal period at 550 °C (Hr)	1			5		
	Air	Oxidation temperature (°C)	500	550	600	500	550	600
Amount of evaporated volatile components of SOF (% of mass)			19.4	19.6	20.0	23.0	22.9	21.8
n_c	Zone1	0.25	0.28	0.19	0.05	0.08	0.09	
	Zone2	0.71	0.83	0.67	0.77	0.75	0.78	
n_{O_2}	Zone1	0.96			0.96			
	Zone2	0.97			0.97			
E_a (kJ/mol)	Zone1	139.5			153.1			
	Zone2	136.3			155.1			
A (1/sec)	Zone1	0.31×10^7			1.27×10^7			
	Zone2	0.05×10^7			1.28×10^7			

Moreover, as expected, the effect of thermal aging on soot oxidation is mostly observed in zone 1. These observations are further confirmed by the comparison of kinetic parameters for the two samples in Table XX. For instance, the reaction order of diesel soot in zone 1 decreases

on an average from 0.26 to 0.08 in zone 1, while the activation energy is increased from 139.6 to 153.1kJ/mol, as the isothermal period is increased from 1 hour to 5 hours. It is important to note that the amounts of volatile SOF evaporated are nearly the same for the two samples, indicating that the effect on the oxidation rate is primarily due to thermal aging. Therefore, an important result here is that the kinetic parameters associated with the oxidation of diesel PM are strongly influenced by the thermal aging, showing reduced reactivity with thermal aging.

Results presented so far pertain to oxidation experiments for diesel PM samples subjected to heat treatment in helium environment prior to oxidation. However, in practical DPF regeneration systems, the diesel PM is exposed to exhaust gas emissions containing oxygen, in which the evaporation/oxidation of volatile components of SOF occur simultaneously with the oxidation of soot. In order to simulate such a scenario, oxidation experiments were also performed with the diesel PM subjected to heating in air environment. The heating mode involved a ramp rate of 10°C/min and the isothermal condition at 500°C, 550°C, or 600°C, as also indicated in Table XXI.

Figure 31 presents the temporal variation of instantaneous mass and rate of mass loss of diesel PM samples for the above case. The initial sample masses were 5.41mg, 5.26mg and 6.86mg, while the residue masses after complete PM oxidation were 0.593mg, 0.37mg and 0.367mg. Also during the heat-up period, the reductions in mass due to evaporation/oxidation of SOF components were 23.0%, 22.9%, and 21.8%, respectively. Similar to our previous study (Chong et al., 2011) concerning the heat release of SOF-containing diesel PM, the oxidation of SOF-containing diesel PM samples exhibits two peaks in the mass loss rate profiles. The first peak near $t=30$ min is due to the evaporation/oxidation of SOF components because of the relatively low temperature, while the second peak near $t=60$ min corresponds to the oxidation of

soot. Using the methodology as described earlier, the data in Fig. 31 were used to extract the oxidation rate parameters, which are in Table XXI. The corresponding values for the sample subjected to heating in the helium environment are listed in this table. The comparison indicates that exposing the sample directly to oxidation during the heating period decreases the overall oxidation rate, as illustrated by the activation energy, which is 150.0 kJ/mol compared to a value of 136.8 kJ/mol for the sample heated in an inert environment.

Table XXI

MEASURED KINETIC PARAMETERS (REACTION ORDERS WITH RESPECT TO SOOT AND OXYGEN, ACTIVATION ENERGY, AND PRE-EXPONENTIAL FACTOR) FOR DIESEL PM SAMPLES EXPOSED TO HELIUM AND AIR ENVIRONMENT DURING HEAT TREATMENT WITH A HEATING RATE OF 10 °C/MIN.

Heating & Flue gas conditions	Heat-up		He			Air		
	Air	Oxidation temperature (°C)	500	550	600	500	550	600
n_c	Zone1		0.24	0.29	0.19	0.25	0.1	0.15
	Zone2		0.72	0.87	0.64	0.72	0.87	0.74
n_{O_2}	Zone1		0.95			0.96		
	Zone2		0.96			0.96		
E_a (kJ/mol)	Zone1		136.8			150.0		
	Zone2		129.5			142.5		
A (1/sec)	Zone1		0.21×10^7			1.6×10^7		
	Zone2		0.1×10^7			0.8×10^7		

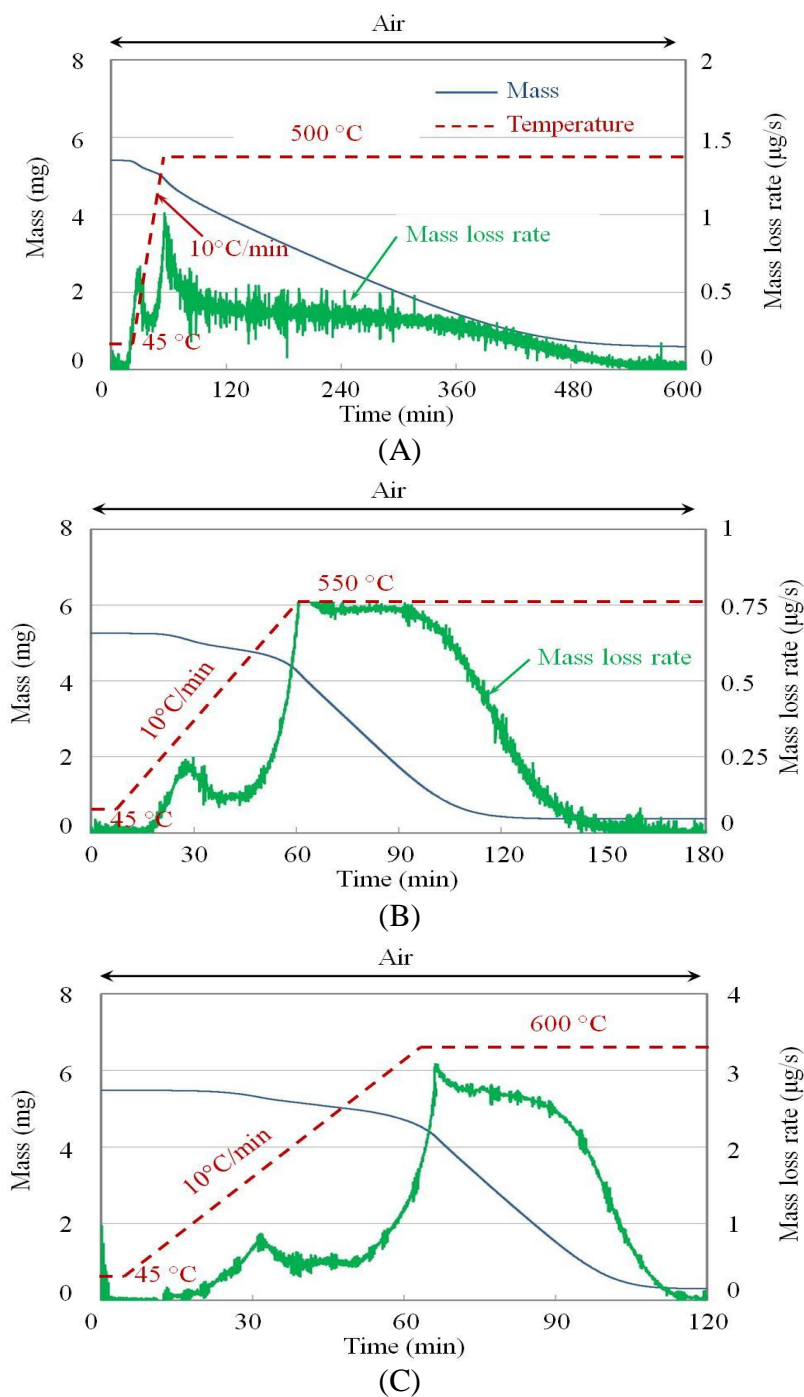


Figure 31. Instantaneous mass and rate of mass loss (oxidation rate) of diesel PM samples exposed to air environment in heating mode with ramp rate of 10 °C/min, followed by isothermal condition at temperatures 500 °C, 550 °C, and 600 °C in Figs. 31A, B, and C, respectively. Initial sample mass and residue mass: 5.41 mg and 0.593 mg in (A), 5.26 mg and 0.372 mg in (B), and 6.861 mg and 0.367 mg in (C).

Suuberg et al. (1989) observed that the surface area of the carbon decreases with increasing aging temperature and exposure time in an oxygen environment. Therefore, it may be speculated that the thermal aging of diesel PM in air may cause loss of surface area and rearrangement of graphitic structure, and thereby the increase in activation energy and reduction in the oxidation rate.

Finally, Table XXII summarizes the kinetic parameters for the oxidation of surrogate soot and diesel PM samples subjected to different heat treatments, followed by oxidation at 550°C. The important observation is that there are significant differences between the oxidation characteristics of surrogate soot and diesel PM. While the oxidation of surrogate soot is characterized by having a single zone, that of diesel PM occurs in two distinct zones. In addition, the kinetic parameters for surrogate soot are essentially independent of the heat treatment schemes, while the oxidation of diesel PM is strongly affected by not the amount of SOF components but the heat treatment schemes.

4.6 Conclusion

In this chapter, we described a detailed experimental study on the oxidation of diesel PM collected from a DPF test system, which was connected to the exhaust stream of a 1.9-L, 4-cylinder light-duty diesel engine. A TGA set-up was used to measure the instantaneous sample mass and the rate of mass loss during its oxidation for a wide range of conditions, which included the initial sample mass, amount of volatile components of SOF in the sample, oxygen concentration, and different heat treatment schemes in both the inert and oxidizing environments. The global kinetic parameters, which include the reaction orders with respect to soot (n_c) and oxygen (n_{o_2}), activation energy (E_a), and pre-exponential factor (A), were determined for both

the diesel PM and surrogate soot samples. The effects of SOF and thermal aging on diesel PM oxidation have also been characterized. Important observations follow.

Table XXII

COMPARISON OF THE KINETIC PARAMETERS FOR THE OXIDATION OF SURROGATE SOOT AND DIESEL PM SAMPLES AT 550 °C WITH DIFFERENT HEAT TREATMENTS.

Sample	kinetics parameters		Heat treatment scheme for evaporation of SOF volatile contents in the sample		
			Heating rate	Isothermal period	Oxidation during heat-up (No helium used)
			100 °C/min	5 hr	
Surrogate soot	n_c		0.8	0.77	0.81
	E_a (kJ/mol)		145.2	149.1	148.1
	n_{O_2}		0.95	0.95	0.74
	A (1/sec)		2.49×10^6	4.54×10^6	3.78×10^6
Diesel PM	n_c	Zone1	0.29	0.08	0.1
		Zone2	0.87	0.75	0.87
	E_a (kJ/mol)	Zone1	139.1	153.1	150.0
		Zone2	133.1	155.1	142.5
	n_{O_2}	Zone1	0.95	0.96	0.96
		Zone2	0.97	0.97	0.96
	A (1/sec)	Zone1	0.68×10^7	1.27×10^7	1.6×10^7
		Zone2	0.18×10^7	1.28×10^7	0.8×10^7

There are significant differences in the oxidation characteristics of diesel PM and surrogate soot. The oxidation behavior of surrogate soot is essentially independent of the various heat treatments and other conditions, while that of diesel soot is strongly influenced by them. For instance, the reaction order of surrogate soot varied in a narrow range of 0.78-0.8, where the diesel soot reaction order had a range of 0.05-0.9, depending upon the test conditions. Similarly, the activation energy range was 145-149 kJ/mol for the surrogate soot, and 130-155 kJ/mol for the diesel soot.

The oxidation of surrogate soot can be characterized by a single zone in which the oxidation rate decreases monotonically as the soot is oxidized. In contrast, the oxidation of diesel soot appears to be characterized by two distinct zones, with the oxidation rate being nearly constant (independent of the instantaneous sample mass) until about 80% of the mass is oxidized (zone 1), and then decreasing continuously as the sample is completely oxidized. Based on the previously reported studies and our data, we may attribute these differences to several processes, including the formation of surface functional groups, presence of heavier SOF components, changes in soot morphology, and build-up of ash layer during the heating and oxidation of diesel soot. Thus an important result from our study is that the data obtained from the oxidation of surrogate soot may not be used for characterizing the oxidation behavior of diesel soot.

The oxidation characteristics of diesel PM are only weakly influenced by the presence of the volatile components of SOF. However, the presence of heavier SOF components and thermal aging seem to have a strong influence on diesel soot oxidation. The diesel soot reactivity is observed to decrease with thermal aging. For example, as the isothermal period in inert environment was increased from 1 to 5 h, the activation energy increased from 139 to 153 kJ/mol, while the soot reaction order reduced from 0.25 to 0.05. The effect of thermal aging

qualitatively provides a measure of differences between the oxidation characteristics of samples collected from the DPF and those collected from the exhaust pipe.

In this work, we have obtained fairly reliable data that may be used for more detailed modeling of diesel soot oxidation. Future studies will focus on characterizing the oxidation behavior of diesel PM in the presence of catalysts and in different oxidizing environments. We have reported that the oxidation of diesel PM is significantly influenced by thermal aging, as described earlier, which corresponds to the experiment result of diesel PM subjected to a wide range of temperature during a certain period under the exhaust gas containing various gas phase chemical components. While we did not investigate the thermal properties of diesel PM collected from the exhaust pipe, the short exposure of PM to exhaust gas leads to weak effect of thermal aging on the diesel PM. Indeed, our experiment result shows that the activation energy of thermally aged diesel PM during 1 hour is lower compared to that during 5 hours, indicating faster oxidation rate. Therefore, the detail investigation on the characterization of oxidation behavior of diesel PM collected from the DPF can provide more relevant information for designing optimum DPF regeneration algorithms. Future studies will focus on characterizing the oxidation behavior of diesel PM in the presence of catalysts and in different oxidizing environments.

CHAPTER 5

MODELING OF HEAT RELEASE RATE

5.1 Introduction

In chapters 3 and 4, oxidation experiments with the diesel PM and surrogate soot subjected to various heat treatments were discussed. A DSC was used to measure the instantaneous heat release during soot oxidation under specified temperature profiles in air, while a TGA was used to measure the amount of volatile components of SOF in soot samples and also to determine the kinetic parameters for diesel PM oxidation relevant DPF regeneration. As described in chapter 3, the DSC mainly measures the amount of heat generated by a given sample undergoing oxidation in flowing gas. In our study, a sample was placed in the reaction chamber of DSC and TGA, and subjected to a specific temperature profile in an air environment. During the oxidation experiment, the temperature of reaction chamber was precisely controlled.

In general, exhaust gas emissions from the engine enter the filter, and then flow through the porous wall of the channel. The soot particles are deposited at the filter surface and inside the porous material, while gaseous emissions flow through the porous wall. The soot particles accumulated over time form a soot cake on the filter surface. As PM oxidizes, the heat dissipated from the accumulated PM layer (i.e. soot cake) is transferred to the exhaust gas directly and indirectly through the soot cake and the channel wall in DPF. This can increase the temperatures of exhaust gas and channel wall, leading to temperatures exceeding the DPF melting temperature. Therefore, the distribution of thermal energy released in regeneration needs to be monitored with care. In Chapter 5, we evaluated the heat release during the soot oxidation, based on the detailed oxidation information, such as total specific heat release and kinetic parameters.

5.2 Modeling of the Heat Release Rate

The heat release rate during soot oxidation under the isothermal condition can be written as follows:

$$(-r)H = q_t + m_c C_{p,s} \frac{\Delta T_s}{\Delta t} \quad (5.1)$$

Here, r is the soot oxidation rate [mg/s], H is the total specific heat release [kJ/mg], q_t is the instantaneous heat release during the soot oxidation [kJ/s], m_c is the soot mass [mg], $C_{p,s}$ is the mass-based heat capacity of soot [kJ/mg·K], T_s is the soot temperature [K], and t is time [s].

Since the soot oxidation rate is defined as

$$-r = A \cdot \exp\left(-\frac{E_a}{R_u \cdot T}\right) \cdot [m_c]^{n_c} \cdot [P_{O_2}]^{n_{O_2}} \quad (5.2)$$

Eq. (5.1) can be rewritten as

$$q_t = H \cdot A \cdot \exp\left(-\frac{E_a}{R_u \cdot T}\right) \cdot [m_c]^{n_c} \cdot [P_{O_2}]^{n_{O_2}} - m_c C_{p,s} \frac{\Delta T}{\Delta t} \quad (5.3)$$

Figure 32 illustrates the schematic apparatus of the DSC used to the oxidation experiment, and its specifications and experiment conditions are presented in Table XXIII. The soot samples were directly exposed to oxidizing environment during the heating mode to measure the heat release rate during the soot oxidation.

With assuming one-dimensional heat conduction and convection problem, heat dissipated in the soot sample is transferred to the air directly from the soot surface and indirectly through the sample pan and the temperature sensor in the sample platform at the DSC. Performing an energy balance on the soot, it follows that, on the basis of a unit surface area,

$$q_t'' = q_1'' + q_2'' \quad (5.4)$$

where q_t'' is the instantaneous heat released during the soot oxidation, q_1'' and q_2'' are the rates of heat transferred to the temperature sensor and the air, respectively.

Since the DSC mainly measures the heat transferred from the soot to the temperature sensor, the measured heat release rate, q_1'' , can be of form on the unit surface area

$$q_1'' = \frac{T_s - T_f}{R_{t,c}'' + (L/k)} \quad (5.5)$$

where, T_s is the soot temperature, T_f is the furnace temperature, $R_{t,c}''$ is the thermal resistance of interface between sample pan and temperature sensor, L is the thickness of pan (0.2 mm), k is the thermal conductivity of pan. Since aluminum-Alloy 195 with 4.5%Cu is known to be the material for the DSC pan, the thermal conductivity is assumed to be 168.7 W/m·K.

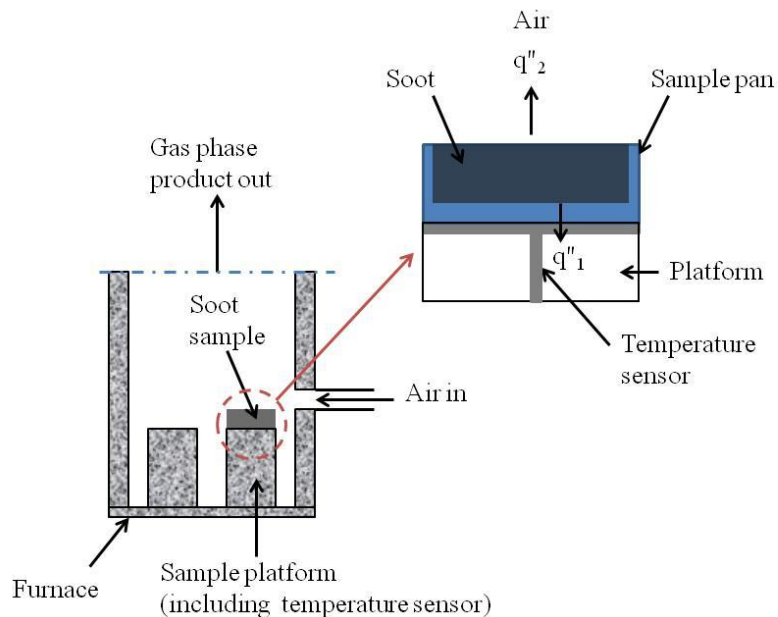


Figure 32. A schematic of differential scanning calorimeter (DSC) and heat dissipation from the soot to the platform and the air.

Table XXIII

DSC SPECIFICATIONS AND OXIDATION EXPERIMENT CONDITION.

DSC manufacturer	TA instrument
Crucible dimension (diameter x height)	$(3 \times 2)10^{-3}$ m
Heating rate accuracy	± 0.1 °C/min
Isothermal stability	0.1 °C
Isothermal temperature accuracy	1 °C
Heating rate	10 °C/min
Max. temperature	550°C
Flue gas & flow rate	Air, 60 ml/min

Thus the soot temperature during the oxidation can be rewritten as

$$T_s = T_f + q_1'' \left\{ R_{t,c}'' + (L/k) \right\} \quad (5.6)$$

The heat flux from the soot to the air during the oxidation, q_2'' , becomes

$$q_2'' = \bar{h}_a (T_s - T_f) + \varepsilon \sigma (T_s^4 - T_f^4) \quad (5.7)$$

where, \bar{h}_a the average convection coefficient [W/(m²·K)], ε is the emissivity (0.7), σ is the Stefan-Boltzmann constant (5.67×10^{-8} W/m²·K⁴).

Table XXIV presents the thermophysical properties of air at 550°C and atmospheric pressure, such as the kinematic viscosity of air, the thermal conductivity, and the Prantle number.

With these given values, the Reynolds numbers can be given as

$$\text{Re} = \frac{u_x \cdot l}{\nu} \quad (5.8)$$

where, Re is the Reynolds number, l the characteristic length, u_x the air flow velocity [m/s], ν the kinematic viscosity of air [m²/s]. Since Reynolds number is evaluated to be 1.12, the air flow can be assumed to be laminar over the entire soot surface. Thus, the average Nusselt number and the average convection coefficient can be evaluated with the following equations as

$$\bar{N}_u = 0.664(\text{Re})^{1/2} (\text{Pr})^{1/3} \quad (5.9)$$

$$\bar{h}_{air} = \frac{\bar{N}_u \cdot k}{l} \quad (5.10)$$

TABLE XXIV

THERMOPHYSICAL PROPERTIES OF AIR AT 550°C AND ATMOSPHERIC PRESSURE

Temperature (°C)	ν (m ² /s)	k (W/m·K)	Pr
550	89.04×10 ⁻⁶	58.37×10 ⁻³	0.712

Here, \bar{N}_u the average Nusselt number, Pr the Prantl number, \bar{h}_a the average convection coefficient [W/(m²·K)], k the thermal conductivity of air. The estimated average convection coefficient is 12.2 W/(m²·K) for 550°C.

5.3 Result and Discussion

Figure 33 depicts the instantaneous heat flow rate of dry surrogate soot samples subjected to a specific temperature profile in helium, and the baseline determined for the data. After the complete evaporation of volatile components in each soot sample, as described in Chapter 3, the soot samples were exposed to helium under the specific temperature profile consisting of two isothermal modes at 45°C to 550°C for 10 minutes and one progressive temperature mode from 45°C to 550°C at a constant heating rate of 10°C/min. Prior to increasing temperature, the DSC was stabilized at 45°C for 10 minutes to eliminate small data fluctuations detected. As noted earlier, the maximum temperature of DSC is 550°C. The heat flow rate curves for three cases, i.e., 6.831mg in sample#1, 6.685mg in sample#2, and 6.525mg in sample#3, indicate the endothermic processes associated with the heating of the sample during the increase of temperature.

For each surrogate soot sample, the specific heat was evaluated as

$$c_{p,s} = \left(\frac{dH}{dt} \right) \times \frac{1}{m_{c,o} (dT/dt)} \quad (5.11)$$

where dH/dt denotes the heat flow rate measured by the DSC [mW], $m_{c,o}$ is the initial mass of soot sample [mg], dT/dt is the temperature increase rate of soot sample [K/s].

Figure 34 shows the heat capacity in the temperature range of 45°C and 550°C for all surrogate soot samples using Eq. (5.11), average values at each temperature, the specific heat function obtained by linear regression analysis for the average data, and a standard National Bureau of Standards (NBS) graphite reference data. As indicated in this figure, the specific heat capacity for surrogate soot is quite similar to the data for pure graphite measured by NBS. Furthermore, this result is also noted that the magnitude of data for the specific heat capacity of surrogate soot is very similar among the three samples, suggesting a good repeatability in

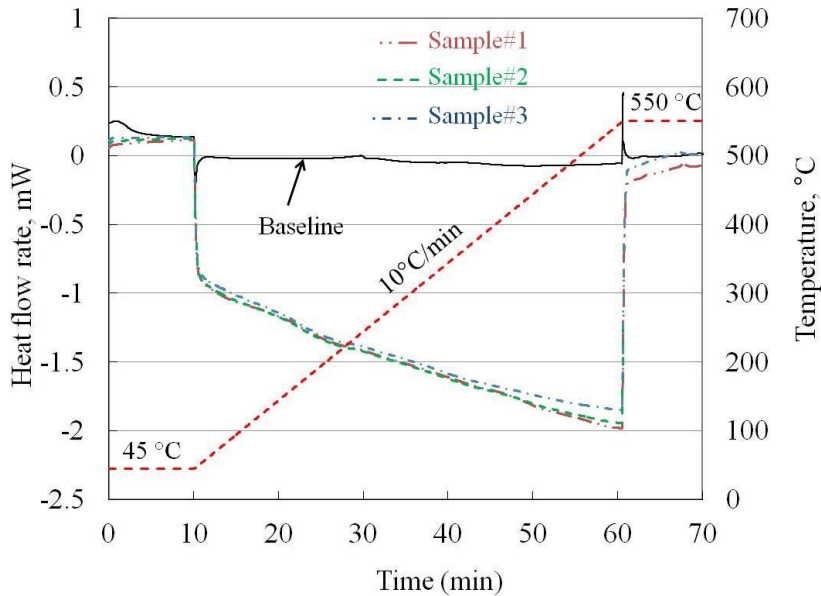


Figure 33. Instantaneous heat flow rate of dry surrogate soot samples subjected to a specific temperature profile in helium, and the baseline determined for the data. Initial sample mass: 6.831mg in sample#1, 6.685mg in sample#2, and 6.525mg in sample#3.

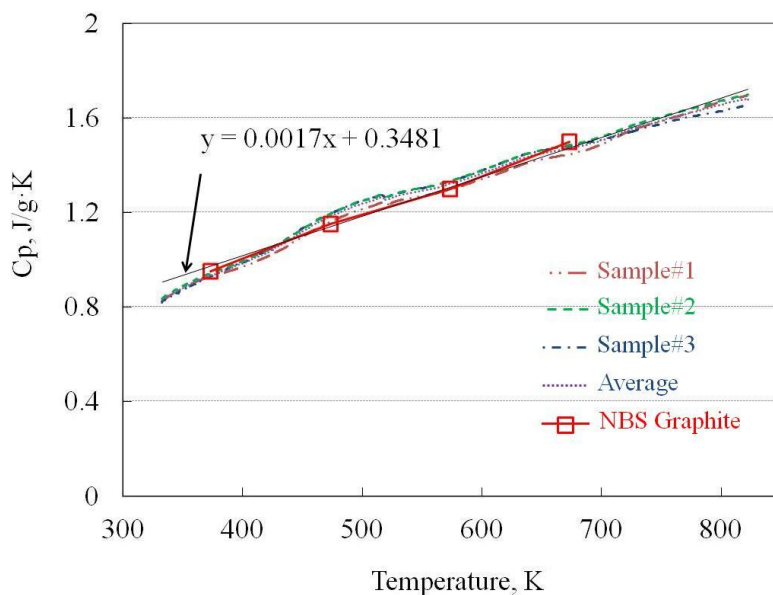


Figure 34. Evaluated heat capacity in the temperature range of 318K(45°C) and 823K(550°C) for all surrogate soot samples using Eq. (5.11), average values at each temperature, the specific heat function obtained by linear regression analysis for the average data, and a standard NBS graphite reference data. Initial sample mass: 6.831mg in sample#1, 6.685mg in sample#2, and 6.525mg in sample#3.

measurement. The specific heat capacity function for surrogate soot can be represented by expression of form

$$c_{p,s} = 0.3481 + 0.0017T(^{\circ}K) \quad (5.12)$$

Figure 35 represents temporal variation of the instantaneous heat release rate for the surrogate soot sample exposed to helium environment in heating mode with temperature gradient of 10°C/min, then maintained at an isothermal temperature of 550°C for 10 min., and then to oxidizing (air) environment at temperatures 550°C.

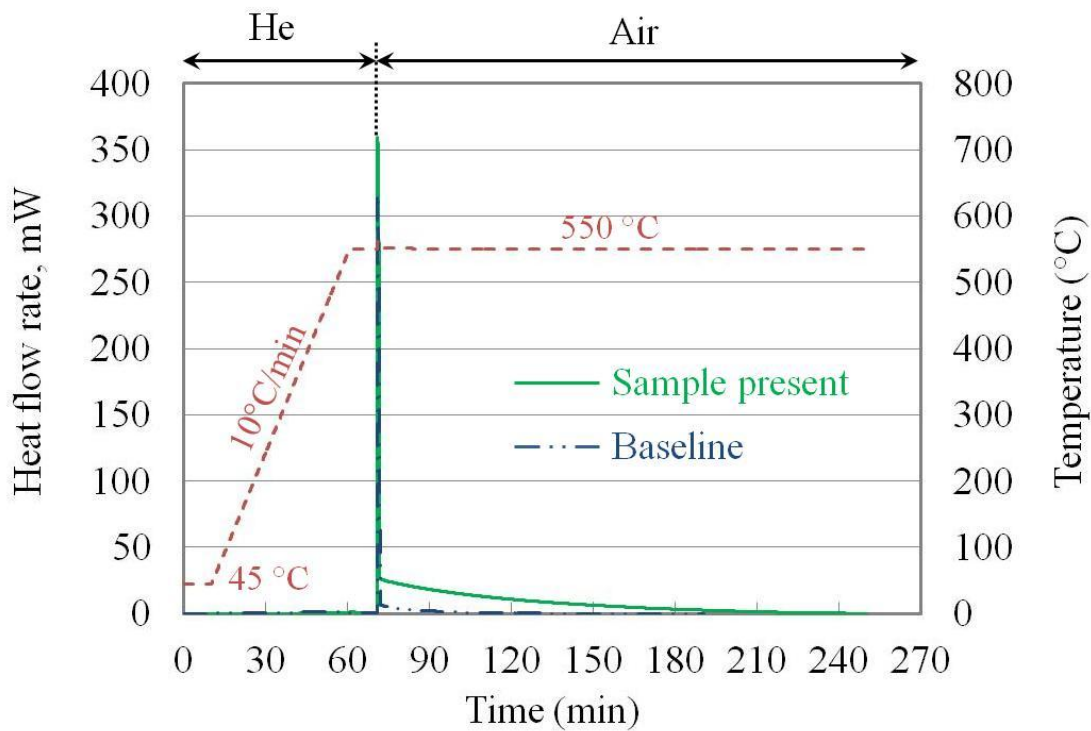


Figure 35. Temporal variation of the instantaneous mass for the surrogate soot sample exposed to helium environment in heating mode with temperature gradient of 10°C/min, then maintained at an isothermal temperature of 550°C for 10 min., and then to oxidizing (air) environment at temperatures 550°C. Initial sample mass: 5.786 mg.

Similar to the TGA oxidation experiment, high purity helium gas flow was used to provide an inert environment to suppress chemical reactions during the heat-up mode. The flow rates of both helium and air were set at 60ml/min. The oxidation experiments were performed with surrogate soot samples of 5.786 mg. The heat release rate rapidly increases and decreases, as helium is being replaced by air, and then gradually decreases as the sample is oxidized. To investigate whether the initial peak is due to the soot oxidation or the change of temperature profile, we established the base line with no sample present. And then the soot sample was exposed to helium environment under the same temperature profile, then maintained at an isothermal temperature of 550°C for 10 min., and then to nitrogen environment at temperatures 550°C. As seen in this figure, the peak is also clearly shown in the heat flow rate curve of baseline, indicating measurement errors associated with the replacement of helium/air. Thus the data during the first increase and decrease is excluded, in performing the comparison of data between calculation with the model and experiment. From this experiment, the amount of heat release per unit mass was evaluated to be 14kJ/g, which is in a good agreement with the value reported previously.

Figure 36 represents the temporal distribution of heat flux transferred to the temperature sensor and the air and the total heat flux to both the air and temperature sensor during the oxidation of surrogate soot in the isothermal temperature at 550°C in the DSC. This figure shows that total heat released from the soot is mainly transferred to the temperature sensor by the conduction, rather than to the air by the convection. In the real condition, the oxygen is supplied by forced convection during DPF regeneration. Thus the total heat in the real DPF regeneration condition is also significantly influenced by heat transferred by the convection. While a more in-

depth description of the effects of convection on the total heat and oxidation behavior of soot is necessary, this investigation is beyond the scope of this study.

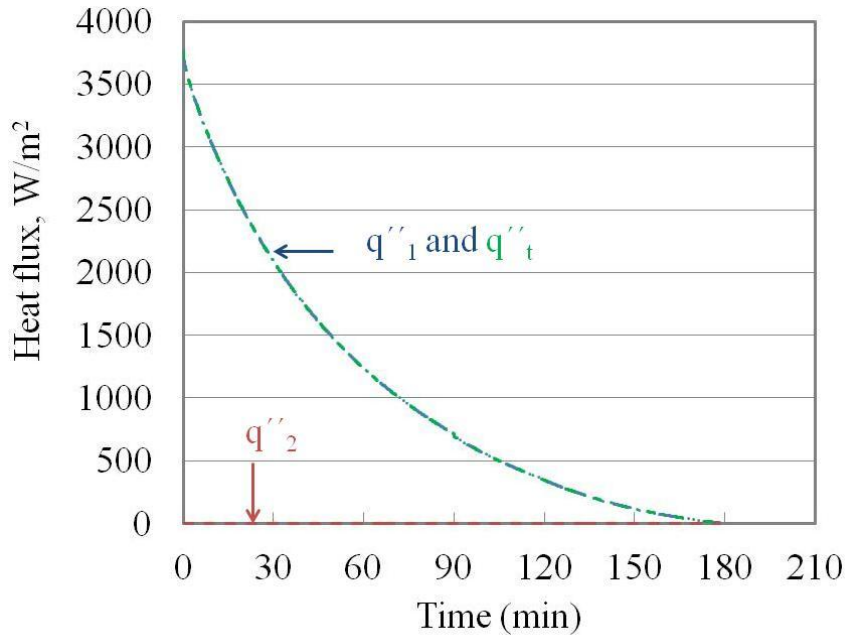


Figure 36. Temporal distribution of heat flux transferred to the temperature sensor (q''_1) and the air (q''_2) and the total heat flux (q''_t) to both the air and temperature sensor during the oxidation of surrogate soot in the isothermal temperature at 550°C in the DSC.

By using Eq. (5.3), the rate of heat release, which was calculated with the determined kinetic parameters and the specific heat capacity of surrogate soot, is displayed as a function of time in Figure 37. To compare with experiment data, we plotted the experiment data following the short transient period. As shown in this figure, the heat flow rate is nearly similar between the two data sets.

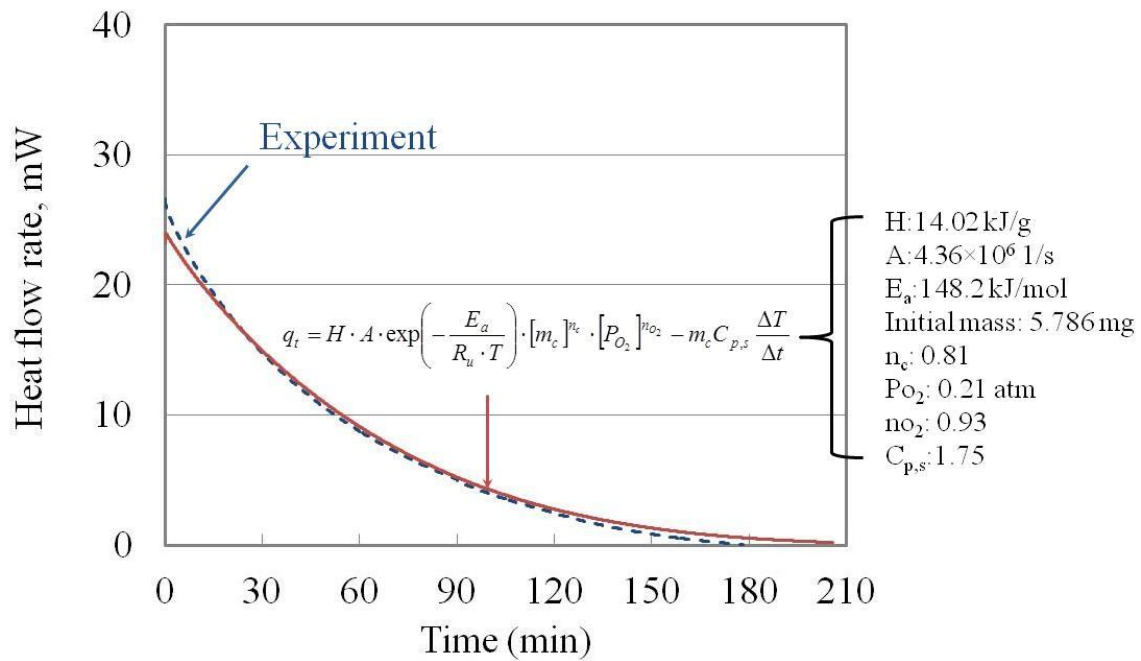


Figure 37. Comparison of data between computation and experiment in terms of heat flow rate (surrogate soot).

We now present results of studying with dry diesel soot. In the same manner of evaluating the specific heat capacity of surrogate soot, the dry diesel soot samples were heated up to 550°C at the rate of 10°C/min followed by an isothermal condition at 45°C for 10 minutes, and then maintained 550°C for 10 minutes in helium environment. Again using Eq. (5.11), the data for specific heat capacity of four different dry diesel soot samples were displayed as a function of temperature in Figure 38. The initial sample masses were 4.81mg in sample#1, 4.852mg in sample#2, 4.845mg in sample#3, and 4.91mg in sample#4, respectively. As shown in this figure, the specific heat capacity exhibits very different values for all samples. While a more in-depth investigation of different values of specific heat capacity will require characterization of

diesel soot speciation, we may ascribe this difference to heavier SOF components and ash particles in diesel soot.

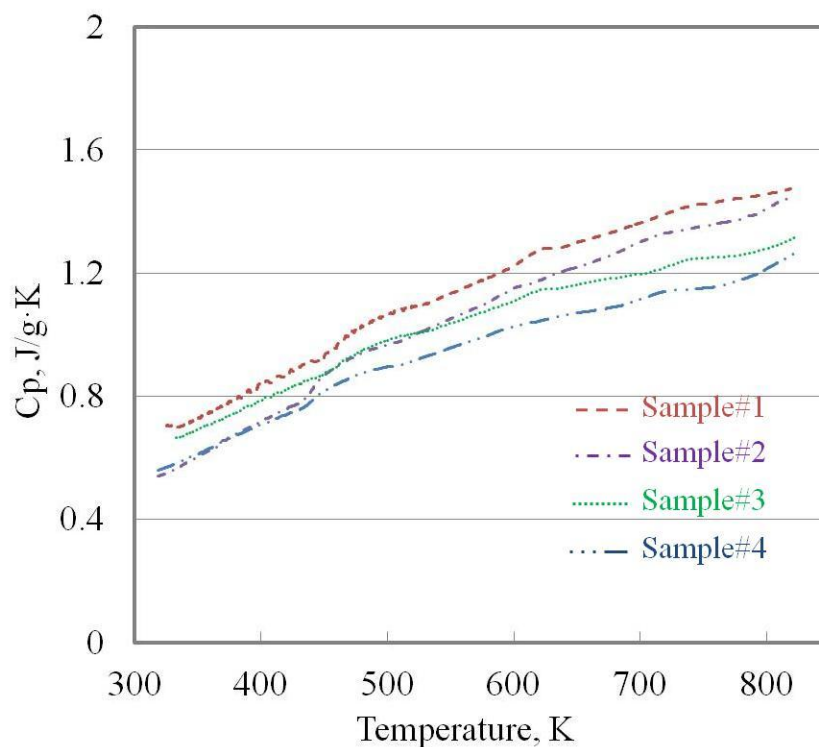


Figure 38. Evaluated heat capacity in the temperature range of 318K(45°C) and 823K(550°C) for four different dry diesel PM samples using Eq. (5.11). Initial sample mass: 4.81mg in sample#1, 4.852mg in sample#2, 4.845mg in sample#3, and 4.91mg in sample#4.

Previous studies have observed different SOF components in diesel PM. Collura et al. (2005) examined the presence of volatile and non-volatile SOF components, as well as surface function groups in the diesel PM, and discussed their effects on reactivity. Chong et al. (2010) have reported ash particles containing complex substance in diesel PM, such as sulfuric compounds,

metal oxides, and their mixture. In particular, the amount of ash was measured to be 3~20% in mass with respect to the initial PM mass. Thus an important observation from this study is that the existence of different SOF components and ash in diesel PM may contribute to differences in the specific heat capacity for the diesel soot samples.

As was the case for the surrogate soot, dry diesel PM was exposed to helium environment in heating mode with temperature gradient of 10°C/min, then maintained at an isothermal temperature of 550°C for 10 min., and then to oxidizing (air) environment at temperatures 550°C, which is presented in Figure 39.

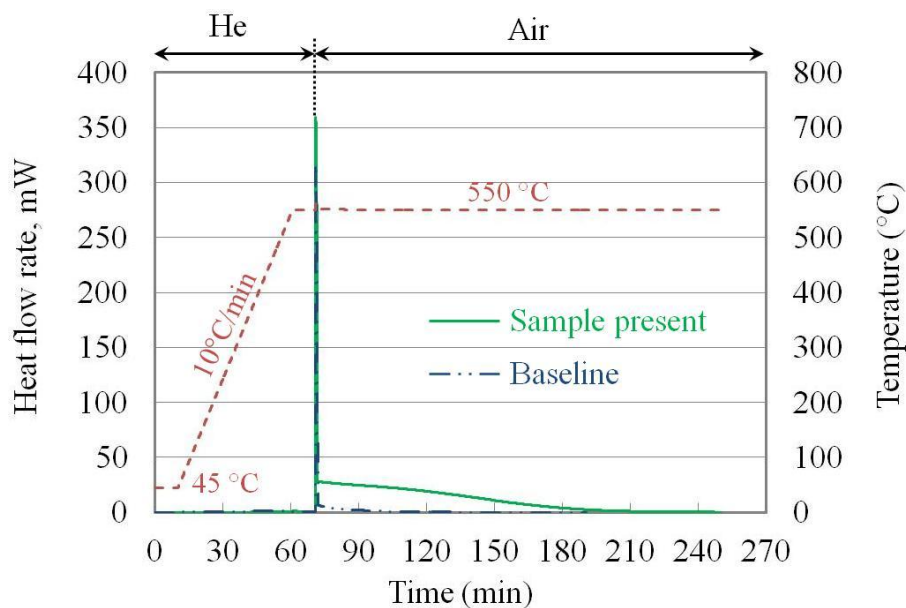


Figure 39. Temporal variation of the instantaneous mass for the dry diesel PM sample exposed to helium environment in heating mode with temperature gradient of 10°C/min, then maintained at an isothermal temperature of 550°C for 10 min., and then to oxidizing (air) environment at temperatures 550°C. Initial sample mass and ash: 5.982mg and 0.285 mg, respectively.

The initial sample mass and ash were 5.982mg and 0.285 mg, respectively. Similar to the oxidation experiment with surrogate soot, the peak is also shown in the heat flow rate curve, after the replacement of helium/air. The data during the first increase and decrease is excluded, in the comparison of data between calculation with the model and experiment. The amount of heat release per unit mass was evaluated to be 17.3kJ/g, which is in a good agreement with the value reported previously.

Figure 40 represents the temporal distribution of heat flux transferred to the temperature sensor and the air and the total heat flux to both the air and temperature sensor during the oxidation of dry diesel PM in the isothermal temperature at 550°C in the DSC.

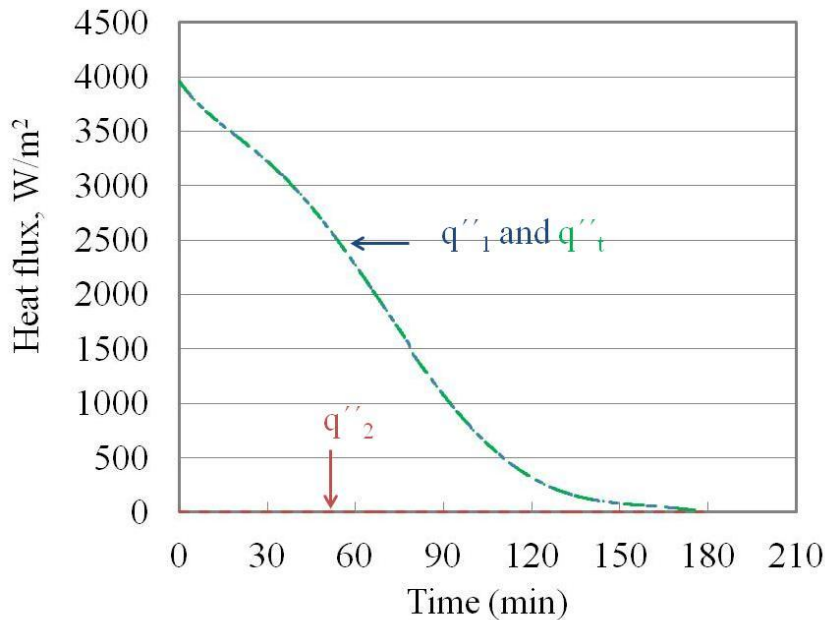


Figure 40. Temporal distribution of heat flux transferred to the temperature sensor (q''_1) and the air (q''_2) and the total heat flux (q''_t) to both the air and temperature sensor during the oxidation of dry diesel PM in the isothermal temperature at 550°C in the DSC.

Similar to the result of surrogate soot, the total heat released from the oxidation of diesel soot in the DSC is also mainly transferred to the temperature sensor by the conduction, while the heat dissipated by the convection is fairly small to be negligible.

Figure 41 presents the temporal variation of instantaneous heat release rate of dry diesel soot sample subjected to the isothermal condition at 550°C in air, which was evaluated with the determined kinetic parameters for zone 1 of diesel soot and the average value of specific heat capacity. The measured heat release rate is also included in the figure.

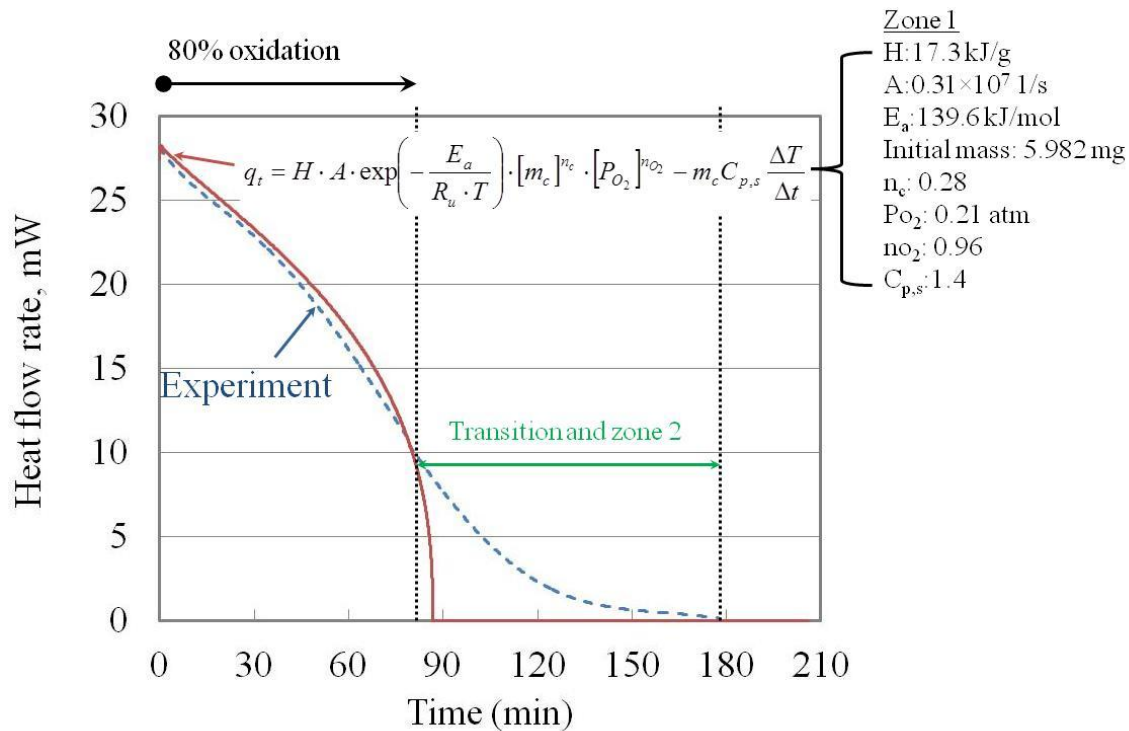


Figure 41. Comparison of data between computation and experiment in terms of heat flow rate (dry diesel soot). The zone 1 and the zone including transition and zone 2 are from the start to 80% of the total heat release and the last 20%, respectively.

As expected, the rate of heat release evaluated with Eq. (5.3) is similar to the experiment data in 80 % of total heat release, while there is a quite difference between the calculated data and experiment in the last 20%. This is due to two different zones occurring during the diesel soot oxidation, as described in chapter 4. To evaluate the instantaneous mass after 80% oxidation in mass occurs, further investigation on the characteristics of the diesel soot oxidation during the transient period from zone 1 to 2 is necessary to fully predict the heat release rate. In particular, the changes of kinetic parameters with respect to the diesel soot morphology and speciation is required to get a complete model for heat released during the diesel soot oxidation.

5.4 Conclusion

In an effort of providing better understanding of heat released during the oxidation of diesel PM, a comprehensive investigation on the oxidation characteristics of diesel PM was performed with the global kinetic parameters from the experiment using TGA, the total specific heat release using DSC, and a mathematical model for predicting heat release rate during the soot oxidation. To control the thermal runaway during the soot oxidation in DPF, the distribution of thermal energy needs to be investigated in detail. As diesel PM on the DPF oxidizes, the transferred heat may contribute to increase the temperatures of exhaust gas and DPF membrane. In this present study, we calculated the heat released during the soot oxidation, using the detailed oxidation experimental data such as total specific heat release and kinetic parameters. Important observations are as follows.

There are significant differences in the specific heat capacity of diesel PM and surrogate soot. The specific heat capacity of surrogate soot is essentially independent of the samples, while

that of diesel soot is strongly influenced by them. For instance, the data for specific heat capacity of surrogate soot varied in a narrow range for all cases, where the specific heat capacity of diesel soot had a wide range, depending upon the samples. This may be due to the difference of chemical components between surrogate soot and diesel PM. While the surrogate soot is ash-free and contains small amount of volatile components, the diesel PM contains various ash and heavier SOF components.

During the soot oxidation in the DSC, the oxygen is mainly supplied by diffusion. And the heat released from the soot is transferred to the temperature sensor by the conduction, rather than to the air by the convection. This result reveals that the heat transferred to the DPF by the conduction should be monitored with care, when the flow of exhaust gas is dominated by diffusion. On the other hand, the oxygen is supplied by forced convection in the real condition during DPF regeneration. Thus the total heat in the real DPF regeneration condition is also significantly influenced by heat transferred by the convection.

The heat release rate of surrogate soot can be modeled with the oxidation rate and total specific heat release, in which the oxidation rate and heat release rate decrease monotonically as the soot is oxidized. In contrast, the heat release rate of diesel soot appears to be characterized by two distinct zones, with the oxidation rate being nearly constant (independent of the instantaneous sample mass) until about 80% of the mass is oxidized (zone 1), and then decreasing continuously as the sample is completely oxidized. The heat release rate of diesel soot can be modeled until the complete of 80% oxidation with the oxidation rate and total specific heat release. However, further investigation on the characteristics of the diesel soot oxidation during the transient period from zone 1 to 2 is necessary to get a complete model of the heat

release rate in the oxidation of diesel soot, such as the changes of kinetic parameters with respect to the diesel soot morphology and speciation.

CHAPTER 6

CONCLUSION

6.1 Summary

Diesel engines typically require DPF systems to reduce PM to meet increasingly stringent emission standards. While there have been noticeable advances in DPF technology, significant efforts are still needed to develop optimum DPF regeneration strategies and achieve efficient removal of diesel PM. In particular, the development of an effective thermal management system is essential to prevent the failure of DPF system by the thermal runaway during the DPF regeneration. In an effort to develop optimum DPF regeneration algorithms, it is important to investigate the oxidation and heat release characteristics of PM collected from the DPF connected to the exhaust pipe of a diesel engine. The experimental approach was to measure directly, by means of a differential scanning calorimeter, the amount of heat release during the oxidation and to elucidate differences in the heat release characteristics of diesel PM and surrogate soot. The TGA experiments involves measurement of the instantaneous sample mass and the rate of mass loss during its oxidation for a wide range of conditions, which includes initial sample mass, amount of volatile components of SOF in the sample, oxygen concentration, and various heat treatment schemes in the inert and oxidizing environments. The global kinetic parameters, which include the reaction orders with respect to soot (n_c) and oxygen (n_{o_2}), activation energy (E_a), and pre-exponential factor (A), were determined for both the diesel PM and surrogate soot samples. The effects of SOF and thermal aging on diesel PM oxidation were also been characterized. Important observations follow.

1. Experiments on the heat release during the oxidation of SOF-containing diesel PM and dry diesel soot (with no SOF) revealed two peaks in heat release rate profiles for the diesel PM, and only one peak for the dry diesel soot. For the diesel PM, the first peak corresponds to exothermic reactions associated with the oxidation of SOFs at temperatures below 400 °C, followed by the second peak corresponding to exothermic reactions for soot oxidation at higher temperatures.
2. The DSC experiments revealed that the amounts of heat released from the oxidation of SOF-containing diesel PM sample, dry diesel soot, and commercially available surrogate soot were approximately 14.67 kJ/g, 17.3 kJ/g, and 14.02 kJ/g, respectively, indicating that the largest heat release was obtained from the dry diesel soot. Furthermore, the specific heat release from the oxidation of SOFs was found to be 5.47 kJ/g.
3. Results also indicated significant differences in the temporal rates of heat release in the oxidation of SOF-containing diesel PM, dry diesel soot, and surrogate soot. In particular, remarkable differences were found on the results for dry diesel soot samples with respect to the oxidation temperatures of 550 °C and below 550 °C in air. The heat release rate of dry diesel soot at the isothermal temperature of 550 °C decreases monotonically as the complete mass is oxidized. In contrast, the rates of heat release at the isothermal temperatures of 535 °C and 525 °C first decrease rapidly, and then slowly.
4. There are significant differences in the oxidation characteristics of diesel PM and surrogate soot. The oxidation behavior of surrogate soot is essentially independent of the various heat treatments and other conditions, while that of diesel soot is strongly influenced by them. For instance, the reaction order of surrogate soot varied in a narrow range of 0.78-0.8, where the diesel soot reaction order had a range of 0.05-0.9, depending upon the test conditions.

Similarly, the activation energy range was 145-149 kJ/mol for the surrogate soot, and 130-155 kJ/mol for the diesel soot.

5. The oxidation of surrogate soot can be characterized by a single zone in which the oxidation rate decreases monotonically as the soot is oxidized. In contrast, the oxidation of diesel soot appears to be characterized by two distinct zones, with the oxidation rate being nearly constant (independent of the instantaneous sample mass) until about 80% of the mass is oxidized (zone 1), and then decreasing continuously as the sample is completely oxidized. Based on the previously reported studies and our data, we may attribute these differences to several processes, including the formation of surface functional groups, presence of heavier SOF components, changes in soot morphology, and build-up of ash layer during the heating and oxidation of diesel soot. Thus an important result from our study is that the data obtained from the oxidation of surrogate soot may not be used for characterizing the oxidation behavior of diesel soot.
6. The oxidation characteristics of diesel PM are only weakly influenced by the presence of the volatile components of SOF. However, the presence of heavier SOF components and thermal aging seem to have a strong influence on diesel soot oxidation. The diesel soot reactivity is observed to decrease with thermal aging. For example, as the isothermal period in inert environment was increased from 1 to 5 h, the activation energy increased from 139 to 153 kJ/mol, while the soot reaction order reduced from 0.25 to 0.05. The effect of thermal aging qualitatively provides a measure of differences between the oxidation characteristics of samples collected from the DPF and those collected from the exhaust pipe.
7. There are significant differences in the specific heat capacity of diesel PM and surrogate soot. The specific heat capacity of surrogate soot is essentially independent of the samples,

while that of diesel soot is strongly influenced by them. This may be due to the difference of chemical components between surrogate soot and diesel PM. While the surrogate soot is ash-free and contains small amount of volatile components, the diesel PM contains various ash and heavier SOF components.

8. Based on the experimental study using TGA and DSC, the heat release rate of diesel PM and surrogate soot have been modeled. Since the surrogate soot oxidation is characterized by a single zone, its heat release rate was successfully predicted. For diesel soot, the oxidation is characterized by two distinct zones. The prediction of heat release rate for zone 1 is in a good agreement with experimental data, while that for zone 2 and transient zone from zone 1 and 2 is quite different from experimental data.

6.2 Future Work

In this work, we have obtained fairly reliable data that may be used for more detailed modeling of diesel soot oxidation. Future studies will focus on characterizing the oxidation behavior of diesel PM in the presence of catalysts and in different oxidizing environments. We have reported that the oxidation of diesel PM is significantly influenced by thermal aging, as described earlier, which corresponds to the experiment result of diesel PM subjected to a wide range of temperature during a certain period under the exhaust gas containing various gas phase chemical components. While we did not investigate the thermal properties of diesel PM collected from the exhaust pipe, the short exposure of PM to exhaust gas leads to weak effect of thermal aging on the diesel PM. Indeed, our experiment result shows that the activation energy of thermally aged diesel PM during 1 hour is lower compared to that during 5 hours, indicating faster oxidation rate. Therefore, the detail investigation on the characterization of oxidation

behavior of diesel PM collected from the DPF can provide more relevant information for designing optimum DPF regeneration algorithms. Future studies will focus on characterizing the oxidation behavior of diesel PM in the presence of catalysts and in different oxidizing environments.

We have reported that the oxidation of diesel PM is characterized by two distinct zones, while the surrogate soot oxidation can be characterized by a single zone. While a more in-depth description of these differences will require investigation on soot morphology and speciation, we may ascribe this behavior to formation of surface intermediates or functional groups during heating and oxidation, which are known to enhance the diesel soot reactivity, presence of heavier SOF components, changes in soot morphology and crystallization. Future work will consider effects of chemical components of soot, morphology, and structure on the oxidation behavior of diesel PM.

We have characterized the oxidation behavior of different soot samples in terms of kinetic study. The global kinetics model was used in this study. With simple algebraic manipulations, the kinetic parameters can be easily determined. To get clear understating of diesel PM oxidation, further investigation will focus on the reaction mechanism of diesel PM and oxygen molecules, the effects of soot morphology and speciation on the kinetic parameters, and the effects of the presence of catalysts and in different oxidizing environments on the kinetic parameters.

REFERENCE

- Abbass, M.K., Shen, Y.J., Abdelhaleem, S.M., Andrews, G.E., Williams, P.T.: Comparison of the methods for the determination of the SOF of diesel particulates and development of a rapid TGA method for the estimation of the unburnt fuel and lubricating oil fractions, **Experimental methods in engine research and development '91**: 109-113, 1991.
- Allanson, R., Blakeman, P.G., Cooper, B.J., Hess, H., Silcock, P.J., Walker, A.P.: Optimizing the low temperature performance and regeneration efficiency of the continuously regenerating diesel particulate filter (Cr-Dpf) System. **SAE Paper** 2002-01-0428, 2002.
- Allansson, R., Gorssmann, C., Lavenius, M., Phillips, P.R., Uusimaki, A.J., Walker A.P.: The development and in-field performance of highly durable particulate control systems. **SAE Paper** 2004-01-0072, 2004.
- Arrhenius, S.: Über die Reaktionsgeschwindigkeit bei der Inversion von Rohrzucker durch Säuren. **Phys.Chem.** 4: 226-248, 1889.
- Barry, A.A.L., van Setten, R., Makkee, M., Moulijn, J.A.: Science and technology of catalytic diesel particulate filters. **Catalysis Reviews** 43 (4): 489-564, 2001.
- Benson, S.W.: The foundation of chemical kinetics. McGraw-Hill, New York, 1960.
- Bhatia, R., Lopipero, P., Smith, A.H.: Diesel exhaust exposure and lung cancer. **Epidemiology**, 9: 84-91, 1998.
- Belisario, M.A., Buonocore, V., De Marinis, E., D. Lorenzo, F.: Biological availability of mutagenic compounds adsorbed onto diesel exhaust particulates. **Mutat. Res.**, 135: 1-9, 1984.
- Boehm, H.P.: Surface oxides on carbon and their analysis: a critical assessment. **Carbon** 40: 145-149, 2002.
- Bradley, L.E., Krishnan, B., Xianjie, Z., Marc, D.R.: Experiments and analysis diesel particulate filter loading and regeneration. **SAE Paper** 2000-01-3087, 2000.
- Bünger, J., Krahl, J., Baum, K., Schröder, O., Müller, M., Westphal, G., Ruhnau, P., Schulz, T.G., Hallier, E.: Cytotoxic mutagenic effects, particle size and concentration analysis of diesel engine emissions using biodiesel and petrol diesel as fuel. **Arch. Toxicol.**, 74: 490-498, 2000.
- Chameides, W.L., Bergin, M.: Climate change-soot takes center stage. **Science**, 297: 2214-2215, 2002.

- Chatterjee, S., McDonald, C., Conway, R., Windawi, H., Vertin, K.D., LeTavec, C.A., Clark, N., Gautam, M.: Emission reductions and operational experiences with heavy-duty diesel fleet vehicles retrofitted with continuously regenerated diesel particulate filters in southern California. **SAE Paper** 2001-01-0512, 2001.
- Chong, H.S., Yang, S.Y., and Lee, K.O.: Accurate measurements of heat release, oxidation rates, and soluble organic compounds of diesel particulates through thermal reaction, **SAE Paper** 2010-01-0814, 2010.
- Ciambelli, P., d'Amore, M., Palma, V., Vaccaro, S.: Catalytic combustion of an amorphous carbon black. **Combust.Flame.** 99: 413–21, 1994.
- Collura, S., Chaoui, N., Azambre, B., Fingueneisel, G., Heintz, O., Krzton, A., Koch, A., Weber, J.V.: Influence of the soluble organic fraction on the thermal behavior, texture and surface chemistry of diesel exhaust soot. **Carbon** 43: 605-613, 2005.
- Cooper, B.J., Thoss, J.E.: Role of NO in diesel particulate emission control. **SAE Paper** 890404, 1989.
- Darcy, P., Costa, P.D., Mellottée, H., Trichard, J.M., Djéga-Mariadassou, G.: Kinetics of catalyzed and non-catalyzed oxidation of soot from a diesel engine. **Catal. Today**, 119: 252-256, 2007.
- Dernaika, B., Uner, D.: A simplified approach to determine the activation energies of uncatalyzed and catalyzed combustion of soot. **Appl. Catal. B** 40: 219–229, 2003.
- Donnet, J.B.: The chemical reactivity of carbons. **Carbon** 6: 161-176, 1963.
- Durán, A., Lucas, A.D., Carmona, M., Ramos, M.J., Armas, O.: Accuracy of the European standard method to measure the amount of DPM emitted to the atmosphere. **Fuels**, 81: 2053-2060, 2002.
- Du, Z., Sarofim, A.F., Longwell, J.P., Mims, C.A.: Kinetic measurement and modeling of carbon oxidation. **Energy Fuels** 5: 214–21, 1991.
- Essenhigh, R. H.: Rate equation for the carbon-oxygen reaction: An evaluation of the Langmuir adsorption isotherm at atmospheric pressure. **Energy Fuel** 5: 41-46, 1991.
- Fábio, S.T., Elisa, B.C., Marcio, S., Isabela, C.L.L., Ricardo, S.A., Martin, S., José, C.P.: Kinetics of the catalytic combustion of diesel soot with MoO₃/Al₂O₃ catalyst from thermogravimetric analyses. **Appl. Catal.A**, 342: 87-92, 2008.

- Farafontov, P., Muter, J.P. Williams, S.: Optimization of partial filter technology for diesel engines. **SAE Paper** 2007-01-4025, 2007.
- Farrauto, R.J., Voss, K.E.: Monolith diesel oxidation catalysts. **Appl. Catal. B**,10: 29-51, 1996.
- Fayard, J.C., Joubert, E.A.: New active DPF system for "Stop & Go" duty cycle vehicles: durability and improvements. **SAE Paper** 2005-01-1754, 2005.
- Fermo, P., Piazzalunga, A., Vecchi, R., Valli, G., Ceriani, M.: A TGA/FT-IR study for OC and EC quantification applied to carbonaceous aerosol collected in Milan (Italy), **Atmos.Chem.Phys.Discuss.**, 5: 4335-4371, 2005.
- Froelund, K., Schramm, J.: PAH-transport in diesel engines. **SAE Paper** 972960, 1997.
- Gamlin, C.D., Dutta, N.K., Choudhury, N.R.: Mechanism and kinetics of the isothermal thermodegradation of ethylene-propylene-diene (EPDM) elastomers. **Polym.Degrad. Stab.** 80: 525-531, 2003.
- Gilot, P., Bonnefoy, F., Marcucilli, F., Prado, G.: Determination of kinetic data for soot oxidation. Modeling of competition between oxygen diffusion and reaction during thermogravimetric analysis. **Combust Flame** 95:87-100, 1993.
- Halsall, R., Mcmillan, M.L., Schwatz, B.J.: An improved method for determining the hydrocarbon fraction of diesel particulates by vacuum oven sublimation. **SAE Paper** 872136; 1987.
- Higgins, K.J., Jung, H.J., Kittelson, D.B., Robert, J.T., Zachariah, M.R.: Sized-selected nanoparticle chemistry: Kinetics of soot oxidation. **J. Phys. Chem. A** 106: 96-103, 2006.
- Hoard, J.W.: Plasma-Catalysis for diesel exhaust treatment: current state of the art. **SAE Paper** 2001-01-0185, 2001.
- Hurt, R. H., Mitchell, R.E.: On the combustion of heterogeneous char particle population. 24th Symposium (International) on Combustion, **The Combustion Institute**, Pittsburgh, PA,; 1233-1241, 1992.
- Hurt ,R.H., Sun, J.K., Lunden, M.: A kinetic model of carbon burnout in pulverized coal combustion. **Combust. Flame** 113:181-197, 1998.

<http://www.dieselnet.com/standards>

- IARC, International Agency for Research on Cancer: Evaluation of carcinogenic risks of chemicals to humans: diesel and gasoline engine exhaust and some nitroarenes. **IARC monographs**, 46: 41-185, 1989.
- Ishiguro, T., Suzuki, N., Fujitani, Y., Morimoto, H.: Micro structural changes of diesel soot during oxidation. **Combust. Flame** 85: 1-69, 1991.
- Jelles, S.J.: Development of catalytic systems for diesel particulate oxidation. Doctoral thesis, Technische Universiteit Delft, Netherlands, 1999.
- Jiang, W., Nadeau, G., Zaghbi, K., Kinoshita, K.: Thermal analysis of the oxidation of natural graphite D effect of particle size. **Thermochim. Acta** 351: 85-93, 2000.
- Johnson, J.H., Bagley, S.T., Gradz, L.D., Leddy, D.G.: A review of diesel particulate control technology and emission effects. **SAE Paper** 94023, 1994.
- Joshi, A.: Development of an actively regenerating DPF System for retrofit applications. **SAE Paper** 2006-01-3553, 2006.
- Jung J., Lee J.H., Song S., Chun K.M.: Measurement of soot oxidation with NO₂-O₂-H₂O in a flow reactor simulating diesel engine DPF. **Int. J. Automotive Technol.** 9: 423-428, 2008.
- Kalogirou, M., Katsaounis, D., Koltsakis, G., Samaras, Z.: Measurements of diesel soot oxidation kinetics in an isothermal flow reactor-catalytic effects using Pt based coatings. **Topics in Catalysis**. 42-43: 247-251, 2007.
- Kasper, M., Matter, U., Burtscher, H.: On-line characterization of particle size and composition. **SAE Paper** 2000-01-1998, 2000.
- Kittelson, D.B.: Engines and nanoparticles: A review, **J. Aeros. Sci.**. 29 (5-6): 575, 1998.
- Kobashi, K., Hayashi, K., Aoki, H., Kurazono, K., Fujimoto, M.: Regeneration capability of diesel particulate filter system using electric heater. **SAE Paper** 930365, 1993.
- Koltakis, G.C. and Stamatelos, A.M.: Modes of catalytic regeneration in diesel particulate filter. **Ind. Chem. Res.** 36: 4155-4165, 1997.
- Kreyling, W. G., Semmler-Behnke, M., Moller, W.: Health implications of nanoparticles. **J. Nanoparticle Res.**8(5):543-562, 2006.
- Laidler, K.J.: Theories of chemical reaction rates. McGraw-Hill, New York, 1969.

- Langley, L.A., Villanueva, D.E., Fairbrother, D.H.: Quantification of surface oxides on carbonaceous materials. **Chem. Mater.** 18:169-178, 2006.
- Lapuerta, M., Ballesteros, R., Rodriguez-Fernandez, J.: Thermogravimetric Analysis of Diesel Particulate Matter. **Meas. Sci. Technol.** 18: 650-658, 2007.
- Laurendeau, N. M.: Heterogeneous kinetics of coal char gasification and combustion. **Prog. Energy Combust. Sci.** 4: 221-270 , 1978.
- Lee, K.O., Cole, R., Sekar, R., Choi, M.Y., Zhu, J., Kang, J., Bae, C.S., Shin, H.D.: Morphological investigation of the microstructure, dimensions, and fractal geometry of diesel particulates. **Proc. Combust. Inst.** 29: 647-653, 2002.
- Lee, K.O., Zhu, J., Ciatti, S., Yozgatligil, A., Choi, M.Y.: Sizes, graphitic structure and fractal geometry of light duty diesel engine particulate. **SAE Paper** 2003-01-3169, 2003.
- Lee, Y.K., Kim, D.J., Kim, H.J., Hwang, T.S., Rafailovich, M., Sokolov, J.: Activation energy and curing behavior of resol- and novolac-type phenolic resins by differential scanning calorimetry and thermogravimetric analysis. **Appl. Polym. Sci.** 89: 2589–2596, 2003.
- Levsen, K.: The analysis of diesel particulate. **Fresenius Z Anal. Chem.** 331: 467-478, 1988.
- Levendis, Y., Larsen, C.A.: Use of ozone-enriched air for diesel particulate trap regeneration. **SAE Paper** 1999-01-0114, 1999.
- Levenspiel, O.: Chemical reaction engineering. John Wiley & Sons, New York, 1999.
- Locker, R.J., Sawyer, C.B., Floerchinger, P., Menon, S., Craig, A.: Diesel particulate filter operational characterization. **SAE Paper** 2004-01-0958, 2004.
- López-Fonseca, R., Landa, I., Elizundia, U., Gutiérrez-Ortiz, M.A., González-Velasco, J.R.: A kinetic study of the combustion of porous synthetic soot. **Chem. Eng.J.** 129: 41-49, 2007.
- Marcucilli, F., Gilot, P., Stanmore, B.R., Prado, G.: Experimental and theoretical study of diesel soot reactivity. 25th Symposium (International) on Combustion, The Combustion Institute, Philadelphia, **The Combustion Institute**,: 619–26, 1994.
- Maricq, M.M.: Chemical characterization of particulate emissions from diesel engine: A review, **J. Aeros. Sci.** 38: 10479-11118, 2007.
- Martirosyan, K.S., Chen, K., Luss, D.: Behavior features of soot combustion in diesel particulate filter. **Chem. Eng. Sci.** 65: 42-46, 2010.

- Messerer, A., Niessner, R., Pöschl, U.: Comprehensive kinetic characterization of the oxidation and gasification of a model and real diesel soot by nitrogen oxides and oxygen under engine exhaust conditions: Measurement, Langmuir-Hinshelwood, and Arrhenius parameters. **Carbon** 44: 307-324, 2006.
- Michelin, J., Figueras, B., Bouly, C., Maret, D.: Optimized diesel particulate filter system for diesel exhaust aftertreatment. **SAE Paper** 2000-01-0475,2000.
- Monson, C.R., Germane, G.J., Blackham, A.U., Smoot, L.D.: Char oxidation at elevated pressure. **Combust. Flame.** 100: 669-683, 1995.
- Muller, J.O., Su, D.S., Jentoft, R.E., Krohnert, J., Jentoft, F.C., Schlogl, R.: Morphology controlled reactivity of carbonaceous materials towards oxidation. **Catalysis Today** 102-103: 259-265, 2005.
- Nejar N., Makkee M., Illán-Gomez M.J.: Catalytic removal of NO_x and soot from diesel exhaust: Oxidation behaviour of carbon materials used as model soot. **Appl. Catal. B** 75: 11-16, 2007.
- Neeft, J.P.A., Hoornaert, F., Makkee, M., Moulijn, J.A.: The effects of heat and mass transfer in thermogravimetry analysis: A case study towards the catalytic oxidation of soot. **Thermochim. Acta** 287: 261-278, 1996.
- Neeft, J.P.A., Nijhuis, T.X., Smakman, E., Makkee, M., Moulijn, J.A.: Kinetics of the oxidation of diesel soot. **Fuel** 76: 1129-1136, 1997.
- Nejar, N., Makkee, M., Illán-Gomez, M.J.: Catalytic removal of NO_x and soot from diesel exhaust: Oxidation behaviour of carbon materials used as model soot. **Appl. Catal. B** 75: 11-16, 2007.
- Ohe, T.: Mutagenicity of photochemical reaction products of polycyclic aromatic hydrocarbons with nitrite. **Sci. Total Environ.**, 39:161-175, 1984.
- Otto, K., Sieg, M.H., Zinbo, M.: The oxidation of soot deposits from diesel engines. **SAE Paper** 800336, 1980.
- Pauli, E., Lepperhoff, G., Pischinger, F.: The description behavior of diesel particulate traps with the aid of a mathematical model. **SAE Paper** 830180, 1983.
- Petersen, R.C.: The oxidation rate of diesel particles which visco AM. Catalytic combustion of diesel soot over metal contain lead. **SAE paper** 870628, 1987.

- Pfeifer, M., Votsmeier, M., Spurk, P.C., Kogel, M., Lox, E., Knoth, J.F.: The Second generation of catalyzed diesel particulate filter systems for passenger cars - particulate filters with integrated oxidation catalyst function., **SAE Paper** 2005-01-1756, 2005.
- Reichert, D., Bockhorn, H., Kureti, S.: Study of reaction of NO_x and soot on Fe₂O₃ catalyst in excess of O₂. **Appl. Catal. B**, 80: 248-259, 2008.
- Riedl, M., Diaz-Sanchez D., Biology of diesel exhaust effects on respiratory function. **J. Allergy Clin. Immunol.** Feb.: 221-228, 2005.
- Saterfield, C.N.: Mass transfer in heterogeneous catalysis. MIT Press, Cambridge, MA, 1970.
- Schramm, J., Hori, S., Abe, T.: An investigation of the effect of the lubricant on the soluble organic fraction of particulate emissions from a DI diesel engine. **J. Synth. Lubr.**, 14(2): 157-168, 1997.
- Schwarze, P. E., Ovrevik, J., Lag, M., Refsnes, M., Nafstad, P., Hetland, R.B., Dybing, E.: Particulate matter properties and health effects: consistency of epidemiological and toxicological studies. **Human & Experimental Toxicology**, 25(10):559-579, 2006.
- Seaton, A., MacNee, W., Donaldson, K., Godden, D., Particle air pollution and acute health effects, **The Lancet**, 345: pp.176, 1995.
- Setiabudi, A., Makkee, M., Moulijn, J.A., The role of NO₂ and O₂ in the accelerated combustion of soot in diesel exhaust gases. **Appl. Catal. B** 50: 185-194, 2004.
- Shirk, R., Bloom, R.L., Kitahara, Y., Shinzawa, M.: Fiber wound electrically regenerable diesel particulate filter cartridge for small diesel engines. **SAE Paper** 950153, 1995.
- Soeger, N., Musmann, L., Sesselmann, R., Leippe, G., Gietzelt, C., Bailey, O., Hori, M.: Impact of aging and NO_x/Soot ratio on the performance of a catalyzed particulate filter for heavy-duty diesel applications. **SAE Paper** 2005-01-0663, 2005.
- Song, Q., He, B., Yao, Q., Meng, Z., Chen, C.: Influence of diffusion on thermogravimetric analysis of carbon black oxidation. **Energy Fuels** 20 (5): 1895-1900, 2006.
- Sorai, M.: Comprehensive handbook of calorimetry and thermal analysis. John Wiley & Sons, Inc., Chichester, 2004.
- Stanmore, B.R., Gilot, P., Prado, G.: The influence of mass transfer in DTG combustion tests. **Thermochim. Acta** 240: 79-89, 1994.

- Stratakis G.A., Stamatelos, A.M.: Thermogravimetric analysis of soot emitted by a modern diesel engine run on catalyst-doped fuel. **Combust. Flame** 132: 157-169, 2003.
- Su, D.S., Jentoft, R.E., Muller, J.O., Rothe, D., Jacob, E., Simpson, C.D., Tomovic, Z., Mullen, K., Messerer, A., Poschl, U., Niessner, R., Schlogl, R.: Microstructure and oxidation behavior of Euro IV diesel engine soot: a comparative study with synthetic model soot substances. **Catalysis Today** 90: 127-132, 2004.
- Suuberg, E.M., Wojtowicz, M., Calo, J.M.: Reaction order for low-temperature oxidation of carbons. **Proc. Combust. Inst** 22:79-87, 1989.
- Tapio, O., Salmi, Jyri-Pekka Mikkola, Johan P. Wärna, Chemical reaction engineering and reactor technology, CRC Press, New York, 2009. (297-325, 549-554)
- Vander Wal, R.L., Mueller, C.J.: Initial investigation of effects of fuel oxygenation on nanostructure of soot from a direct-injection engine. **Energy and Fuels** 20: 2364-2369, 2006.
- Vander Wal, R.L., Yezerets, A., Currier, N.W., Kim, D.H., Wang, C.M.: HRTEM study of diesel soot collected diesel particulate filters. **Carbon**, 45: 70-77, 2007.
- Vincent, M.W., Richards, P., Novel-Cattin, F., Marcelly, B., Favre, C.: Fuel additive performance evaluation for volume production application of a diesel particulate filter. **SAE Paper** 2001-01-1286, 2001.
- Vincenti, W.G. and Kruger, G.H.Jr.; Introduction of physical gas dynamics. Wiley, New York, 1965.
- Walker, P.L., Austin, L.G., Nandi, S.P.: In Chemistry and Physics of Carbon, Walker PL, Ed.; Marcel Dekker: New York, 1966.
- Yamamoto, T., Okubo, M., Kuroki, T., Miyairi, Y.: Nonthermal plasma regeneration of diesel particulate filter. **SAE Paper** 2003-01-1182, 2003.
- Yang, S.Y., Lee, K.O. and Chong, H.S.: Characterization of oxidation behaviors and chemical-kinetics of diesel particulates relevant to DPF regeneration. **SAE Paper** 2010-01-2166, 2010.
- Yezerets, A., Neal, .W. C., Eadler H.A.: Experimental determination of the kinetics of diesel soot oxidation by O₂- modeling consequences. **SAE Paper** 2003-01-0833, 2003.

- Yezerets, A., Currier, N.W., Kim, D.H., Eadler, H.A., Epling, W.S., Peden, C.G.F: Differential kinetic analysis diesel particulate matter (soot) oxidation by oxygen using a step-response technique. **Appl. Catal. B**, 61: 120-129, 2005.
- Zhi, N., Guanglong, Z., Yong, L., Junmin, L., Xiyan, G., Lunhui, L., Jiahua, C.: Analysis of characteristic of microwave regeneration for diesel particulate filter. **SAE Paper** 952058, 1995.
- Zinbo, M., Skewes, L.M., Hunter, C.E., Shuetzle, D.: Thermogravimetry of filter-borne diesel particulates, **Thermochim. Acta**, 198: 249-275, 1992.
- Zinbo, M., Korniski, T.J., Weir, J.E.: Relationship between the composition of engine particulate emissions and emission control system performance, **Ind. Eng. Chem. Res.**34: 619-625, 1995.

ARGONNE NATIONAL LABORATORY Argonne, USA
Co-op Researcher, Transportation Technology R&D Center May 2008 – May 2010

- Development of an advanced DPFs regeneration system
- Development of a high speed system for sampling emissions in diesel engines

HYUNDAI HEAVY INDUSTRIES Ulsan, Korea
Researcher, Engine and Machinery Division Jul. 2000 – Jun. 2003

- Development of laser-based optical diagnostic system for research on diesel engines
- Investigation on the effect of iso-octane, biodiesel, and liquefied natural gas addition on diesel engine performance and emissions characteristics
- Research on the effects of in-take swirl and tumble flows on the efficiency of diesel engines
- Development of thermal performance test procedures of advanced diesel engines for marine propulsion and industrial power plants
- Development of a diesel PM filtration systems using dielectrophoresis
- Prepare, plan, and execute performance test on advanced turbomachineries developed by ABB for diesel engines
- Prepare, plan, and execute functionality test for diesel engines in engine test cells
- Analyze data, diagnose and evaluate testing issues
- Communication with customers regarding testing data, schedules, and technical issues.

MILITARY **KOREA ARMY** Hwachon, Korea
Platoon Leader Mar. 1996 – Jun. 1998

- Administered a platoon

PUBLICATIONS Thesis:

- *An Experimental Investigation of the Oxidation Characteristics of Diesel Particulate Matter, 2012 (Doctor of Philosophy)*
- *Investigation on the in-cylinder flow fields using PTV measurement, 2000 (Master of Science)*

Conference proceeding/Journal:

H.S. Chong, S.Y. Yang, K.O. Lee, "Accurate Measurement of Heat Release, Oxidation rates and Soluble Organic Compounds of Diesel Particulates through Thermal Reactions", SAE PAPER 2010-01-0814

S. Yang, K. Lee, H. Chong, "Characterization of Oxidation Behaviors and Chemical-Kinetics of Diesel Particulates Relevant to DPF Regeneration", SAE PAPER 2010-01-2166

H.S. Chong, S.K. Aggarwal, K.O. Lee, S.Y. Yang, "Measurement of Heat Release of Diesel PM for Advanced Thermal Management Strategies for DPF Regeneration", Combust.Sci.and Technol., 183: 1-14, 2011

H.S. Chong, S.K. Aggarwal, K.O. Lee, S.Y. Yang, H. Seong "Experimental Investigation on the Oxidation Characteristics of Diesel Particulates Relevant to DPF Regeneration", Combust.Sci.and Technol., Accepted 13 Sep. 2012.

PRESENTATIONS

“Accurate Measurement of Heat Release, Oxidation rates and Soluble Organic Compounds of Diesel Particulates through Thermal Reactions”, SAE (Society of Automotive Engineers) 2010 WORLD CONGRESS, 2010.

“Experimental Investigation on the Oxidation Characteristics of Diesel Particulates”, CLEERS (Cross-cut Lean Exhaust Emissions Reduction Simulations) 2012 CONFERENCE (Poster), 2012.

COMPUTER

Simulation Tools (CONVERGE, KIVA-III, ANSYS, CHEMKIN)

Design Tools (AUTOCAD, PRO-E)

Programming Languages (C/C++, MATLAB)

MS Office (Word, Excel, PowerPoint)